On the long-term stability of the solar system

by

Garett Brown

A thesis submitted in conformity with the requirements
for the degree of Doctor of Philosophy

Department of Physics
University of Toronto

On the long-term stability of the solar system

Garett Brown
Doctor of Philosophy

Department of Physics
University of Toronto
2025

Abstract

The long-term evolution of the solar system is inherently chaotic, arising from the overlap of secular resonances determined by the system's secular modes. The extents of the overlapping regions are determined by the amplitudes of the solar system's secular modes, resulting from the planets' eccentric and non-coplanar orbits, challenging formation theories that predict nearly circular and coplanar orbits. Upon entering a linear secular resonance, planetary eccentricities can rapidly increase, potentially leading to instability. To accurately model the solar system's long-term evolution and predict its potential instability, it is essential to incorporate general relativistic precession. General relativity introduces small but significant corrections to the planets' orbits, particularly Mercury's, without which can significantly alter the dynamics of the system and accelerate its approach to a secular resonance with Jupiter. A Fokker–Planck, advection–diffusion model demonstrates that while ignoring general relativistic precession brings Mercury closer to a secular resonance with Jupiter, this closeness alone does not explain the excessive instability rate. External perturbations from stellar flyby encounters also affect the long-term stability of the solar system. A substellar flyby encounter offers a plausible explanation for the moderate eccentricities and inclinations of the planets, with at best a 1-in-1000 chance of producing a solar system–like architecture. Moreover, weak stellar encounters can perturb the solar system's dynamical state, with small perturbations to the outer planets' orbits being transferred inwards and increasing the likelihood of inner solar system destabilization. Relative perturbations to Neptune's semi-major axis of 0.1 per cent can significantly increase the probability of solar system destabilization within 5 Gyrs. In conclusion, the long-term stability of the solar system is a chaotic and complex interplay of secular resonances, general relativistic effects, and external perturbations from flyby encounters. Understanding these factors is vital for unraveling the history and future of our planetary system.

To my children, Ælwyn and Maelie.
You are the chaos in my universe and sparks of joy in my life.

Acknowledgements

No one can complete the requirements of a PhD alone and my experience has not been an exception. Therefore, I have done my best here to express my gratitude and thank those who have supported and encouraged me. I cannot list you all, but I could not have done this without you.

To my advisor, Hanno Rein, I owe my deepest appreciation and sincerest thanks. From the moment we first met in March 2017[1], my experiences with you have only been positive and constructive[2]. Thank you for your kindness and advocacy as I not only endeavoured to complete this monumental undertaking, but also as I embarked on the path of parenthood. I will always be grateful for your patience and support as I have navigated this journey. I am grateful for our conversations and how you brought me from student to collaborator. I find it difficult to capture the positive feelings of being invited by you to weigh in on a project that you are working on.

To the additional academic advisors who supported me, encouraged me, and taught me in personal conversations, committee meetings, classroom discussions, or group meetings. Thank you Norm Murray, Chris Thompson, Jo Bovy, Cristobal Petrovich, Yanqin Wu, Marten van Kerkwijk, Noah Hammond, and Nathan Sandholtz. Thank you Sam Hadden for your patient discussions of secular dynamics. A special thank you to Dan Tamayo. Your incredible support early on and your letters of recommendation enabled so much of what I was able to do later on. Your ability to teach and inspire is unparalleled. A particular thanks to Krystyna Beil. I think it is very clear that no one would graduate from the Department of Physics without your support and the work that you do. Thank you for the often thankless work that you do and specifically for helping me along my journey through the department. Finally, thank you, Renu Malhotra. Your support and encouragement were an integral part of helping me rebuild my scientific self-confidence[3]. Additionally, my collaborative work with you was a joy to wrestle with and is the highlight of this work.

Thank you to my cohort for the good conversations and listening ears. Even if I was silently frustrated at times, thank you for the interruptions. I did miss our conversations during lockdowns and when I was working remotely in South Korea. Thank you Mykhaylo Plotnykov, Bo Peng, Michael Poon, Alysa Obertas, David Veitch, Mark Dodici, Rejean Le Blanc, Fergus Horrobin, Shayne Gryba, Jesse Velay-Vitow, and my original office mates Ilan Tzitrin and Eli Bourassa. A special thanks for you Dang Pham. Our frequent discussions were a staple highlight of the latter part of my degree. Also, thank you to the Graduate Astronomy Students Association (GASA) and the SciFi Lunches for welcoming me from Physics.

Thank you to my undergraduate advisor, Manuel Berrondo. Thank you for allowing me to explore the world of boids with you and for helping me develop my emerging research skills. I am very grateful to my undergraduate professors at Brigham Young University (BYU) for your dedication to good pedagogical practices and support of curious students like me. Thank you Mark Transtrum, Gus Hart, Denise Stephens, Lawrence Rees, John Colton, Steve Turley, and Rob Davies. And thank you to John Ellsworth for taking me under your wing and teaching me about vacuums,

[1] You were wearing a bow-tie in our first meeting and, as I am also an avid wearer of bow-ties, I was excited about the prospect of working with you. I don't remember the details about the conversation we had (though it was likely about numerical methods), but I remember feeling like we connected, that we were both excited about similar things, and I felt good about the opportunity to work with you.

[2] Thank you for helping me navigate the mess of funding sources, parental leave requirements, reimbursement requests, and unexpected issues. I apologize for my lack of communication and unintentional complications at times.

[3] Managing the rollercoaster of the false self-confidence following my undergraduate degree and the ensuing imposter syndrome was a long and existential process.

high voltage systems, hazardous chemicals, and life in general. Also, thank you to Priscilla Canizares for the firehose introduction to gravitational waves during my brief summer in Cambridge. I am also grateful for your letters of recommendation that supported my graduate career.

Thank you to my good friends from BYU who helped me get through some of the most demanding parts of my academic career. A special thanks to Kyle Matt and Kolten Barfuss. Thank you for being such true friends, for helping me relax and unwind, and for being there with me through the difficult nights of homework assignments. Thank you for keeping in touch and helping me make sense of this ever-changing world.

To my high school physics teacher, Farouq Hassanali, and my high school chemistry teacher, Kim Houlder. Thank you for inspiring me and showing me the beauty of science. Thank you for the conversations and the genuine interest in my life.

I am grateful to my parents and family for all of your support over the decades. Thank you for encouraging me to pursue an education and for all of your financial and emotional support along the way. Thank you for creating a home that I am welcomed back to and for enabling me to find my path in life.

Lastly, and most importantly, I am grateful for my partner Jessica. You have been my biggest supporter in this entire endeavour. You are my best friend and trusted confidante. Thank you for the endless conversations. Your dedication and love of learning always inspires me to be better. Your love of travel always brings me new experiences. Your support in our parenting leads me to be a better father and a better person. You are a source of so much happiness in my life. Thank you for sharing the sky with me. I love you for eternity. Thank you for everything.

Contents

List of Tables viii

List of Figures ix

List of Works x

1 Introduction 1
- 1.1 Brief Historical Overview . . . 1
- 1.2 Computational Advances . . . 4
- 1.3 This Work . . . 7

2 On the origin of the secular modes 9
- 2.1 Introduction . . . 10
- 2.2 Introduction . . . 11
- 2.3 Methods . . . 12
  - 2.3.1 Stellar Environment . . . 12
  - 2.3.2 Integration Methods . . . 13
  - 2.3.3 Metric for secular architectures . . . 13
  - 2.3.4 Reference Systems . . . 14
- 2.4 Results and Discussion . . . 15
  - 2.4.1 Best Match . . . 15
  - 2.4.2 Inner Solar System . . . 18
  - 2.4.3 Kuiper Belt . . . 19
  - 2.4.4 Probabilities . . . 20
- 2.5 Conclusions . . . 21
- 2.A Appendix . . . 23
  - 2.A.1 Likelihood of Multiple Flybys . . . 23
  - 2.A.2 Success Criteria . . . 23
  - 2.A.3 Angular Momentum Deficit . . . 23

3 On the role of general relativity 27
- 3.1 Introduction . . . 28
- 3.2 The path to instability . . . 29
- 3.3 N-body simulations . . . 30
  - 3.3.1 Methods . . . 30

3.3.2 Perihelion precession from general relativity . . . 30
3.3.3 N-body results . . . 32
3.4 Advection–diffusion model . . . 32
3.4.1 Fokker–Planck equation . . . 32
3.4.2 Model with general relativistic precession . . . 34
3.4.3 Model without general relativistic precession . . . 34
3.4.4 Model with time-dependent general relativistic precession . . . 35
3.5 Results . . . 35
3.6 Conclusions . . . 37

4 On flybys and long-term stability **39**
4.1 Introduction . . . 39
4.2 Weak perturbations to planetary systems . . . 40
4.2.1 Stellar environments . . . 40
4.2.2 One planet . . . 42
4.2.3 Successive flybys . . . 44
4.2.4 Two planets . . . 46
4.2.5 More than two planets . . . 47
4.3 Long-term stability . . . 48
4.3.1 Numerical methods . . . 48
4.3.2 Solar system stability . . . 48
4.3.3 Secular resonances . . . 49
4.4 Discussion and Conclusions . . . 50
4.A Adiabatic change in energy from a stellar flyby . . . 51
4.B Angular momentum deficit . . . 52
4.C Details of numerical results . . . 53

5 Conclusions **55**

A `AIRBALL` **59**

Bibliography **70**

List of Tables

2.1 A comparison of the secular frequencies and amplitudes of the giant planets (SS) and our best matching flyby system that experienced a $m_\star = 8.27\,\mathrm{M_J}$ encounter at $q_\star = 1.69\,\mathrm{AU}$, with $v_\infty = 2.69\,\mathrm{km\,s^{-1}}$. By convention, s_5 is the null frequency when inclinations are designated with respect to the invariant plane. 18

2.2 Averaged over 20 Myr, we show a comparison of the eccentricities and inclinations (with respect to the invariant plane) of the giant planets (SS) and our best matching flyby system that experienced a $m_\star = 8.27\,\mathrm{M_J}$ encounter at $q_\star = 1.69\,\mathrm{AU}$, with $v_\infty = 2.69\,\mathrm{km\,s^{-1}}$. 24

4.1 A summary of stellar environment parameters for different regions of the galaxy. . . 41

List of Figures

1.1 Illustration of the Keplerian orbital elements, by Lucas Snyder (CC BY-SA 3.0) . . . 2
1.2 History of solar system integration times. 6

2.1 A snapshot from our best matching flyby simulation and the time evolution of the orbital elements of the gas giants before, during, and after the flyby. 16
2.2 The power spectra of the solar system compared to our best matching flyby. 17
2.3 The impact of our best matching flyby on the cold, classical Kuiper Belt. 19
2.4 The distributions of the flyby parameters for all our simulations. 21
2.5 The distribution of the angular momentum deficit (AMD) for all the flyby systems. . 24
2.6 The distributions of all the flyby parameters in all our simulations. 25

3.1 The instability time of simulations with respect to time varying general relativity. . . 32
3.2 A comparison of our advection–diffusion model with previous work. 33
3.3 The survival fraction of the entire ensemble of simulations compared to our model. . 36
3.4 The survival fraction of the simulations (divided into four bins) compared to our model. 36

4.1 The average time until a stellar flyby occurs for various stellar environments. 44
4.2 The impact of successive flybys on the binding energy of a Sun-Neptune system. . . 45
4.3 Changes to the secular mode frequncy g_1 with respect to the relative change in Neptune's semi-major axis. 47
4.4 The fraction of simulations that lead to an instability before 5 Gyr with respect to the relative change in Neptune's semi-major axis. 48
4.5 Secular resonant angle between Earth and Mars with respect to the relative change in Neptune's semi-major axis. 50
4.6 Relative changes to the angular momentum deficit (AMD) of the entire solar system with respect to the relative change in Neptune's semi-major axis. 53
4.7 All events that triggered the simulations from Section 4.3.2 to end before 5 Gyr. . . 54

List of Works

Papers

8. **Garett Brown**, Renu Malhotra, Hanno Rein, "A substellar flyby that shaped the orbits of the giant planets", *Submitted* (5 Dec 2024, *Preprint*).

7. **Garett Brown**, Hanno Rein, "General relativistic precession and the long-term stability of the solar system", *MNRAS*, Volume 521, Issue 3, May 2023, Pages 4349–4355.

6. **Garett Brown**, Linda He, James Unwin, "The Potential Impact of Primordial Black Holes on Exoplanet Systems", *MIT PRIMES* (28 Jan 2023, *Preprint*).

5. **Garett Brown**, Hanno Rein, "On the long-term stability of the Solar System in the presence of weak perturbations from stellar flybys", *MNRAS*, Volume 515, Issue 4, October 2022, Pages 5942-5950.

4. **Garett Brown**, Hanno Rein, "A Repository of Vanilla Long-term Integrations of the Solar System", *RNAAS*, Volume 4, Number 12, 9 December 2020.

3. Hanno Rein, **Garett Brown**, Daniel Tamayo, "On the accuracy of symplectic integrators for secularly evolving planetary systems", *MNRAS*, Volume 490, Issue 4, December 2019, Pages 5122–5133.

2. Hanno Rein, Daniel Tamayo, **Garett Brown**, "High order symplectic integrators for planetary dynamics and their implementation in REBOUND", *MNRAS*, Volume 489, Issue 4, November 2019, Pages 4632–4640.

1. Hanno Rein, David M. Hernandez, Daniel Tamayo, **Garett Brown**, Emily Eckels, Emma Holmes, Michelle Lau, Rejean Leblanc, Ari Silburt, "Hybrid Symplectic Integrators for Planetary Dynamics", *MNRAS*, Volume 485, Issue 4, June 2019, Pages 5490–5497.

Presentations

- "`AIRBALL`", Invited Presentation, *REBOUND 2024*, 9 July 2024, Online.
- "The effects of stellar flybys on the formation and stability of the Solar System", Submitted Presentation, *DDA*, 13 May 2024, University of Toronto, Toronto, Ontario, Canada.
- "On the Long-term Stability of the Solar System", Submitted Presentation, *GSSS*, 20 Mar 2024, University of Toronto Scarborough, Scarborough, Ontario, Canada.

- "On the Long-term Stability of the Solar System", Invited Presentation, *Exoplanets/Stars Seminar*, 27 Feb 2024, Yale University, New Haven, Connecticut, USA.
- "Long-term Solar System Survival (Analysis)", Submitted Presentation, *StellarStats 2023*, 4 May 2023, University of Toronto, Toronto, Ontario, Canada.
- "Too Close For Comfort", Submitted Presentation, *DPS54*, 4 Oct 2022, RBC Place London, London, Ontario, Canada.
- "Too Close For Comfort", Submitted Presentation, *CITA Planet Day*, 9 Aug 2022, University of Toronto, Toronto, Ontario, Canada.
- "Quantifying the Effects of Stellar Flybys on Planetary Systems", Submitted Presentation, *ERES 2019*, 18 Jun 2019, Cornell University, Ithaca, New York, USA.
- "Quantifying the Effects of Stellar Flybys on Planetary Systems", Submitted Presentation, *Planetary Dynamics Conference 2019*, 6 Jun 2019, Max-Planck Institute for Astronomy, Heidelberg, Germany.

Posters

- "Small Changes with Big Consequences: Solar System Stability", Submitted Poster, *ERES 2022*, 1 Aug 2022, Penn State, State College, Pennsylvania, USA.
- "Quantifying the Effects of Weak Stellar Flybys on the Solar System", Submitted Poster, *ERES 2021*, 25 May 2021, Princeton University, Online
- "Coordinate Interpolation and Data Compression Using REBOUND", Submitted Poster, *Theory Canada 13, 2018*, 8 Jun 2018, St-Francis Xavier University, Antigonish, Nova Scotia, Canada.

Chapter 1

Introduction

The solar system is perhaps the oldest and most studied dynamical system. Over the millennia, astronomers have dedicated their best work to unraveling its complexities, employing increasingly refined mathematical models to diminish discrepancies with observations. However, as one mystery would become known, another would appear to replace it, creating cycles of confusion and clarity. The growing precision and predictive power of these mathematical models, made the question of the long-term stability of the solar system of great interest to natural philosophy. Building upon this foundation of knowledge, this work investigates the long-term stability of the solar system using various mathematical and numerical techniques while considering how various effects may be significant or relevant.

1.1 Brief Historical Overview

From antiquity, it has been known that the planets are not fixed in the firmament. Indeed, the name "*planet*" comes from the Greek "$\pi\lambda\alpha\nu\acute{\eta}\tau\eta\sigma$" (wanderer). Thus, these objects wander the sky, but always within the zodiac—an 18°–wide strip of sky centred on the ecliptic[1] (Jacobsen, 1999). However, the seemingly regular motion of the planets remained puzzling for centuries, even to the greatest philosophers, due to the planet's occasionally observed retrograde motion. Eventually, through dedicated observation and computation, Ptolemy was able to make precise predictions (within a sixth of a degree) using a system of epicycles (Babb, 1977). Even though Ptolemy also observed deviations between the mean and observed longitudes of the planets, finding larger discrepancies at perigee[2] (Jacobsen, 1999), Ptolemy's predictions were the most accurate of all his contemporaries. Because of this unparalleled accuracy, Ptolemy's system of epicycles would be used for centuries to make predictions of the motion of the planets.

More than a millenium after Ptolemy, Copernicus developed a heliocentric model of the solar system—one of his many contributions to astronomy which also includes laying out the relative mean distance of the (known) planets from the Sun (to within 4 per cent). Through deep dedication and meticulous perseverance, Kepler took Tycho Brahe's extensive and precise observations and proved Copernicus' heliocentric model showing that the motion of Mars was, in fact, an ellipse with the

[1] The ecliptic is the path of the Sun across the sky; it is a great circle on the celestial sphere.
[2] This discrepancy was not understood at the time, but was later described by Kepler's second law.

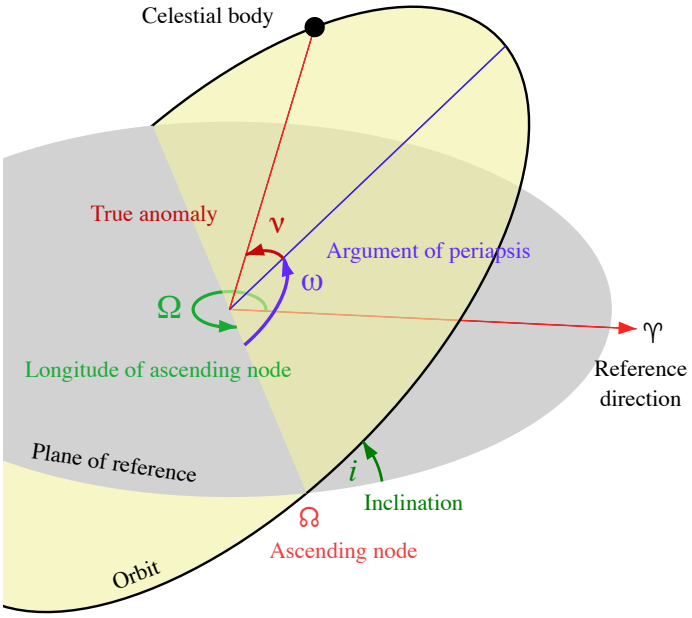

Figure 1.1: Illustration of the Keplerian orbital elements and their relation to the reference plane. Original work by Lucas Snyder (username Lasunncty) at the English Wikipedia (CC BY-SA 3.0).

Sun at one of the foci (Jacobsen, 1999). Kepler's work improved the accuracy of predictions of the motion of the planets by an order of magnitude (Gingerich, 1985). Through his work, Kepler gave three laws of orbital motion (Kepler, 1609, 1619; Kepler & Donahue, 1992; Kepler et al., 1997):

1. All planets move about the Sun in elliptical orbits, having the Sun as one of the foci.

2. A line drawn between a planet and the Sun sweeps out equal areas during equal time intervals.

3. The squares of the planets' orbital periods are directly proportional to the cubes of their mean distances from the Sun.

Proving the elliptical orbits of the planets provided a more complete visualization of their motion through space. In addition to the semi-major axis a and eccentricity e of an orbit, Fig. 1.1 shows the relationship of the remaining orbital elements established by Kepler. Namely, the inclination i with respect to a reference plane, the longitude of ascending node Ω, the argument of periapsis ω, and the true anomaly ν. While Kepler gave his own justifications for why the planets move as they do (Kepler, 1609; Kepler & Donahue, 1992), his reasons would soon be replaced by a groundbreaking new theory called gravity.

Building on the shoulders of giants, Isaac Newton developed three laws of motion[3] along with a universal theory of gravity: every object attracts every other object in the universe with a force proportional to the product of their masses and inversely proportional to the square of the distance between their centres (Newton, 1687; Newton et al., 1999). In modern scalar notation, the universal law of gravitation for two massive bodies m_1 and m_2 is written as

$$F = \frac{Gm_1m_2}{r^2}\,, \tag{1.1}$$

[3]First law: bodies remain at rest or in uniform motion in a straight line unless acted on by an external force. Second law: the acceleration of an object is equal to the ratio of an external force and its mass, $F = ma$. Third law: for every action (force) there is an equal and opposite reaction, $F_{12} = -F_{21}$.

where G is the universal constant of gravitation and r is the distance between the two bodies. With these laws, Newton was able to show that for two massive bodies, their orbits are ellipses with their mutual centre of mass at one of the foci. With this new formalism and a developing theory of infinitesimal calculus, significant improvements to the predictions of the locations of the planets could be made (Gingerich, 1985). The equations of motion describing the motion of N planets could be derived using Newton's second law, described in modern vector notation as

$$\ddot{\mathbf{r}}_i = \sum_{\substack{j=0 \\ j\neq i}}^{N} G m_j \frac{\mathbf{r}_j - \mathbf{r}_i}{|\mathbf{r}_j - \mathbf{r}_i|^3}, \tag{1.2}$$

for the i^{th} planet in the system with m_0 being the mass of the central body or Sun. Similarly, using Hamilton's formalism, the equations of motion could be derived from Hamilton's equations using, for example, the Hamiltonian defined in Jacobi coordinates. Writing the generalized positions and momenta as Q_i and P_i, Jacobi coordinates are referenced from the centre-of-mass of all interior particles, with $j < i$ (Rein & Tamayo, 2019). Thus, the Hamiltonian for the N-body problem can be written in Jacobi coordinates as

$$\mathcal{H} = \frac{P_0^2}{2M_N} + \sum_{i=1}^{N}\left(\frac{P_i^2 M_i}{2m_i M_{i-1}} - \frac{GM_{i-1}m_i}{Q_i}\right) + \sum_{i=1}^{N}\frac{GM_{i-1}m_i}{Q_i} - \sum_{i=0}^{N}\sum_{j=i+1}^{N}\frac{Gm_i m_j}{|\mathbf{r}_i - \mathbf{r}_j|}, \tag{1.3}$$

where $M_i = \sum_{j=0}^{i} m_j$. However, attempts to determine the general solution for the motion of the planets in a system with more than two bodies proved difficult even though an exact solution for describing the motion of two bodies under the mutual influence of gravity was known. Nevertheless, significant advancements to the emerging field of perturbation theory, by Laplace and Lagrange, enabled new insights into this intractable problem. Laplace and Lagrange's work on the long-term, or secular, evolution of the solar system laid out a theory for describing the slow variations in the orbital elements of the planets over thousands of years (Laplace, 1775, 1776; Lagrange, 1776, 1778, 1781, 1782, 1783a,b, 1784); see Laskar (2013) for a comprehensive historical review.

Laplace and Lagrange's secular description of the solar system averages over the mean motions of the planets and considers how weak interactions affect their long-term evolution[4]. This groundbreaking, linear, secular theory is a perturbation theory of first-order in the masses with a disturbing function of second-order in the eccentricities and inclinations. The linear, secular expansion exhibits no changes to the semi-major axes of the planets and shows only small changes to the eccentricities and inclinations, but not by an amount to allow for orbit crossing scenarios. The solutions contain the perihelion precession of planetary orbits as well as the precession of the ascending nodes of the planets, but fundamentally they are perfectly periodic. This initially seemed to *prove* that the solar system is dynamically stable for all time, but these successive approximations did not provide rigorous bounds to actually prove it analytically (Poincaré, 1898). When Le Verrier (1840, 1841) continued the perturbative expansion to higher order, significant terms emerged that make crucial corrections to the linear equations showing that the *linear* theory could not be used for an indefinite period of time. Subsequently, using the infinite series solution presented by Newcomb

[4]Consider the averaged motion of the planets as smeared out rings of mass along the planet's orbital paths. Laplace-Lagrange theory considers how the shapes (eccentricities) and relative inclinations of these rings change over time due to their mutual torques.

(1874), Poincaré (1899) went on to prove the impossibility of an analytical solution to multi-planetary dynamics over an infinite time interval.

Alongside these theoretical developments, improvements in astronomical observations with more advanced telescopes and measuring techniques led to new discrepancies between the predicted locations of the planets and their observed locations (Clerke, 1902; Mills et al., 1979; English, 2011). Most successfully, Le Verrier's work on deviations to the predicted orbit of Uranus eventually led to the prediction—and observational discovery—of Neptune (Clerke, 1902; Baum & Sheehan, 1997). This was a monumental achievement for Newton's theory of gravity, as quasi-periodic approximations were still the most accurate models at the time. However, observational evidence in the perihelion precession rate of Mercury indicated that additional non-Newtonian gravitational effects were yet unaccounted for (Le Verrier, 1845; Park et al., 2017). Attempts to explain this discrepancy were unsuccessful until the paradigm shift of general relativity (GR), introduced by Einstein (1915), further increased our understanding and ability to model the motion of the solar system precisely. As Einstein's equations were cumbersome and difficult to work with, post-Newtonian corrections derived from the equations of general relativity provided a simpler approach to more accurately model the discrepancies previously found through observation (Eddington, 1923).

Further mathematical developments by Kolmogorov (1954), Arnol'd (1963), and Möser (1962) (KAM) showed that for systems with a few degrees of freedom and in small regions around the initial conditions, the dynamical trajectories in phase space remain constrained to quasi-periodic solutions. However, these KAM toroidal regions are only isolating for systems with two degrees of freedom. As such, for systems with more degrees of freedom, like the solar system, these constrained regions overlap and allow trajectories to pass into chaotic regions and effectively diffuse through phase space (Laskar, 2013). With the aid of computer algebra systems, the integration of high-order secular expansions by Laskar (1985, 1986, 1988, 1989, 1990) showed that the inner solar system is indeed chaotic—not quasi-periodic. Thus, long-term predictions of the solar system are mathematically impossible. However, high-order, computer algebra–assisted expansions continue to reveal insights into the dynamical richness of the solar system unachievable by N-body integrations alone (Mogavero & Laskar, 2021, 2022; Hoang et al., 2022; Mogavero et al., 2023).

1.2 Computational Advances

Numerical integration techniques have been used from antiquity, going hand in hand with a desire to understand the motion of the planets (Ossendrijver, 2016). At a basic level, the idea of numerical integration is to closely estimate a definite integral. Often for differential equations describing a dynamical system, the objective of numerical integration is to transform the state variables of the system to approximate what state the system will be in after some amount of time (often called a timestep). In the limit of an infinitesimally small timestep, the expectation is that the numerical solution converges to the true solution. Euler's method (Euler, 1768) considers the position and velocity of a body as an initial value problem to determine the evolution of position and velocity over time[5]. Runge and Kutta set out to improve on the Euler's scheme by using the midpoint and trapezoidal rule (Runge, 1895; Kutta, 1901; Butcher, 1996). These improvements reduce the

[5]In 1980, high school student Abby Apsel discovered an improved, symplectic scheme when she accidentally swapped two lines of code during a class assignment (Cromer, 1981).

error associated with discretization, as can a sufficiently small timestep. Over short integrations, there is some tolerance for these errors that may result in artificial excitation or dampening, or the slow integration speeds that result from a small timestep (Yoshida, 1993). However, long-term integrations of planetary systems can require more than a trillion timesteps, making Runge–Kutta style integrators unsuited for simulating the time-evolution of planetary systems, even if they are modified to preserve the total energy and angular momentum of the system (Hairer et al., 2009; Ranocha & Ketcheson, 2020).

The advent of Hamiltonian mechanics opened new approaches and methods for studying dynamics and its applications to astronomy (Hamilton, 1833). Canonical transformations—a change of coordinates that preserve the form of Hamilton's equations—not only enabled new insights into celestial mechanics, such as those made by Delaunay, but also enabled the development of symplectic integrators (Tremaine, 2023). While it is not known who developed the first symplectic integrator[6] (De Vogelaere, 1956; Skeel & Cieśliński, 2020), symplectic integrators are canonical transformations and their time evolution is area-preserving in their canonical coordinates. Thus, for dynamical systems that can be described by a Hamiltonian, like the motion of the planets, symplectic integrators preserve multiple quantities (Donnelly & Rogers, 2005). While symplectic integrators do not conserve the energy directly, it has been shown that in most cases they oscillate around the conserved energy value (Tremaine, 2023). Every integrator type has a different set of trade-offs, but symplectic integrators do not suffer from unphysical changes to the semi-major axes, making them well suited for long-term integrations of the solar system.

There were many ventures to directly integrate the equations of motion for the (outer) solar system planets during the computing era when hardware was slow and storage was scarce, see Fig. 1.2 (Eckert et al., 1951; Cohen & Hubbard, 1965; Cohen et al., 1973; Feuchter, 1984; Newhall et al., 1983; Kinoshita & Nakai, 1984; Quinn et al., 1991). Closing that era, the two ultimate collaborations were the Digital Orrery[7] (Applegate et al., 1986) and LONGSTOP[8] (Roy et al., 1988). Their work focused on investigating the long-term stability of the outer planets[9] while also showing that the numerical error accumulation from long-term solar system integrations could be managed to provide meaningful and insightful results. Long-term integrations require managing both truncation error and round-off error; truncation error is due to substituting a continuously dynamical system with one represented by a finite difference model; round-off error is due to the mapping of real numbers to floating point numbers with a finite mantissa (Applegate et al., 1986; Roy et al., 1988). The LONGSTOP integrations used Encke's method, while not symplectic, utilizes conic section coordinates to describe the path of each planet while comparing to the real coordinates; when the discrepancy grows too large, the osculating orbit is rectified (Roy et al., 1988; Roy, 2004). The Digital Orrery used a combination of a fourth order Runge-Kutta scheme in combination with the Störmer method[10] (Applegate et al., 1986). Even though both of these collaborations were ground breaking in the direct integration of the equations of motion, their efforts to build a synthetic secular model of the solar system were quickly out-done by the work of Jacques Laskar.

[6] The leapfrog integrator is symplectic, ubiquitous, and can be traced back to Newton (1687) (see Hairer et al., 2006, for details).

[7] Applegate et al. (1986) commissioned a special purpose computer named the Digital Orrery.

[8] The **LON**g-term **G**ravitational **ST**udy of the **O**uter **P**lanets used a commercially available CRAY-1S computer.

[9] Both collaborations modelled the gas giants as point-mass particles with Pluto as a massless test particle. The Digital Orrery modelled the terrestrial planets by adding their masses to the mass of the Sun, while LONGSTOP modelled them as solar rings by extending the Sun's J_{20} moment.

[10] Störmer's method is a symplectic integration scheme equivalent to leapfrog or Verlet's method (Skeel, 1993).

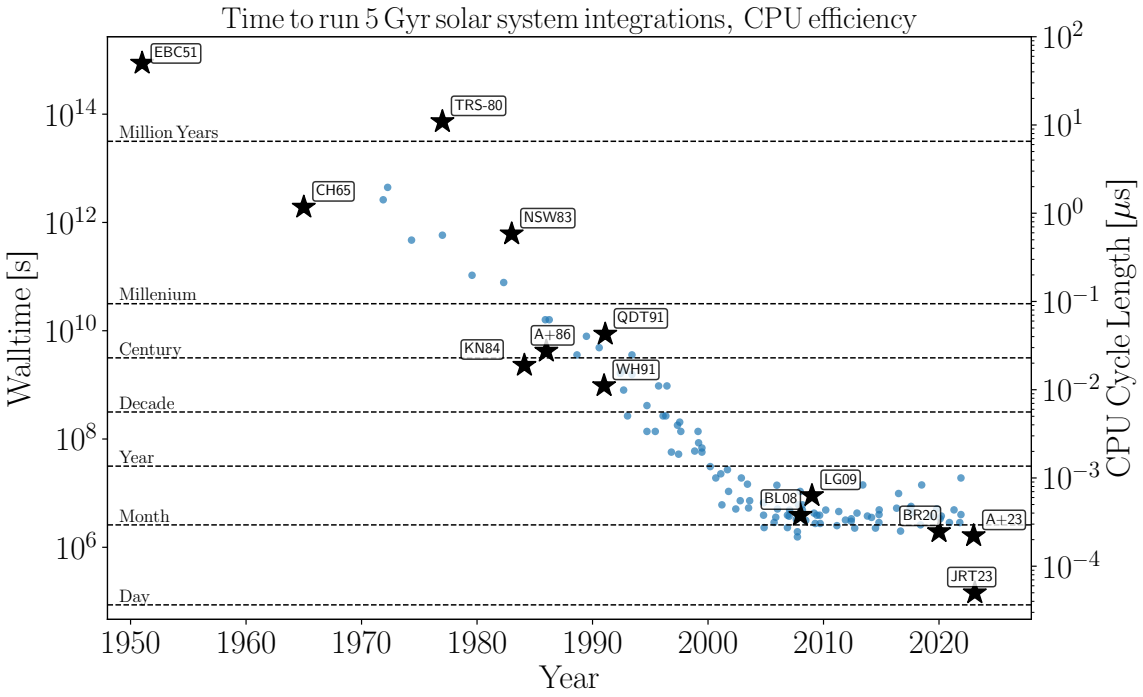

Figure 1.2: The history of solar system integration times (black stars) are overlaid with CPU processor speeds (blue circles). Advancements in integration times are a combination of both processor, algorithm, and implementation improvements. Data by Hadden (2023); Rupp (2020) with EBC51 (Eckert et al., 1951), CH65 (Cohen & Hubbard, 1965), TRS-80 (Feuchter, 1984), NSW83 (Newhall et al., 1983), KN84 (Kinoshita & Nakai, 1984), A+86 (Applegate et al., 1986), QTD91 (Quinn et al., 1991), WH91 (Wisdom & Holman, 1991), BL08 (Batygin & Laughlin, 2008), LG09 (Laskar & Gastineau, 2009), BR20 (Brown & Rein, 2020), A+23 (Abbot et al., 2023), and JRT23 (Javaheri et al., 2023).

The seminal work of Laskar (1985, 1986, 1988) was to build a secular model of all eight planets that is second-order in the masses and fifth-order in the eccentricities and inclinations, including the effects of the Moon and general relativity. This results in an expansion with 153824 polynomial terms. Using this model, Laskar (1989, 1990) not only showed that the motion of the solar system is chaotic[11], but also identified which overlapping secular resonances drive the chaos, something N-body integrations cannot do alone (Laskar et al., 1992; Sussman & Wisdom, 1992; Lithwick & Wu, 2011). These chaotic zones are sufficient to induce large variations in the secular dynamics of the inner solar system, seen specifically in the changes to the secular frequencies associated with Earth and Mars. The development of a modified Fourier transform (MFT) (Laskar, 1989, 1990, 1993, 2003; Šidlichovský & Nesvorný, 1996) to precisely identify frequency values[12] was essential to these discoveries and is fundamental to this work.

Shortly after Laskar's foundational work, a significant breakthrough in direct N-body integration was developed by Wisdom & Holman (1991). Enabled by the standard map for oscillating systems

[11]The chaos of the solar system was confirmed by direct integration (Sussman & Wisdom, 1992; Wisdom, 2018).

[12]The MFT (or frequency modified Fourier transform, FMFT) is an optimization algorithm that enables the determination of frequency values more precisely than a discrete Fourier transform (FFT). It does this by searching for a frequency value that maximizes the Fourier transform in a narrow region—typically in the vicinity of a frequency with a large amplitude given by the FFT.

(Chirikov, 1979), Wisdom and Holman (WH) devised an integrator that enabled an order of magnitude speed up over traditional integrators (Wisdom & Holman, 1991). The significant advancement of this second-order, symplectic integrator was to split the Hamiltonian of the planetary problem into a dominating, Kepler step and a perturbing, interaction step. This allows for larger timesteps by solving Kepler's equation to determine the arc of the planets along their orbital motion around the Sun, with adjustments from the planet-planet interactions. High-order correctors were developed to improve the accuracy of the integrations over longer integration times by reducing the truncation errors (Wisdom et al., 1996). Other symplectic integrators based on the WH scheme were developed, experimenting with different splitting techniques or approaches (Laskar & Robutel, 2001; Blanes et al., 2013); however, for the last few decades, the most significant advancements in wall-time came from improvements in CPU clock speeds. Additional improvements to integration times were made through implementation optimizations (Rein & Tamayo, 2015), with the fastest integrations of the solar system to date by Javaheri et al. (2023)[13] enabled by AVX512 instructions[14].

1.3 This Work

This work is made possible by the advancements in analytic and computational techniques developed over the past few centuries, along with an increase in computing availability. This work has been an effort to understand the dynamical life of the solar system, with a focus on flyby encounters. It is divided into three main parts that tell a story of the life and interconnected, long-term stability of the solar system.

First, Chapter 2 is an exploration into the origin of the secular modes of the solar system planets via a substellar flyby. For much of the history of astronomy, there has been an attempt to describe the motion of the planets. In some ways, the original expectations that planets move in perfect circles aligns with the modern expectations that planets emerge from protoplanetary disks in nearly perfectly circular and coplanar orbits. However, just as the eccentric and non-coplanar orbits of the planets posed a challenge to ancient astronomers, these modest deviations from expectations continue to puzzle astronomers today. Before this work, the prevailing hypothesis has been to invoke planet-planet interactions to explain the eccentricities and inclinations of the planets. The work in Chapter 2 differs by investigating the possibility of a substellar-mass flyby encounter as a plausible explanation for the origins of the secular mode amplitudes—with as high as a 1-in-1000 chance. These secular modes are fundamental to understanding the long-term stability of the solar system and this work offers a plausible explanation for their origin.

Second, Chapter 3 is an exploration into the role that general relativity plays in the long-term stability of the solar system. The main mechanism for dynamical instability in the solar system arises from a secular resonance between Mercury and Jupiter—specifically, a resonance between their perihelion precession rates manifest in the secular modes. This resonance rapidly increases the eccentricity of Mercury, significantly increasing the likelihood of a Mercury–Venus collision (this is considered a Mercury instability). Since the perihelion precession rate described by general relativity differs from the classical, Newtonian description and running full general relativistic simulations of

[13] Using `WHFast512` to integrate the solar system (the Sun and eight planets with general relativistic corrections) for 5 Gyr can be accurately achieved in 1 day! See Fig. 1.2.

[14] AVX512 are 512-bit extensions to the Advanced Vector Extensions SIMD instructions for x86 instruction set architecture and SIMD stands for single instruction, multiple data.

the solar system is unnecessarily burdensome, the inclusion of general relativistic corrections to Newtonian models is vital for accurate long-term integrations of the solar system. The work in Chapter 3 investigates the impact of general relativistic contributions on the long-term stability of the solar system showing that, one, general relativistic corrections are necessary for achieving accurate solar system simulations using Newtonian models, and two, the expected instability time of Mercury can be modelled using a Fokker–Planck, advection–diffusion model.

Third, Chapter 4 is an exploration into the impact of weakly interacting stellar flybys on the long-term stability of the solar system. Previous work has investigated the role of stellar flybys on the dynamics of planetary systems. However, little attention has been given to understanding how stellar encounters might affect the long-term stability of planetary systems—over the entire lifetime of the system, rather than a mere fraction of the lifetime. With an understanding that a secular resonance between Mercury and Jupiter is the main driver of instability in the solar system, the work in Chapter 4 undertakes to find a threshold of perturbation that results in a significant increase in instability. It is shown that changing the semi-major axis of Neptune by a relative amount more than 0.1 per cent increases the probability of destabilizing the solar system within 5 Gyr by one order of magnitude. While it is unlikely that the solar system will experience a flyby of this kind in the near future, this work shows that while the solar system is on the edge of stability, its stability is robust to perturbations below a specific threshold.

In addition to the three main parts of this work outlined here, this work also contributes to the development and accessibility of high-order symplectic integrators, see List of Works. This work shares in the development of a hybrid integration scheme, known as `MERCURIUS` (Rein et al., 2019). `MERCURIUS` utilizes a simplified switching scheme to handle close encounters between planets, something that the WH method fails to do as close encounters breaks the Kepler–Interaction splitting assumption. Additionally, this work assists in making publicly accessible a suite of high-order symplectic integrators using `REBOUND` (Rein & Liu, 2012). Specifically, while exploring the effect of high-order symplectic correctors on the accuracy of calculating the secular modes of the solar system (Rein et al., 2019a), this work led to an investigation into how different symplectic correctors impact the long-term precision of solar system integrations (Rein et al., 2019b). Furthermore, this work has produced `AIRBALL` (Brown et al., 2024), publicly available code for managing and simulating flyby encounters using `REBOUND`, see Appendix A.

Finally, Chapter 5 concludes by summarizing the most significant results of this work, along with suggestions for future exploration and investigation. As the study of the long-term stability of the solar system is rich with discoveries, efforts to understand the origins of the secular modes continue to reveal surprising and difficult to reconcile results. The various features of the solar system range from clear to complex. Placing the solar system in the context of the growing number of known exoplanet systems is also an area of active and ongoing research. Lastly, this work has been one small step towards understanding the solar system's place in the universe and it has been a privilege to share in that.

Chapter 2

On the origin of the secular modes

A version of the following chapter has been submitted for publication, overseen by Hanno Rein and Renu Malhotra. In this chapter, this work explores the effects of stellar and substellar flybys on the origins of the secular mode amplitudes of the solar system. Before this work, much effort had been given to investigating the secular mode amplitudes via planet-planet scattering. Additionally, much effort had been given to understanding the impact of stellar flybys on the dynamics of planetary systems. However, no work had yet undertaken to show the impact of substellar flybys on the solar system, especially as an attempt to explain the origins of the secular mode amplitudes. The novelty of this work is two fold. First, we invoke external perturbations to account for the solar system's secular modes. Secondly, we include the parameter space of substellar mass objects (down to Jupiter mass) and extremely close flyby distances, representing parameter regimes that have been overlooked in previous studies of flyby encounters of the solar system. Our results further show that there is about a 1-in-100 chance that such a flyby produces a dynamical architecture similar to that of the solar system offering a plausible explanation for the origin of the moderate eccentricities and inclinations of the planets.

Abstract

The modestly eccentric and non-coplanar orbits of the giant planets pose a challenge to solar system formation theories which generally indicate that the giant planets emerged from the protoplanetary disk in nearly perfectly circular and coplanar orbits. We demonstrate that a single encounter with a 2–50 Jupiter-mass object, passing through the solar system at a perihelion distance less than 20 AU and a hyperbolic excess velocity less than $6\,\mathrm{km\,s^{-1}}$, can excite the giant planets' eccentricities and mutual inclinations to values comparable to those observed. We estimate that there is about a 1-in-100 chance that such a flyby produces a dynamical architecture similar to that of the solar system. We describe a metric to evaluate how closely a simulated system matches the eccentricity and inclination secular modes of the solar system. The scenario of a close encounter with a substellar object offers a plausible explanation for the origin of the moderate eccentricities and inclinations and the secular architecture of the planets.

2.1 Introduction

Since antiquity, astronomers have sought to unravel the intricate patterns of planetary motion, refining their models over centuries to better align with empirical observations. In some ways, the historical expectations that planets move in perfect circles align with modern planet formation theories which suggest that planets emerge from protoplanetary disks in nearly circular and coplanar orbits (Goldreich & Tremaine, 1980; Artymowicz, 1992; Pollack et al., 1996; Lubow et al., 1999; Papaloizou et al., 2001; Ida & Lin, 2004; Kley & Nelson, 2012; Armitage, 2020). Consequently, the origin of the modestly eccentric and modestly non-coplanar orbits of the giant planets of the solar system has been an abiding puzzle (Tsiganis et al., 2005; Morbidelli et al., 2007; Nesvorný & Morbidelli, 2012; Raymond et al., 2020; Nesvorný, 2018; Clement et al., 2021; Griveaud et al., 2024). In this paper, we investigate external perturbations from flybys of stellar and substellar objects as a mechanism for the origins of the dynamical architecture of the planets.

As background to our investigation, we note that the present-day eccentricities and inclinations of the solar system planets are the instantaneous manifestations of their long-term variations under mutual planetary perturbations. In the linear approximation of the Laplace-Lagrange secular perturbation theory, these long-term (secular) variations of the eccentricities are separable from those of the inclinations, and both are approximated by the superposition of linear modes whose frequencies are determined by the planetary masses and semi-major axes (Brouwer & Clemence, 1961; Murray & Dermott, 1999; Tremaine, 2023). The secular modes and their long-term variations have been the subject of many studies as they are crucial for understanding the long-term dynamical stability of the solar system (Laskar, 1988, 1990, 1996; Ito & Tanikawa, 2002; Laskar & Gastineau, 2009; Zeebe, 2015; Mogavero & Laskar, 2021, 2022; Hoang et al., 2022) as well as the climate cycles of Earth (e.g. Laskar et al., 2004; Laskar et al., 2011). These studies show that the semi-major axes and the secular mode amplitudes of the planets are largely well preserved over billion-year timescales. Assuming that the giant planets' masses and orbital separations were largely determined by formation processes in the primordial protoplanetary disk (with only minor changes subsequently), one infers that the amplitudes of the eccentricity and inclination secular modes must originate from some form of internal or external perturbation in the ancient solar system, after planet formation. Possible internal perturbations include planet-planet interactions, either from scattering encounters or mean motion resonances; external perturbations include stellar flybys.

In our investigation of perturbations from flybys of stellar and substellar objects, we initially focus on the giant planets because their secular modes are nearly unaffected by the terrestrial planets (Laskar, 1990). Later we also include the terrestrial planets in our analysis. Previous studies to constrain possible signatures of stellar flyby events in the solar system's history have looked at the orbital configuration of the small bodies in the outer solar system (the Kuiper belt, Sednoids, and Oort Cloud) (Levison et al., 2004; Morbidelli & Levison, 2004; Kenyon & Bromley, 2004; Brasser et al., 2006; Adams, 2010; Huang & Gladman, 2024; Pfalzner et al., 2024), and the long-term stability of the solar system (Li & Adams, 2015; Li et al., 2019; Brown & Rein, 2022; Raymond et al., 2024). Indeed, significant effort has been undertaken to investigate the stability and dynamics of planetary systems in general within the context of stellar flyby encounters (Laughlin & Adams, 1998, 2000; Malmberg et al., 2007; Spurzem et al., 2009; Malmberg et al., 2011; Hao et al., 2013; Cai et al., 2017; Li et al., 2020; Schoettler & Owen, 2024, and references therein). However, none of these investigations consider both extremely close (periastron distance less than 20 AU) and substellar-

mass objects (masses less than $50\,M_J$) together in the Sun's primordial star cluster.

In this paper, we consider close encounters from a typical open star cluster environment using an initial mass function that includes sub-stellar objects with masses ranging between $10^{-3}\,M_\odot$ and $10^2\,M_\odot$. We focus on encounters with perihelia less than 20 AU of the Sun. Due to the closeness of the flybys, we run full N-body simulations rather than analytical estimates to accurately resolve the close encounters. In total, we simulate $5 \cdot 10^4$ flybys with the solar system giant planets initially on circular, coplanar orbits at their current semi-major axes.

We first describe the methods and our initial conditions in detail in Section 2.3. We then present the results of our simulations, including our best matching flyby and the bigger statistical picture in Section 2.4. Finally, we detail our conclusions in Section 2.5.

2.2 Introduction

Since antiquity, astronomers have sought to unravel the intricate patterns of planetary motion, refining their models over centuries to better align with empirical observations. In some ways, the historical expectations that planets move in perfect circles align with modern planet formation theories which suggest that planets emerge from protoplanetary disks in nearly circular and coplanar orbits (Goldreich & Tremaine, 1980; Artymowicz, 1992; Pollack et al., 1996; Lubow et al., 1999; Papaloizou et al., 2001; Ida & Lin, 2004; Kley & Nelson, 2012; Armitage, 2020). Consequently, the origin of the modestly eccentric and modestly non-coplanar orbits of the giant planets of the solar system has been an abiding puzzle (Tsiganis et al., 2005; Morbidelli et al., 2007; Nesvorný & Morbidelli, 2012; Raymond et al., 2020; Nesvorný, 2018; Clement et al., 2021; Griveaud et al., 2024). In this paper, we investigate external perturbations from flybys of stellar and substellar objects as a mechanism for the origins of the dynamical architecture of the planets.

As background to our investigation, we note that the present-day eccentricities and inclinations of the solar system planets are the instantaneous manifestations of their long-term variations under mutual planetary perturbations. In the linear approximation of the Laplace-Lagrange secular perturbation theory, these long-term (secular) variations of the eccentricities are separable from those of the inclinations, and both are approximated by the superposition of linear modes whose frequencies are determined by the planetary masses and semi-major axes (Brouwer & Clemence, 1961; Murray & Dermott, 1999; Tremaine, 2023). The secular modes and their long-term variations have been the subject of many studies as they are crucial for understanding the long-term dynamical stability of the solar system (Laskar, 1988, 1990, 1996; Ito & Tanikawa, 2002; Laskar & Gastineau, 2009; Zeebe, 2015; Mogavero & Laskar, 2021, 2022; Hoang et al., 2022) as well as the climate cycles of Earth (e.g. Laskar et al., 2004; Laskar et al., 2011). These studies show that the semi-major axes and the secular mode amplitudes of the planets are largely well preserved over billion-year timescales. Assuming that the giant planets' masses and orbital separations were largely determined by formation processes in the primordial protoplanetary disk (with only minor changes subsequently), one infers that the amplitudes of the eccentricity and inclination secular modes must originate from some form of internal or external perturbation in the ancient solar system, after planet formation. Possible internal perturbations include planet-planet interactions, either from scattering encounters or mean motion resonances; external perturbations include stellar flybys.

In our investigation of perturbations from flybys of stellar and substellar objects, we initially

focus on the giant planets because their secular modes are nearly unaffected by the terrestrial planets (Laskar, 1990). Later we also include the terrestrial planets in our analysis. Previous studies to constrain possible signatures of stellar flyby events in the solar system's history have looked at the orbital configuration of the small bodies in the outer solar system (the Kuiper belt, Sednoids, and Oort Cloud) (Levison et al., 2004; Morbidelli & Levison, 2004; Kenyon & Bromley, 2004; Brasser et al., 2006; Adams, 2010; Huang & Gladman, 2024; Pfalzner et al., 2024), and the long-term stability of the solar system (Li & Adams, 2015; Li et al., 2019; Brown & Rein, 2022; Raymond et al., 2024). Indeed, significant effort has been undertaken to investigate the stability and dynamics of planetary systems in general within the context of stellar flyby encounters (Laughlin & Adams, 1998, 2000; Malmberg et al., 2007; Spurzem et al., 2009; Malmberg et al., 2011; Hao et al., 2013; Cai et al., 2017; Li et al., 2020; Schoettler & Owen, 2024, and references therein). However, none of these investigations consider both extremely close (periastron distance less than 20 AU) and substellar-mass objects (masses less than $50\,\mathrm{M_J}$) together in the Sun's primordial star cluster.

In this paper, we consider close encounters from a typical open star cluster environment using an initial mass function that includes sub-stellar objects with masses ranging between $10^{-3}\,\mathrm{M_\odot}$ and $10^{2}\,\mathrm{M_\odot}$. We focus on encounters with perihelia less than 20 AU of the Sun. Due to the closeness of the flybys, we run full N-body simulations rather than analytical estimates to accurately resolve the close encounters. In total, we simulate $5 \cdot 10^4$ flybys with the solar system giant planets initially on circular, coplanar orbits at their current semi-major axes.

We first describe the methods and our initial conditions in detail in Section 2.3. We then present the results of our simulations, including our best matching flyby and the bigger statistical picture in Section 2.4. Finally, we detail our conclusions in Section 2.5.

2.3 Methods

2.3.1 Stellar Environment

We use a Monte Carlo approach to investigate the impact of various flybys on the solar system by simulating $5 \cdot 10^4$ flyby objects from an open star cluster environment with a mass density of $n = 100\,\mathrm{M_\odot\,pc^{-3}}$. For each flyby, we sample a mass, velocity, and impact parameter along with a random orientation centered on the Sun (Zink et al., 2020). The initial mass function (IMF) we use to generate the flyby masses $m_\star$ is the Maschberger IMF (Maschberger, 2013) which smoothly combines a log-normal IMF for single stars (Chabrier, 2003) with masses less than one solar mass and the standard power-law IMF (Salpeter, 1955) for masses above one solar mass. Our full IMF contains objects with masses ranging from $10^{-3}\,\mathrm{M_\odot}$ to $10^{2}\,\mathrm{M_\odot}$ and a median object mass of about $80\,\mathrm{M_J}$. We note that extending of the stellar IMF well into the substellar regime is somewhat uncertain but is consistent with microlensing observations (Chabrier & Lenoble, 2023). We sample hyperbolic excess velocities v_∞ from a Maxwell-Boltzmann distribution with a velocity dispersion of $1\,\mathrm{km\,s^{-1}}$ (Girard et al., 1989; Adams, 2010). We sample impact parameters $b_\star$ to uniformly cover the cross-sectional area out to 75 AU. Gravitational focusing (Binney & Tremaine, 2008) naturally gives a perihelion which is less than the impact parameter with the host star. For our simulations, all perihelia come within 55 AU with 90% coming within 20 AU. We sample the incident angles isotropically to allow for all possible encounter geometries. We initialize the solar system with the

four giant planets on circular and coplanar orbits at their current semi-major axes, and randomly initialize their true anomalies.

2.3.2 Integration Methods

We use the open-source N-body integrator `REBOUND` (Rein & Liu, 2012) along with `AIRBALL` (Brown et al., 2024), a python package for setting up and running simulations of flybys. We use the `IAS15` (Rein & Spiegel, 2015) integrator (with the improved criteria for the timestep presented by Pham et al. 2024) to integrate the flyby in a heliocentric reference frame starting at a distance of 10^5 AU which is on the order of the Sun's current Hill sphere with the Galaxy (Pham & Rein, 2024). When the flyby object has receded to a distance of 10^5 AU, we remove it from the simulation, and then propagate the planetary system for another 20 Myr using the `WHCKL` or `WHFast512` integrators (Rein et al., 2019b; Javaheri et al., 2023) depending on whether we are integrating the giant planets or all eight planets respectively.

For each flyby system that did not experience any planetary ejections, we then compute the power spectra of the complex eccentricities and complex inclinations of the planets and compare those to the solar system using the log-spectral distance metric (see below).

2.3.3 Metric for secular architectures

For the purpose of comparing the similarity of two systems, the approximately conserved quantity of the angular momentum deficit (AMD) (Laskar, 1997, 2000; Turrini et al., 2020) is not a good measure because the AMD can be dominated by a single planet—a common result of flyby encounters. A comparison of the instantaneous eccentricities and inclinations alone is insufficient when comparing the dynamical architectures of two systems because these represent only a snapshot of the time evolution of a system and not the overall structure. Even measuring the minimum-to-maximum range of the eccentricities and inclinations of each of the planets is insufficient because it does not measure the distribution of power spread across different secular modes. Measuring the closeness of the secular modes using their frequencies and amplitudes is also not straightforward because of the many degrees of freedom. We also would like to include the long-term variations of the secular modes, since secular modes are merely the linearized approximation of an inherently non-linear system. All the above reasons motivate us to develop a new metric which measures the distance of a simulated system from the real solar system without making any initial assumptions regarding their dynamical structure or architecture.

Let us start by defining the root-mean-square log-spectral distance (Gray & Markel, 1976; Rabiner & Juang, 1993) which compares the power spectra of two signals to evaluate the similarity of the amplitudes for each frequency as

$$\mathcal{D}(X, \hat{X}) = \sqrt{\frac{1}{N} \sum_{k=1}^{N} \left(\log_{10} |X_k| - \log_{10} |\hat{X}_k| \right)^2} \tag{2.1}$$

where X_k and $\hat{X}_k$ are the complex-valued, discrete Fourier transforms (FFT) for the k^{th} frequency of the two signals being compared. We make sure that the two signals are identical in length and sample spacing so that the amplitudes from the same frequencies are being compared. This

distance measure $\mathcal{D}$ also satisfies the properties of a metric, i.e. it satisfies the triangle inequality, is symmetric, and when $\mathcal{D} = 0$ there is a perfect match between the power spectra. This can also be interpreted such that if the average ratio between the two spectra is 10^p, i.e. $\hat{X} = 10^p X$, then $\mathcal{D}(X, \hat{X}) = \mathcal{D}(X, 10^p\, X) = \mathcal{D}(X, 10^{-p}\, X) = p$.

When we apply this distance measure to build a metric we equally consider it using the time evolution of both the complex eccentricities and inclinations of two systems. The complex eccentricities and inclinations of a secular system for a given planet j are defined as (Laskar, 1990)

$$z_j = e_j \exp\left(\mathtt{i}\varpi_j\right) \tag{2.2}$$

and

$$\zeta_j = \sin(i_j/2) \exp\left(\mathtt{i}\Omega_j\right) \tag{2.3}$$

where e_j is the eccentricity, i_j is the inclination with respect to the invariant plane, Ω_j is the longitude of the ascending node, $\varpi_j = \omega_j + \Omega_j$ is the longitude of the periapsis, ω_j is the argument of the periapsis, and $\mathtt{i} = \sqrt{-1}$. We sample these values on evenly spaced time intervals over 20 Myr integrations with $N = 2^{11}$ samples to then process with an FFT. We use $\mathcal{D}$ in equation (2.1) to build a metric that evenly weighs the signals of the complex eccentricities and complex inclinations for each planet. We define our metric as

$$\mathcal{M} = \frac{1}{2n} \sum_{j=1}^{n} \left(\mathcal{D}(\mathcal{F}[z_j], \mathcal{F}[\hat{z}_j]) + \mathcal{D}(\mathcal{F}[\zeta_j], \mathcal{F}[\hat{\zeta}_j]) \right) , \tag{2.4}$$

comparing one system (identified using a hat) with n planets to another system with n planets, where $\mathcal{F}[\cdot]$ is the discrete Fourier transform. Thus, $\mathcal{M}$ is the averaged values given by $\mathcal{D}$ over the FFTs of the complex eccentricities and inclinations of all the planets.

2.3.4 Reference Systems

In order to make a fair comparison between the flyby systems and the observed solar system, we use a reference set of solar system realizations from an ensemble of integrations (Brown & Rein, 2020). This ensures that our reference set representing the solar system's secular architecture samples not just one single 20 Myr realization but also samples the effect of uncertainties of the initial conditions and of the small changes in the solar system's secular modes over long times, both of which arise from nonlinear effects. Indeed, the secular mode frequencies of the giant planets change by at most $15\,\mathrm{mas\,yr^{-1}}$ and their amplitudes vary by at most $9.5 \cdot 10^{-4}$ over billions of years.

We start with the nominal initial conditions that are identical to what we see today using NASA's Jet Propulsion Laboratory (JPL) Horizons data at the J2000 epoch. Our solar system ensemble uses these nominal initial conditions that are identical in every way except for a small variation ($< 0.5\,\mathrm{m}$) in the semi-major axis of Mercury from the present-day value (see Brown & Rein 2020 for more details). We use all 96 of the 5 Gyr solar system simulations and divide them into 20 Myr non-overlapping segments from which we sample the complex eccentricities and inclinations to process with our metric.

Using the metric $\mathcal{M}$ and this set of 20 Myr segments from our reference solar system ensemble, we cross compare each segment of a random subset of 2500 segments against another randomly

selected subset of 2500 segments to compute the distribution of values. This distribution of values of $\mathcal{M}$ quantifies how similar the solar system is to itself at different times and with slightly different initial conditions (within observational uncertainties). The range of values given by $\mathcal{M}$ for this cross comparison of the solar system are between 0 and 0.434.

We want to determine the similarity of each post-flyby system to the solar system. To do that, we compare each post-flyby system to every 20 Myr segment of our full solar system ensemble. This yields a distribution of values of the metric $\mathcal{M}$ for the simulated systems compared to the solar system. We can then compare this distribution to the distribution we obtain for the solar system compared to itself.

We found that this procedure provides a clear way of evaluating how close two systems are to each other and, most importantly, allows us to sort and rank them in closeness. More over, this procedure avoids over-fitting to a specific manifestation of the solar system's long and diverse dynamical evolution. What is not immediately clear is how to define the cutoff that determines if a given system is considered to be a *close match* to the solar system or not. For the present study, we define any flyby system with a metric value that overlaps with the reference solar system distribution as a *close match* to the solar system. However, we acknowledge that this choice is somewhat arbitrary and comes with several caveats. Note that the maximum value of $\mathcal{M}$ could be limited by the ensemble size. Our ensemble size is large, $2500^2 > 6 \cdot 10^6$, so we don't expect this to be important in practice. However, there exists the rare possibility that a solar system trajectory will eventually go unstable, for example with a Mercury–Venus collision (Laskar et al., 2004). The closer we get to such an instability, the more the trajectory diverges from what is a more 'typical' realization of the solar system. Such a divergent trajectory will cause the range of metric values to increase significantly above the typical range and thus lead to more *closely matching* flyby simulations. However, if there aren't any significantly divergent trajectories (as is the case with our solar system ensemble, see Brown & Rein 2020), then to use anything less than the entire range of the metric would be to claim that the solar system is not a close match to itself. In summary, although it may be possible to find a better metric, the definition of what is considered a *close match* to the solar system will likely always be subject to some reasonable but arbitrary quantitative choices.

2.4 Results and Discussion

2.4.1 Best Match

For each flyby simulation, we calculate the power spectrum of the complex eccentricities and inclinations over 20 Myr and compute its value of $\mathcal{M}$ relative to all the solar system power spectra. Of the $5 \cdot 10^4$ simulated flybys, we found 422 cases (approximately 1%) that lie within the range of the solar system's own $\mathcal{M}$ values. As we described above, we consider these to be a *close match* to the orbital architecture of our solar system.

Fig. 2.1a visualizes the encounter that produces the best match to the solar system's secular architecture according to our metric. In this case, the flyby object has a mass of $m_\star = 8.27\,\mathrm{M_J}$, a perihelion of $q_\star = 1.69\,\mathrm{AU}$, a hyperbolic excess velocity of $v_\infty = 2.69\,\mathrm{km\,s^{-1}}$, and an inclination of $i_\star = 131°$ with respect to the initial common plane of the planets. Fig. 2.1b shows the time evolution of the semi-major axes a of the giant planets along with the perihelia q, aphelia Q, and inclinations

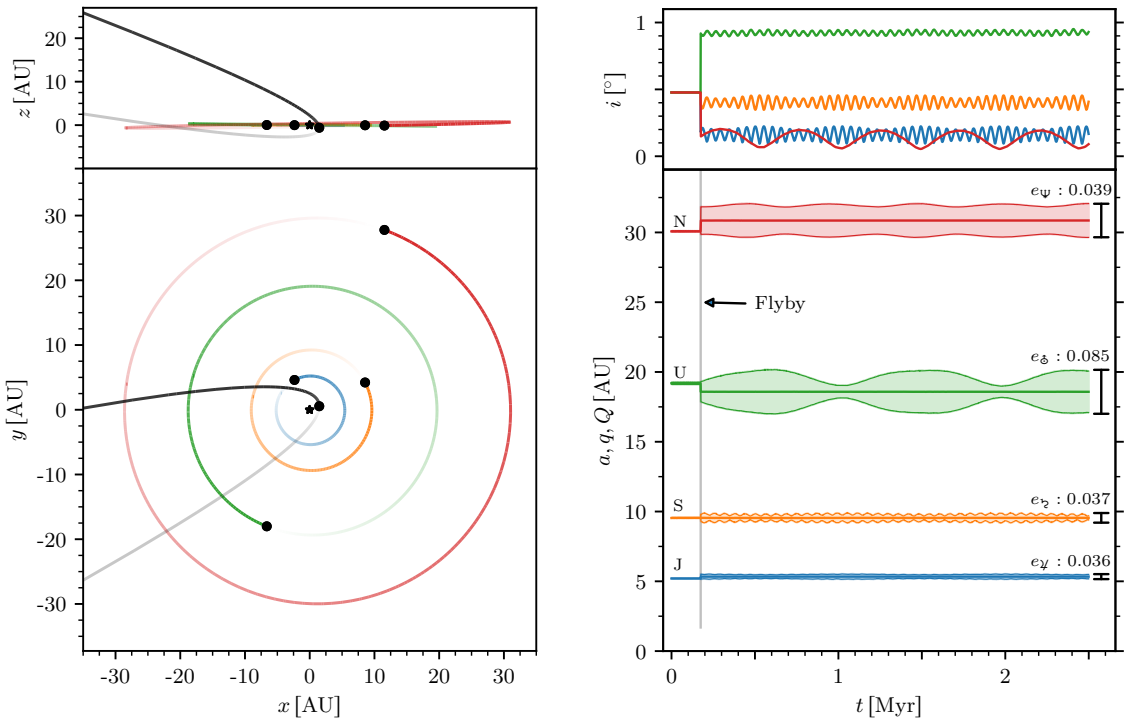

(a) (b)

Figure 2.1: **(a)** A snapshot of the flyby simulation that produces the best match to the solar system. The flyby parameters for the encounter are $m_\star = 8.27\,\mathrm{M_J}$, $q_\star = 1.69\,\mathrm{AU}$, $v_\infty = 2.69\,\mathrm{km\,s^{-1}}$, and $i_\star = 131°$. **(b)** The time evolution of the giant planets before, during, and after the flyby shown on the left. The encounter time is indicated by the vertical line at $t \approx 0.2\,\mathrm{Myr}$. The upper panel shows the inclination of the planets (with respect the the final invariant plane) while the lower panel shows the semi-major axes, the perihelia, aphelia distances. The maximum eccentricity range of each planet is also indicated.

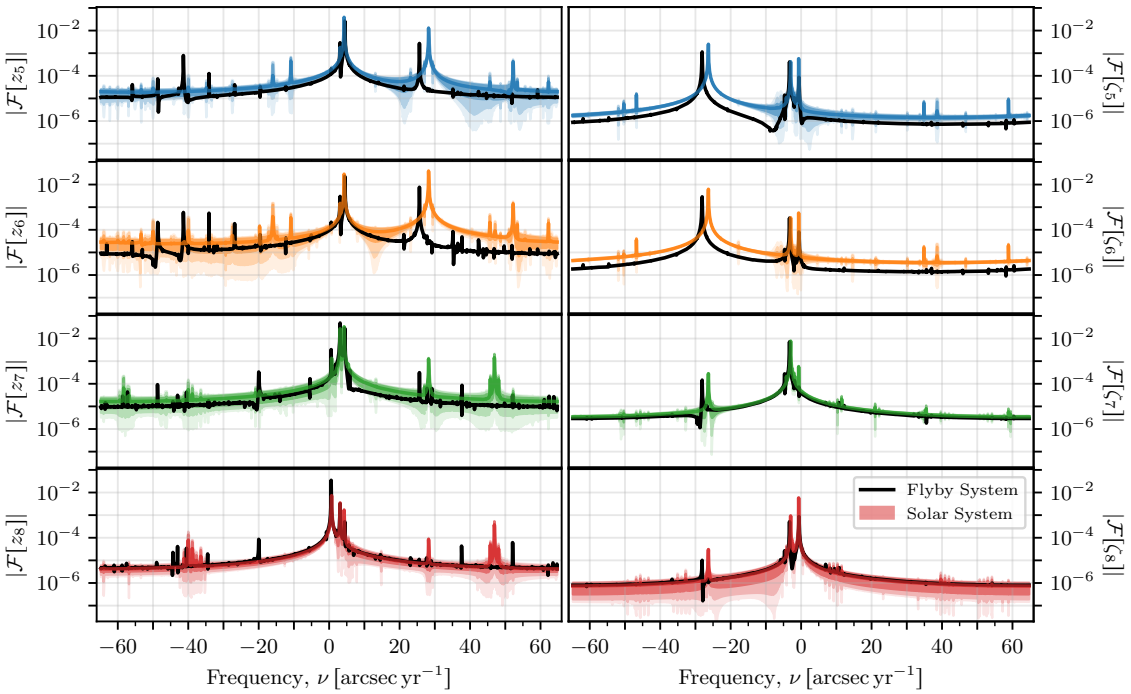

Figure 2.2: Power spectra of the complex eccentricities (left column) and complex inclinations (right column). The black line shows the best matching flyby case (as in Figures 2.1a and 2.1b), while the color-shaded plots show the ensemble of spectra of the solar system taken in 20 Myr–long segments from an ensemble of 5 Gyr–long integrations. The median power at each frequency of the solar system ensemble is shown as a dark coloured line, with lighter shaded regions representing the first three standard deviation percentiles. The median power spectrum of the solar system is very similar to the simulated best case flyby.

i of the giant planets before, during, and after the flyby encounter. The maximum eccentricities for each planet are indicated on the right.

Fig. 2.2 shows the power spectra from the FFTs of the complex eccentricities and complex inclinations for the best matching flyby system (black line) overlaid with the ensemble of power spectra of the solar system. In order to see how a particular flyby system compares to the spectral variation present in the true solar system, we determine the spread in the power for each frequency of the FFTs using the reference set of solar system integrations marking the median and the first three standard deviation percentiles. The peaks in these spectra correspond to the frequencies of the secular modes (Laskar, 1988, 1990, 1993; Šidlichovský & Nesvorný, 1996; Laskar, 2003). One can see that the amplitudes of the secular modes of the giant planets have been excited with a single flyby event to values similar to those of the real solar system.

Table 2.1 provides a more quantitative comparison between the present-day Laplace–Lagrange secular modes of the giant planets and the best matching flyby simulation. For the four giant planets, there are four mode frequencies in the complex eccentricities, traditionally denoted as g_5, g_6, g_7, g_8, and three in the complex inclinations, s_6, s_7, s_8 (Brouwer & Clemence, 1961). Table 2.1 shows that all the linear secular mode frequencies of the flyby system are a close match with those of the solar system. This follows from the circumstance that the best matching flyby only mildly disturbs the semi-major axes of the planets: by +2.6%, −0.03%, −3.2%, and +2.6% for Jupiter, Saturn, Uranus,

Mode	Freq. [arcsec yr^{-1}] SS	Flyby	Amp. $\lvert A\rvert \cdot 10^3$ SS	Flyby
g_5	4.26	4.44	44.17	28.76
g_6	28.25	25.62	48.21	7.91
g_7	3.09	3.08	29.03	54.31
g_8	0.67	0.56	9.14	35.11
s_5	$--$	$--$	$--$	$--$
s_6	-26.35	-28.12	7.85	3.50
s_7	-2.99	-3.31	8.87	8.02
s_8	-0.69	-0.61	5.81	1.20

Table 2.1: A comparison of the secular frequencies and amplitudes of the giant planets (SS) and our best matching flyby system that experienced a $m_\star = 8.27\,\mathrm{M_J}$ encounter at $q_\star = 1.69\,\mathrm{AU}$, with $v_\infty = 2.69\,\mathrm{km\,s^{-1}}$. By convention, s_5 is the null frequency when inclinations are designated with respect to the invariant plane.

and Neptune respectively. (Recall that the linear mode frequencies depend only upon the semi-major axes and masses.) We also see in Table 2.1 that the mode amplitudes of the best matching flyby system have magnitudes of a few hundredths in the eccentricity modes and a few thousandths in the inclination modes. While similar in order-of-magnitude to those of the solar system, they differ in detail. The amplitudes of the inclination modes are a closer match than those of the eccentricity modes.

In particular, it has been recognized for some time that it is most challenging to excite the amplitude of the g_5 mode to values similar to the observed value by any of a number of plausible mechanisms considered in previous studies (Nesvorný & Morbidelli, 2012; Griveaud et al., 2024). This is because the g_5 mode dominates Jupiter's orbit. As Jupiter has the largest planetary mass in the solar system, it is consequently the most resistant to orbital perturbations. In that light, note that in the best matching flyby case, we find that the amplitude of the g_5 mode is about 65% that of the present-day solar system. Overall, we find that in 40% of the 422 *closely matching* flyby systems, the amplitude of the g_5 mode is within a factor of two of the solar system's. This is a notable success of the substellar flybys as a mechanism to explain the secular mode amplitudes.

For the g_6 mode, there is mismatch in Table 2.1 as the amplitude of this mode in the best matching flyby simulation is much smaller than in the present-day solar system. We do not consider this significant because our simulations include other *close matching* flyby systems that are more similar in the g_6 mode amplitude than our best matching case (though less similar in other ways), while still being close matches with the range of the solar system's power spectrum over billion-year timescales.

2.4.2 Inner Solar System

Because many of the *closely matching* systems experience flybys at perihelion distances in the region of the terrestrial planets, we simulate an additional 10^4 circular, coplanar systems. We use the exact same initial conditions for the giant planets and the exact same flyby event as shown in Figs. 2.1a and 2.1b, but include the terrestrial planets at their current average semi-major axes, also on circular, coplanar orbits but with random phases, as well as the effect of general relativity

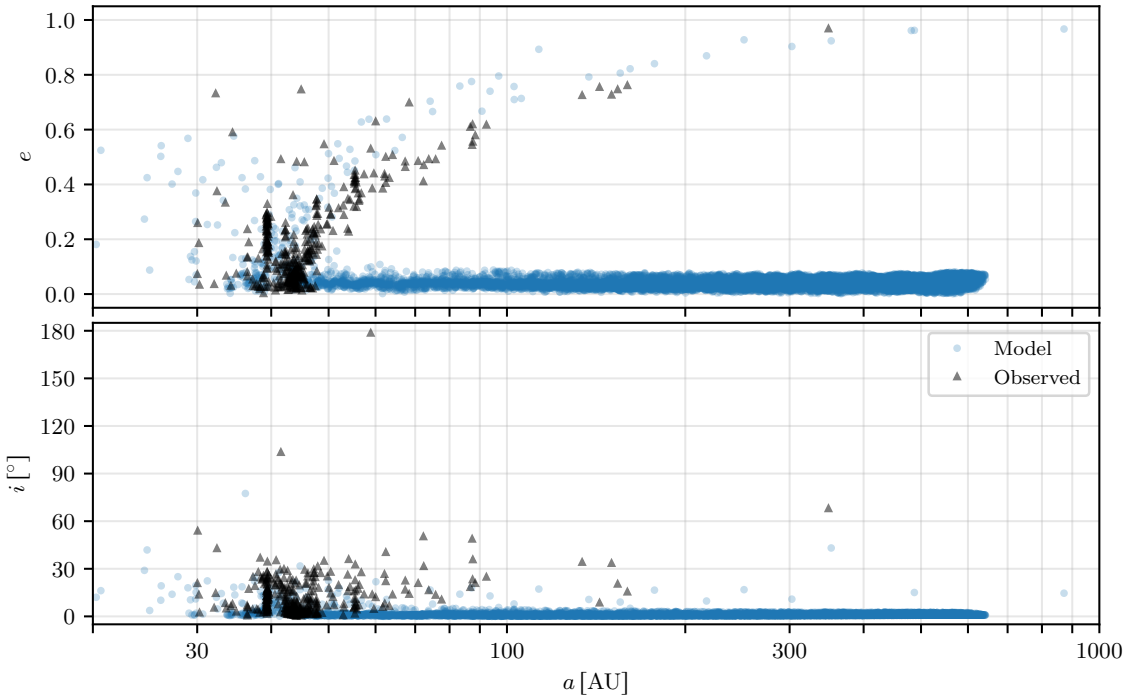

Figure 2.3: We show here the impact of our best matching flyby on the cold, classical Kuiper Belt. We preliminarily find that the best matching flyby does *not* over-excite the cold, classical Kuiper Belt, but rather produces features similar to those observed in the solar system. The top panel shows the distribution of eccentricities with respect to their semi-major axes and the lower panel similarly shows the distribution of inclinations.

(Brown & Rein, 2023). The terrestrial planets are initialized on circular coplanar orbits with their present day semi-major axes. We use a hybrid flyby method that utilizes `WHCKL` until the flyby object is about 3000 AU away before switching to `IAS15` until the flyby object returns to 3000 AU before switching back to `WHCKL`. We find this manual hybrid approach offers a good balance between accuracy and efficiency. After the flyby object is removed at 10^5 AU, we employ the `WHFast512` (Javaheri et al., 2023) integrator and simulate the solar system with general relativistic corrections for an additional 20 Myr.

Remarkably, in the majority of cases we roughly reproduce the secular modes and amplitudes of the entire solar system. In these simulations, we find that within the first 20 Myr following the flyby encounter, only 2% of cases result in an ejected planet, with 4% having at least one planet that reaches an eccentricity greater than 0.6. However, it becomes more difficult to make a specific claim of similarity because there are even more degrees of freedom and larger range of variation, particularly in the power spectra of the terrestrial planets.

2.4.3 Kuiper Belt

Any flyby that overexcites the cold, classical Kuiper Belt would not be consistent with the observed solar system, so it is important to understand how much of an impact the flyby will have on this region of the solar system. As such, we also briefly investigated the effect that the best matching flyby would have on the Kuiper Belt since we expect some disturbance to the cold, classical Kuiper

Belt from a substellar flyby. We simulate the Kuiper Belt using 12,000 test particles initialized on perfectly circular, coplanar orbits, with uniformly random true anomalies, and with semi-major axes uniformly distributed from 30 AU – 600 AU. We preliminarily find that the best matching flyby does *not* over-excite the cold, classical Kuiper Belt, see Fig. 2.3. Actually, in the scatter comparison between semi-major axis and eccentricity or inclination, as shown in Fig. 2.3, there are some similarities between the observed Kuiper Belt objects and the resulting test particles. However, significantly more work needs to be done in order to make full comparisons between the distributions of observed Kuiper Belt objects and the test particles in our simulation. The most notable difference is the remaining extended disk in our simulation and whether or not that extended disk is present in the solar system. Additional work needs to be considered to understand the impact of the best matching flyby on all the various populations of Kuiper Belt objects, such as the scattered disk objects and the resonant populations.

2.4.4 Probabilities

The standard estimation for the flyby encounter rate considers the average of the product of the spatial number density n, the average relative velocity v, and the cross-sectional area σ (Adams, 2010), $\Gamma = \langle n v \sigma \rangle$. Assuming these variables are uncorrelated, the typical approach is to approximate the average of the product with the product of the averages. For a given object density (mass density divided by median mass) and average velocity, the difference in flyby rates depends on the chosen cross-sectional area. With our adopted parameters, we find $\Gamma \approx 10^{-3}\,\mathrm{Myr}^{-1}$. Given that it is estimated that the solar system formed in an open star cluster that dispersed over a timescale of 10–100 Myr (van den Bergh, 1981; Elmegreen & Clemens, 1985; Battinelli & Capuzzo-Dolcetta, 1991; Adams & Myers, 2001; Lada & Lada, 2003; Adams, 2010; Pfalzner, 2013), for a flyby with $b_\star \leq 75\,\mathrm{AU}$ and $m_\star \geq 1\,\mathrm{M_J}$ there is a 1-in-100 chance of a flyby within 10 Myr and a 1-in-10 chance of a flyby within 100 Myr (assuming the density remains constant). This occurrence probability for extremely close encounters may seem surprising compared with previous work that have investigated stellar flybys of the solar system (Jiménez-Torres et al., 2013; Pfalzner et al., 2018; Pfalzner & Vincke, 2020; Batygin et al., 2020; Brown & Rein, 2022). The reason for this significant probability is primarily because of the large population of substellar and super-Jovian mass objects estimated in our implementation of the Maschberger IMF which extends the Chabrier 2003 stellar IMF into the substellar regime (Maschberger, 2013). This extension of the stellar IMF well below the substellar regime is consistent with microlensing observations. However, we note that considerable uncertainties exist in the abundance of super-Jovian and Brown Dwarf objects that form via the same mechanism as stars (Chabrier & Lenoble, 2023) which may affect these probabilistic estimates.

As discussed above, our simulations show that, starting with initially coplanar and circular orbits, approximately 1% of such close flybys result in secular mode amplitudes similar to those of the real solar system. Thus, the overall probability of the solar system acquiring its current dynamical state via a close encounter with a substellar object is roughly 1 in 10^4 (becoming as likely as 1 in 10^3). Fig. 2.4 shows the encounter parameters of all the flyby objects drawn from our cluster parameters, highlighting in blue the *close matches* to the solar system. See also Fig. 2.6 which shows all flyby parameters. From here, we can see that the *closest matching* simulations result from flybys are those with substellar masses ($m_\star < 50\,\mathrm{M_J}$) and pass between the orbits of Mercury and Uranus ($\sim 0.4 < q_\star < 20\,\mathrm{AU}$ from the Sun). For typical velocities within an open star cluster, extremely

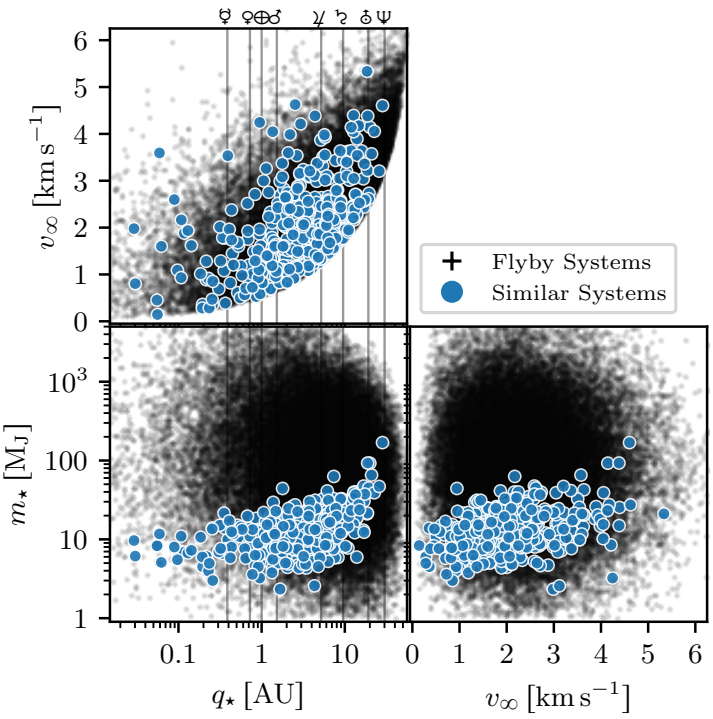

Figure 2.4: Here we show the distributions of the flyby parameters ($m_\star$, $q_\star$, v_∞) in our simulations as well as the subset of those parameters that led to a *close match* with the solar system. We highlight in blue the flyby systems that are similar to the solar system when compared to itself.

close flybys ($q_\star < 50\,\mathrm{AU}$) with stellar masses ($m_\star > 80\,\mathrm{M_J}$) almost always result in ejected planets or over-excited secular modes. About 60% of our $5 \cdot 10^4$ simulations had at least one ejected planet in the first 20 Myr. Stellar mass flybys at greater distances are much less likely to eject a planet, but are also unable to sufficiently excite the eccentricity modes, particularly Jupiter's eccentricity (Nesvorný & Morbidelli, 2012; Griveaud et al., 2024; Brown & Rein, 2022). It may be possible for a stellar mass encounter to enable the same degree of similarity between an initially circular, coplanar system and the solar system. However, such a stellar flyby would need to be moving significantly faster than what is typically found within an open star cluster system, while also passing extremely close, making such cases exceedingly low probability.

2.5 Conclusions

In this paper, we explore a new scenario for the origin of the secular mode amplitudes of the giant planets. We show that a single substellar object making a hyperbolic close encounter with the ancient solar system can account for the observed amplitudes in both the eccentricity and inclination secular modes. We find the most favorable encounter to be a substellar object with encounter parameters $m_\star = 8.27\,\mathrm{M_J}$, $q_\star = 1.69\,\mathrm{AU}$, $v_\infty = 2.69\,\mathrm{km\,s^{-1}}$, and $i_\star = 131°$. Our numerical simulations indicate that there is approximately a 1-in-10^3 to 1-in-10^4 chance of the necessary encounter parameters being realized with random encounters within an open star cluster having properties expected for where the solar system formed. Given that the estimated population of Sun-like stars in the Galaxy is on the order of 10^{10} and that stars are commonly formed in open star clusters, the 1-in-10^4 chance is *not* negligible. In other words, we don't need to look for a needle in a haystack to find a suitable encounter. Additional numerical simulations also demonstrate that the terrestrial planets have a

high probability of not only surviving such an encounter but also themselves acquiring secular mode amplitudes similar to those observed today.

The novelty of this work is two fold. First, we invoke external perturbations to account for the solar system's secular modes; this is in contrast to invoking internal, planet-planet interactions of the giant planets (Tsiganis et al., 2005; Morbidelli et al., 2007; Nesvorný & Morbidelli, 2012; Raymond et al., 2020; Nesvorný, 2018; Clement et al., 2021; Griveaud et al., 2024). Secondly, we include substellar mass objects (down to Jupiter mass) and extremely close flyby distances in the Sun's primordial star cluster in our simulations. This represents parameter regimes that have not been considered in previous studies of flyby encounters of the ancient solar system (Levison et al., 2004; Morbidelli & Levison, 2004; Kenyon & Bromley, 2004; Brasser et al., 2006; Adams, 2010; Huang & Gladman, 2024; Pfalzner et al., 2024; Li & Adams, 2015; Li et al., 2019; Brown & Rein, 2022; Raymond et al., 2024).

Note that there is a very large parameter space of initial conditions to explore in this scenario (velocity, direction, and mass of the flyby object, as well as the orbital phases of all planets) and the outcomes are sensitive to these initial conditions. That we found a substantial fraction of *close matches* to the solar system shows that this scenario is not only possible but surprisingly efficient. This result holds regardless of the specific measure of closeness adopted (see Appendix 2.A.2 for more details). However, let us acknowledge that identifying with very high precision the one specific set of flyby encounter parameters that reproduces every observed dynamical feature of the solar system is not possible—it would be as unique as the solar system itself.

Nevertheless, further exploration of this scenario is warranted. For example, simulations could include a wider range of initial semi-major axes. This would allow us to connect the present scenario to other earlier phases in planet formation theories including planet-disk interactions. Future investigations might also look into a more detailed study of the effects on the terrestrial planets, as well as the effect of substellar flybys on the dynamical excitation of minor planets in the asteroid belt and the trans-Neptunian belts, and the capture probability of irregular satellites by the giant planets. Our results suggest that substellar flyby encounters should be taken into account when studying the formation and evolution of the Kuiper belt, trans-Neptunian objects (TNOs), and the Sednoids (Pfalzner et al., 2024). The preliminary work shown in Section 2.4.3 indicates that even a substellar flyby may be able to produce some of the features of the TNOs. However, a more thorough investigation is needed. Whereas this study focused on finding *close matches* for our own solar system, a statistical analysis of all flyby outcomes might also reveal new insights into the formation history of extrasolar planetary systems which show different architectures compared to the solar system (Winn & Fabrycky, 2015; Kane & Wittenmyer, 2024).

Lastly, let us also acknowledge that internal perturbations during the planetesimal-driven migration of the giant planets, such as planet-planet resonant encounters and scatterings (Tsiganis et al., 2005; Morbidelli et al., 2009) could have also played a role in establishing the secular architecture of the giant planets. Considering the robust statistics in the substellar flyby scenario found in our study, a combination of internal and external perturbations appears to be a likely part of the story of the solar system.

2.A Appendix

2.A.1 Likelihood of Multiple Flybys

We can model the likelihood of the solar system experiencing a specific number of flyby encounters using the Poisson distribution. This expresses the probability of a given number of events in a fixed time interval. We can use the Poisson distribution because the number of flyby events does not depend on any previous flyby events and we model the encounter rate using a constant (static) object density, velocity dispersion, and cross-section. Given the encounter rate of $\Gamma \approx 10^{-3}\,\text{flybys}\,\text{Myr}^{-1}$ (see above), the probability of k flyby events in time interval Δt is given by ($k \in \mathbb{N}, t \in \mathbb{R}^+$)

$$P(k, \Delta t) = \frac{(\Gamma \Delta t)^k e^{-\Gamma \Delta t}}{k!}\,. \tag{2.5}$$

Therefore, the likelihood of zero flybys in 100 Myr is $P(0, 100\,\text{Myr}) \approx 0.881$. Similarly, $P(1, 100\,\text{Myr}) \approx 0.112$, $P(2, 100\,\text{Myr}) \approx 0.007$, and so on. We can express the probability of having *at least* k flybys as

$$\hat{P}(k \geq n, \Delta t) = 1 - \sum_{k=0}^{n-1} P(k, \Delta t)\,, \tag{2.6}$$

such that the likelihood of the solar system experiencing *at least* one flyby is $\hat{P}(k \geq 1, 100\,\text{Myr}) \approx 0.119$.

2.A.2 Success Criteria

We discuss here the success rate for the four criteria defined in Section 3 of (Nesvorný & Morbidelli, 2012) resulting from the flyby simulations of this study. Criterion A is that four planets remain in the simulation. Criterion B has three parts: all of the semi-major axes are within 20% of the current solar system, the average eccentricities are all less than 0.11, and the average inclinations are less than 2°. See Table 2.2 for the average eccentricity and inclination values for the best matching flyby case. Criterion C, discussed in this study, requires the amplitude of the g_5 mode in Jupiter's orbit to be greater than 0.022. Criterion D is not applicable to our study because the giant planets do not migrate in our simulations. Instead, a specific study of the effect of each flyby on the terrestrial planets should be considered. The criteria are dependent; C can only be successful if B is successful, and B can only be successful if A is successful. Using these criteria with our data we find success rates of A (41.33%), B (19.33%), and C (1.63%). These success rates also show that 1% of flyby simulations result in a 'close match' with the solar system. If we consider an intersection of successful matches from these criteria with $\mathcal{M}$ the success rate is 0.23%.

2.A.3 Angular Momentum Deficit

As discussed in Section 2.3.3, we found that, for purpose of comparing the similarity between two systems, the angular momentum deficit (AMD) is not a good parameter because the AMD can be dominated by a single planet which is a common result of flyby encounters. There are many more flyby systems with AMD similar to the solar system than there are *closely matching* flyby systems, see Fig. 2.5. Flyby encounters tend to increase the eccentricities of the outermost planets more than the innermost planets (Heggie & Rasio, 1996). The results from our simulations are generally

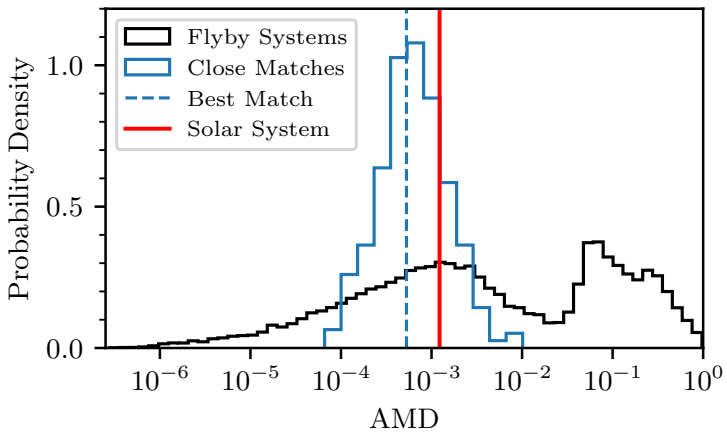

Figure 2.5: Here we show in black the distribution of the normalized angular momentum deficit (AMD) compared to the solar system (shown in red). We highlight in blue the 422 flyby systems that are a *close match* to the solar system according to our metric $\mathcal{M}$ along with the best matching system. We note that of the $5 \cdot 10^4$ flyby systems, 15737 have AMD within the range of our *closely matching* systems; 6679 are within the range of the best matching system; and 567 are within 1% of the solar system.

Table 2.2: Averaged over 20 Myr, we show a comparison of the eccentricities and inclinations (with respect to the invariant plane) of the giant planets (SS) and our best matching flyby system that experienced a $m_\star = 8.27\,\mathrm{M_J}$ encounter at $q_\star = 1.69\,\mathrm{AU}$, with $v_\infty = 2.69\,\mathrm{km\,s^{-1}}$.

Planet	Eccentricity		Inclination [°]	
	SS	Flyby	SS	Flyby
Jupiter	0.0456	0.0289	0.366°	0.164°
Saturn	0.0536	0.0259	0.902°	0.402°
Uranus	0.0435	0.0593	1.022°	0.920°
Neptune	0.0096	0.0352	0.669°	0.146°

consistent with this theoretical expectation. Note that this is opposite to the solar system where Neptune has the smallest eccentricity out of the giant planets. Approximately 8% of the *closely matching* cases have the same trend as in the solar system.

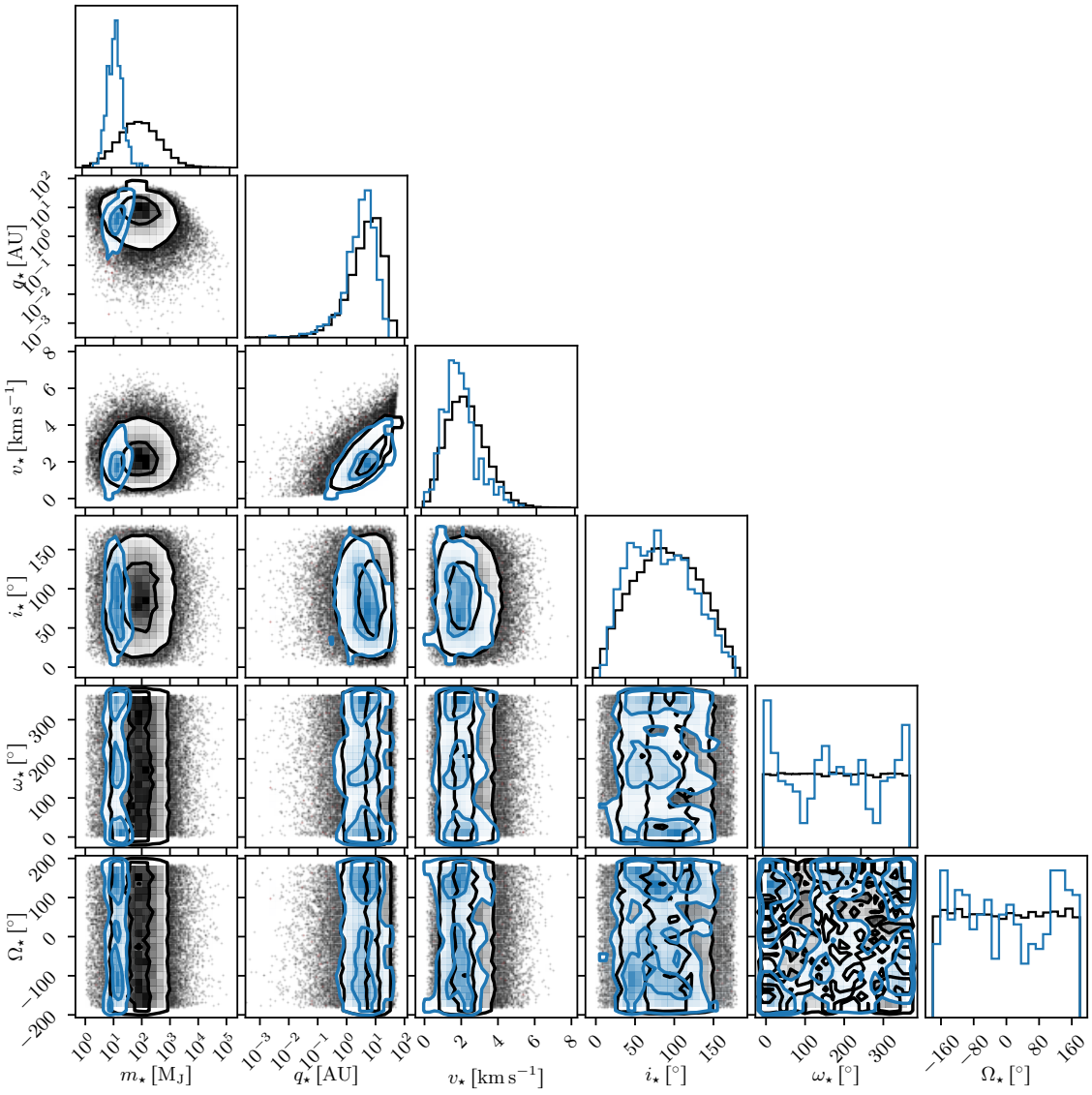

Figure 2.6: Here we show the distributions of all the flyby parameters in our simulations (black) as well as the subset of those parameters that led to a *close match* with the solar system (blue). The contours show the first two standard deviations.

Acknowledgments

G.B. is grateful to Mykhaylo Plotnykov, Dang Pham, and Sam Hadden for useful discussions. R.M. is grateful to the Canadian Institute for Theoretical Astrophysics (CITA) for hosting a sabbatical visit during which this project began. The citations in this paper have made use of NASA's Astrophysics Data System Bibliographic Services. The research of G.B. and H.R. has been supported by the Natural Sciences and Engineering Research Council (NSERC) Discovery Grants RGPIN-2014-04553 and RGPIN-2020-04513. Their research was enabled in part by support provided by Digital Research Alliance of Canada (formerly Compute Canada; `https://alliancecan.ca/en`). Computations were performed on the Niagara supercomputer (Loken et al., 2010; Ponce et al., 2019) at the SciNet HPC Consortium (`www.scinethpc.ca`). SciNet is funded by the following: the Canada Foundation for Innovation; the Government of Ontario; Ontario Research Fund – Research Excellence; and the University of Toronto. R.M. acknowledges research support from NASA grant 80NSSC18K0397 and from the program "Alien Earths" (supported by the National Aeronautics and Space Administration under agreement No.80NSSC21K0593) for NASA's Nexus for Exoplanet System Science (NExSS) research coordination network sponsored by NASA's Science Mission Directorate.

The solar system ensemble used in this study can be found at `https://doi.org/10.5281/zenodo.4299102`. A repository containing the code and data underlying this article can be found at `https://github.com/zyrxvo/Secular-Origin`. This research was made possible by the open-source projects `Jupyter` (Kluyver et al., 2016), `iPython` (Pérez & Granger, 2007), `matplotlib` (Hunter, 2007; Droettboom et al., 2016), `joblib` (Joblib Development Team, 2024) and `gnu-parallel` (Tange, 2023). The author's open-source projects `REBOUND` (Rein & Liu, 2012) and `AIRBALL` (Brown et al., 2024) that enabled this research are also available online.

Chapter 3

On the role of general relativity

A version of the following chapter was published as Brown & Rein (2023), overseen by Hanno Rein. In this chapter, this work explores the effects of different strengths of general relativity on the long-term stability of the solar system. Before this work, little effort had been given to investigating the effect of general relativity on the dynamical stability of planetary systems. However, Laskar & Gastineau (2009) had established a baseline level of expected instability over 5 Gyr both with and without the effect of general relativity. Therefore, this work takes to understanding the effect of different strengths of general relativity on the long-term dynamical stability of the solar system. The significance of this work was using the dynamical stability of the solar system to show the smooth relationship between the cases with and without general relativity.

Abstract

The long-term evolution of the solar system is chaotic. In some cases, chaotic diffusion caused by an overlap of secular resonances can increase the eccentricity of planets when they enter into a linear secular resonance, driving the system to instability. Previous work has shown that including general relativistic contributions to the planets' precession frequency is crucial when modelling the solar system. It reduces the probability that the solar system destabilizes within 5 Gyr by a factor of 60. We run 1280 additional N-body simulations of the solar system spanning 12.5 Gyr where we allow the GR precession rate to vary with time. We develop a simple, unified, Fokker–Planck advection–diffusion model that can reproduce the instability time of Mercury with, without, and with time-varying GR precession. We show that while ignoring GR precession does move Mercury's precession frequency closer to a resonance with Jupiter, this alone does not explain the increased instability rate. It is necessary that there is also a significant increase in the rate of diffusion. We find that the system responds smoothly to a change in the precession frequency: There is no critical GR precession frequency below which the solar system becomes significantly more unstable. Our results show that the long-term evolution of the solar system is well described with an advection–diffusion model.

3.1 Introduction

For many centuries, the motion of the solar system has been a subject of interest to many cultures. Since Newton (1687) formulated his universal law of gravitation, there has been a formal and precise way to describe this motion. The paradigm shift of general relativity (GR) introduced by Einstein (1915) further increased our understanding and ability to model the motion of the solar system precisely. Shortly afterwards, post-Newtonian corrections derived from the equations of general relativity provided a simpler approach to more accurately model the discrepancies previously found through observation (Eddington, 1923). Today, a combination of these precise numerical models together with modern computational resources have made extensive studies on the long-term behaviour of the solar system feasible. Modern numerical studies of the solar system that focus primarily on its dynamical stability have considered the classical solar system, which assumes no additional forces or effects beyond Newtonian gravity, or they consider a constant strength of general relativity (Batygin & Laughlin, 2008; Laskar & Gastineau, 2009; Zeebe, 2015; Abbot et al., 2021, 2022). We consider in more detail here how the dynamical stability of the solar system depends on the general relativistic perihelion precession rate of the planets.

We do this by artificially adjusting the strength of the first-order post-Newtonian correction over time, decreasing it from the values observed today to completely absent. General modified versions of gravity have been developed to account for dynamical features seen in galactic and galactic cluster scales and are proposed to mimic the effect of dark matter (Milgrom, 1983; Moffat & Toth, 2008; Verlinde, 2017). However, some of these theories result in changes to the perihelion precession rate of Mercury that are not compatible with current observations (Chan & Lee, 2023). We investigate a decrease in the GR precession rate not because we think this mimics these modified theories of gravity, but because it offers a clean way to experiment with the dynamics of the solar system.

By comparing to previous work, we determine the effect the perihelion precession rate of Mercury from general relativistic corrections has on the probability that the system goes unstable. The results of this work reconfirm the work of Laskar & Gastineau (2009), showing that the stability of the solar system is highly dependent on the presence of general relativity. What is new in this paper is that we also smoothly vary the strength of general relativistic corrections to the perihelion precession over the lifetime of the solar system and consider the implications for the long-term evolution of the solar system. We develop a physical model based on a diffusion process (Mogavero & Laskar, 2021) that can explain the observed instability rate in our numerical experiments. Our results show that a change in general relativistic corrections does not only change the planets' perihelion precession rate, but also the rate at which the precession rate diffuses with time. We find that the dependence of the diffusion coefficient and the general relativistic corrections is smooth. We find no evidence of any critical strength of GR that is required for stability.

To do this, we begin with a discussion of Mercury's path to instability and the role of secular resonances in Section 3.2. In Section 3.3 we describe the numerical set-up for our long-term ensemble of integrations of the solar system, how we modify the first-order post-Newtonian corrections that affect the perihelion precession from general relativity, and the results of the integrations. The diffusion model we use to interpret our results is developed and compared to previous work in Section 3.4. In Section 3.5 we compare the model to our new N-body data. Finally, we close in Section 3.6 with the conclusions and implications.

3.2 The path to instability

The secular evolution of the solar system was first described by Laplace and Lagrange (Laplace, 1775, 1776; Lagrange, 1776, 1778, 1781, 1782, 1783a,b, 1784); see Laskar (2013) for a comprehensive historical review. This description of the solar system averages over the mean motions of the planets. The ground-breaking linear expansion is a perturbation theory of first-order in the masses with a disturbing function of second order in the eccentricities and inclinations. It exhibits no changes to the semi-major axis of the planets and over time shows only small changes to the eccentricities and inclinations, but not by an amount to allow for orbit crossing scenarios. The solutions contain the perihelion precession of planetary orbits as well as the precession of the ascending nodes of the planets, but fundamentally they are perfectly periodic. This initially seemed to *prove* that the solar system is dynamically stable for all time, but these successive approximations did not provide rigorous bounds to actually prove it analytically (Poincaré, 1898).

From this Laplace-Lagrange linear expansion, the fundamental eigenmodes for the variations in the eccentricities and inclinations of the solar system can be calculated (Murray & Dermott, 1999). When Le Verrier (1840, 1841) continued the perturbative expansion to higher order, significant terms emerged that make crucial corrections to the linear equations and showed that the linear theory could not be used for an indefinite period of time. In spite of Poincaré (1899) proving the impossibility of an analytical solution to multi-planetary dynamics over an infinite time interval, quasi-periodic approximations were still the most accurate models at the time. Further mathematical developments by Kolmogorov (1954), Arnol'd (1963), and Möser (1962) (KAM) showed that for systems with a few degrees of freedom and in small regions around the initial conditions, the trajectories remain constrained to quasi-periodic solutions. These KAM toridal regions are only isolating for systems with two degrees of freedom. As such, for systems with more degrees of freedom, these constrained regions overlap and allow trajectories to pass into chaotic regions and effectively diffuse through phase space (Laskar, 2013). With the aid of computer algebra systems, the integration of high-order secular expansions by Laskar (1985, 1986, 1990) showed that the inner solar system is indeed chaotic. Recent developments in high-order expansions continue to reveal insights into the dynamical richness of the solar system unachievable by N-body integrations alone (Mogavero & Laskar, 2021, 2022; Hoang et al., 2022).

Over short time-scales of $\sim 1\,\mathrm{Myr}$ the evolution of the secular frequencies is regular and can be calculated accurately either with computer-aided expansion to higher order or with direct N-body simulations. However, on time-scales greater than $\sim 50\,\mathrm{Myr}$, the changes in secular frequencies are chaotic (Laskar, 1990; Lithwick & Wu, 2011). This chaos in the solar system is largely driven by overlapping secular resonances (Laskar, 1989). Various resonances driving chaos in the inner solar system are at play, e.g. the Earth–Mars secular resonance $2(\varpi_4 - \varpi_3) - (\Omega_4 - \Omega_3)$ and the Mercury–Venus–Jupiter secular resonance $(\varpi_1 - \varpi_5) - (\Omega_1 - \Omega_2)$ (Laskar et al., 1992; Sussman & Wisdom, 1992), where $\varpi_1, ..., \varpi_8$ are the longitudes of the perihelia and $\Omega_1, ..., \Omega_8$ are the longitudes of the ascending nodes of the planets. Sometimes, these secular resonances are also expressed in terms of the eigenfrequencies $g_1, ..., g_8$ and $s_1, ..., s_8$ of the solar system associated with the precession of the perihelia and ascending nodes, respectively. We follow the traditional convention to associate g_1 with Mercury, g_2 with Venus, and so forth, with our discussion focusing mainly on Mercury and Jupiter, and therefore g_1 and g_5. Thus, the Earth–Mars resonance mentioned above would be $2(g_4 - g_3) - (s_4 - s_3)$.

Instabilities from the g_1–g_5 resonance can be seen in long-term solar system integration of N-body models (Laskar & Gastineau, 2009; Zeebe, 2015; Abbot et al., 2021, 2022; Brown & Rein, 2022). As the solar system evolves, the planets push each other into or out of secular resonances through exchanges of angular momentum (Laskar, 2000; Zakamska & Tremaine, 2004). Reduced models help us to understand the nature of this process, specifically how the g_1–g_5 resonance affects the eccentricity pumping of Mercury, and how Mercury falls into the resonance in the first place after a diffusive walk through phase space (Lithwick & Wu, 2011; Batygin et al., 2015; Mogavero & Laskar, 2021). Although the frequencies of the secular eigenmodes of the solar system are fixed in the simplest model, they do in fact show small variations. In particular, the secular frequencies corresponding to the inner solar system change as a result of mutual interactions of the inner planets and the interactions of the inner planets with the outer gas giants (Laskar, 1990). As we will show in Section 3.4, a simple diffusion process is often a remarkably accurate model that can explain most of the results seen in ensembles of direct N-body integrations.

3.3 *N*-body simulations

3.3.1 Methods

We run direct N-body simulations of the solar system that we will later compare to our advection–diffusion model. All of our simulations for the solar system (the Sun and eight planets) use *exactly* the same initial conditions that are taken from NASA Jet Propulsion Laboratory (JPL) Horizons data at the J2000 epoch. Even though all the initial conditions are the same, because the systems are chaotic and we use slightly different general relativistic corrections in each simulation, the simulations diverge quickly. This is effectively the same as varying the initial conditions of one planet by a tiny amount (Laskar & Gastineau, 2009). We integrate simulations forward in time using `REBOUND` (Rein & Liu, 2012) and the Wisdom-Holman integrator `WHFast` (Wisdom & Holman, 1991; Rein & Tamayo, 2015) with symplectic correctors and the lazy implementation of the kernel method, `WHCKL` (Wisdom et al., 1996; Rein et al., 2019b). The `WHCKL` integrator is well suited to provide highly accurate results for secularly evolving systems (Rein et al., 2019a). We used a fixed timestep of $dt = \sqrt{11}\,\text{days} \approx 3.317\,\text{days}$.

The aim of our simulations is not to exactly reproduce the solar system, but to have a well-defined model that can reproduce the most important dynamical effects. Specifically, we do not consider the stellar evolution of the Sun even though we integrate beyond the end of its life on the main sequence. We also neglect the effects resulting from the solar oblateness, moons, asteroids, tides, and other non-gravitational effects.

3.3.2 Perihelion precession from general relativity

Of all the contributions to Mercury's perihelion precession, the most important are the gravitational interactions from the other solar bodies contributing $g_{1,\text{planets}} = 5.323\,''\text{yr}^{-1}$ (arcseconds per year), followed by the precession from GR (the gravitoelectric effect) with $g_{1,\text{gr}} = 0.4298\,''\text{yr}^{-1}$, followed by other less significant contributors such as solar oblateness that provide $g_{1,\text{other}} = 2.8\times10^{-4}\,''\text{yr}^{-1}$ (Park et al., 2017). Thus, the impact of general relativity follows closest behind Newtonian planet-planet interactions and is more than three orders of magnitude more influential than any additional

effects. As discussed in Section 3.2, the long-term stability of the solar system is connected to Mercury's perihelion precession rate and thus the general relativistic effects are very important (Laskar & Gastineau, 2009).

In this paper, we consider an N-body Newtonian model of the solar system. To have a perihelion precession that is consistent with general relativity, we include an additional potential term in our force calculation:

$$\Phi_{\rm gr} = \alpha(t,\tau)\frac{6G^2M^2}{c^2r^2} \tag{3.1}$$

where r is the distance of the planet to the Sun and M, G, and c are the mass of the Sun, the gravitational constant, and the speed of light, respectively. The perihelion precession rate caused by $\Phi_{\rm gr}$ is

$$\dot{\varpi}_{\rm GR} = \alpha(t,\tau)\frac{3GMn}{ac^2(1-e^2)} \tag{3.2}$$

where $n = \sqrt{GM/a^3}$ is the mean motion of a planet with semi-major axis a and e is the planet's eccentricity.

The time-dependent parameter $\alpha(t,\tau)$ in the above equations enables us to experiment with different strengths for the general relativistic corrections. With $\alpha = 1$, we refer to this potential as the standard first-order post-Newtonian corrections. This assumes that the Sun is the only body in solar system massive enough so that particles orbiting it experience general relativistic precession. This commonly used model gets the general relativistic precession frequency right, but at the expense of introducing an error on the mean motions on the order of $\mathcal{O}(GM/ac^2)$ (Nobili & Roxburgh, 1986; Saha & Tremaine, 1994). For this paper, the accuracy in the mean motion does not affect the results because of the relative importance of Mercury's perihelion precession rate to its stability compared to its mean motion (there are no mean motion resonances in the inner solar system).

With $\alpha = 0$, we recover the purely classical regime with no general relativistic precession. Although this is clearly inconsistent with many observations that confirm general relativity, it can act as a useful case to study if we want to understand the dynamics of the solar system. In previous work, Laskar & Gastineau (2009) integrated thousands of solar system simulations for billions of years and showed that without general relativistic corrections, 60 per cent of the solutions resulted in an unstable solar system after 5 Gyr (defined as Mercury having an eccentricity beyond 0.9). Conversely, when general relativistic corrections were included, only 1 per cent of the solutions were unstable (Laskar & Gastineau, 2009). See also Fig. 3.2 below.

In this paper, we go beyond simply turning general relativistic precession on or off and allow for a time-dependent parameter α defined as

$$\alpha(t,\tau) = \begin{cases} 1 & t < 0 \\ 1-(t/\tau) & 0 \le t \le \tau \\ 0 & t > \tau \end{cases}. \tag{3.3}$$

At the beginning of a simulation, $t = 0$, the full GR corrections are taken into account, consistent with present-day observations. After $t = \tau$ no more general relativistic corrections are applied and the simulation evolves classically. We include the general relativistic corrections using `REBOUNDx` (Tamayo et al., 2020a) and the `gr_potential` module, modified to allow for the time-varying form given in equation (3.1).

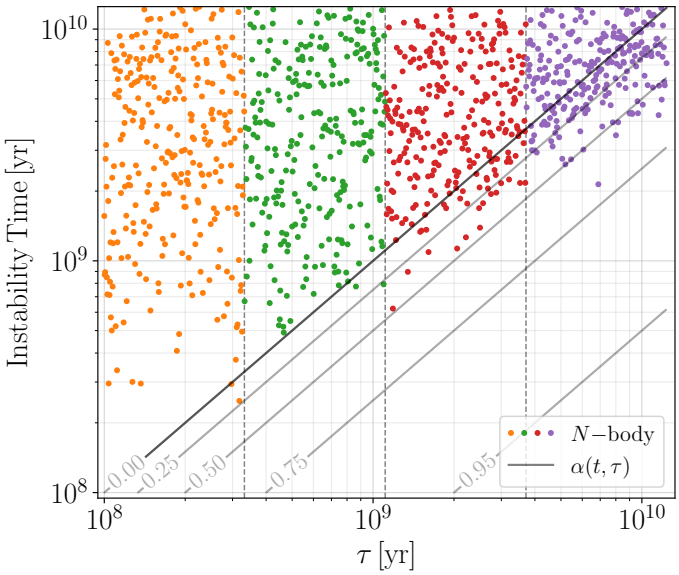

Figure 3.1: The instability time of simulations in our ensemble that went unstable as a function of the control parameter τ that determines the time when general relativistic corrections to the perihelion precession are turned off. Simulations are significantly more likely to go unstable before 12.5 Gyr when no general relativistic corrections are present (upper left portion). The four different colours show the binning made for comparison to the model in Section 3.5 and Fig. 3.4.

3.3.3 *N*-body results

In this section we present the stability results of an ensemble of 1280 long-term integrations of the solar system. We decrease the coupling strength, $\alpha(t,\tau)$, of the general relativistic corrections to perihelion precession linearly from the current value, 1, to 0 as defined in equation (3.3). For each simulation, we assign a different value for τ. We sample τ log-uniformly between 0.1 and 12.5 Gyr. We then integrate the simulations for 12.5 Gyr, or until a collision or escape event occurs. We do not carry out any simulations beyond the first physical collision or escape.

We find that 1072 out of 1280 or 83.8 per cent of the simulations end up in an instability, all involving a Mercury-Venus close encounter or collision. 175 simulations go unstable while some fractional GR precession is still present. We present the instability times with respect to τ in Fig. 3.1. The instability time is shown on the y-axis, τ is shown on the x-axis. The uppermost diagonal line is when $\alpha(t,\tau) = 0$ at $t = \tau$. The remaining diagonal lines indicate the times when $\alpha(t,\tau)$ reaches $0.25, 0.5, 0.75$, and 0.95 (from top to bottom).

3.4 Advection–diffusion model

3.4.1 Fokker–Planck equation

In this section, we develop a simple model that is physically motivated and can explain results from our new N-body simulations as well as the results from previous studies that have both included and excluded general relativistic corrections.

Our model describes the evolution of Mercury's precession frequency g_1 as an advection–diffusion

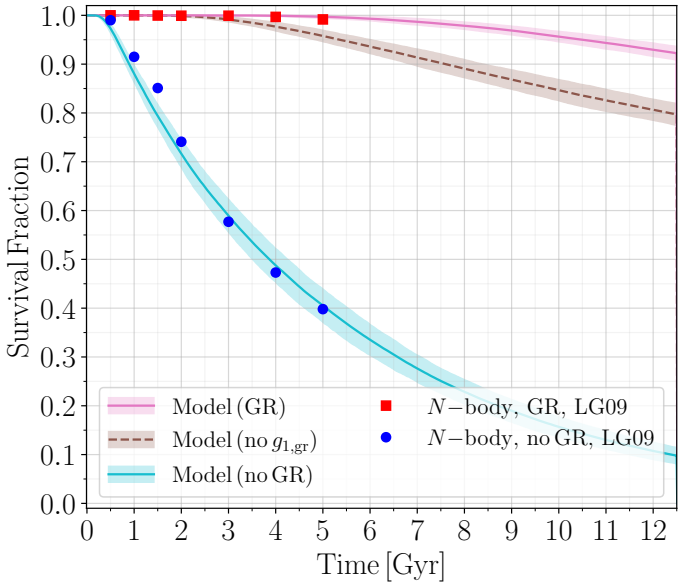

Figure 3.2: A comparison showing the implementation of our model against the previous work of Laskar & Gastineau (2009). The mean and 2σ uncertainties of the model are in good agreement with these numerical results in both cases with and without GR. The dashed curve shows the effect of changing the initial starting location of g_1 by removing $g_{1,\mathrm{gr}}$ from the GR model without altering the diffusion coefficient. The fact that this curve does not match the numerical experiments without GR reveals that the initial proximity between g_1 and g_5 alone does not account for the increase in instabilities.

process. This can be seen as a natural extension of the model used by Mogavero & Laskar (2021) who use a stochastic–Wiener process to describe the evolution of Mercury's precession frequency g_1 (see their section 8.2).

We use the Fokker–Planck equation to describe the evolution of $p(g_1, t, \tau)$, the probability density of the secular frequency g_1 as a function of time t and our model parameter τ:

$$\frac{\partial p(g_1,t,\tau)}{\partial t} = -\mu(t,\tau)\frac{\partial p(g_1,t,\tau)}{\partial g_1} + D(t,\tau)\frac{\partial^2 p(g_1,t,\tau)}{\partial g_1^2}. \tag{3.4}$$

Here $\mu(t,\tau)$ describes the advection and $D(t,\tau)$ the diffusion of g_1. We use the current precession frequency of Mercury, $g_{1,0} = 5.577''\mathrm{yr}^{-1}$, as the initial condition:

$$p(g_1, 0, \tau) = \delta(g_1 - g_{1,0}). \tag{3.5}$$

There is an upper boundary that acts as a reflecting barrier at $g_{1,\max} = 5.72367''\mathrm{yr}^{-1}$ (Mogavero & Laskar, 2021). We also have a lower boundary where g_1 overlaps with $g_5 = 4.257''\mathrm{yr}^{-1}$, the perihelion precession frequency of Jupiter. When this lower boundary is hit, the system is assumed to go unstable on a very short time-scale because of the g_1–g_5 secular resonance.

3.4.2 Model with general relativistic precession

In the limit where general relativistic corrections are present during the entire simulation, Mogavero & Laskar (2021) show that the results of high-order secular simulations can be closely matched with a constant diffusion coefficient $D_{\rm gr}$ and a vanishing convection term $\mu = 0$.

A more intuitive understanding of these quantities can be achieved by rewriting the diffusion coefficient D and the initial precession frequency $g_{1,0}$ into a diffusion time-scale T_D and a dimensionless parameter β that describes how close the initial condition for g_1 is to the lower boundary g_5 where we expect an instability to occur. Making use of $(g_{1,\max} - g_5)$, the distance between the two boundaries, we can define the characteristic diffusion time-scale as

$$T_D = \frac{(g_{1,\max} - g_5)^2}{4D}. \tag{3.6}$$

and the parameter[1] β that describes our initial conditions as

$$\beta = (g_{1,0} - g_5)/(g_{1,\max} - g_5). \tag{3.7}$$

Using $g_5 = 4.257''\mathrm{yr}^{-1}$, we have $\beta = 0.9$. Mogavero & Laskar (2021) show that a value of $T_{D,\rm gr} = 27.6\,\mathrm{Gyr}$ reproduces the statistical results from their simulations (which include general relativistic corrections) remarkably well. The survival fraction as a function of time corresponding to this model is the uppermost line plotted in Fig. 3.2. N-body data (an ensemble of 2501 simulations) from the previous work by Laskar & Gastineau (2009) are overlaid as red squares for comparison. It shows how this advection–diffusion model captures the instability rates of Mercury in N-body solar system simulations for the first 5 Gyr very well. Obtaining a meaningful number of instabilities beyond the remaining lifetime of the sun is costly, but we show below that this model can also be used to give accurate results well beyond 5 Gyr.

3.4.3 Model without general relativistic precession

We can repeat the analysis from the previous section for the case without general relativistic precession. In our notation, this is the case where $\tau \to 0$ and $\alpha = 0$. The contribution from general relativity to the precession frequency of Mercury is $g_{1,\rm gr} = 0.4298''\mathrm{yr}^{-1}$. Without general relativity, our initial condition is therefore shifted to

$$p(g_1, 0, 0) = \delta(g_1 - (g_{1,0} - g_{1,\rm gr})), \tag{3.8}$$

or equivalently $\beta = 0.607$. If we assume this is the only change to the system, then we end up with a survival fraction shown as a dashed line in Fig. 3.2. Clearly, although the rate of instability is higher, this does not fit the numerical experiments by Laskar & Gastineau (2009).

This leads to the conclusion that we need to change not only the initial conditions but also the diffusion coefficient. To find the diffusion coefficient, we can make use of the N-body results by Laskar & Gastineau (2009) who find that 60 per cent of all simulations have gone unstable after 5 Gyr, using an ensemble of 201 simulations. Choosing $T_{D,\rm nogr} = 3.22\,\mathrm{Gyr}$ results in a model that fits those results well, as can be seen in Fig. 3.2. While there are some discrepancies between the model

[1] This parameter is equivalent to the parameter α in Mogavero & Laskar (2021).

and N-body results, especially in the 1–2 Gyr regime, we attribute this discrepancy to the relatively small number of simulations used in the ensemble.

3.4.4 Model with time-dependent general relativistic precession

We are now in a position to describe a model for our case where we have a time-dependent $\alpha(t, \tau)$ given by equation (3.3), leading to a time-dependent general relativistic precession. In this paper, τ is the model parameter that describes the time-scale on which the general relativistic precession changes.

For our model, the initial conditions are the present-day precession frequency $g_{1,0}$, i.e.

$$p(g_1, 0, \tau) = \delta(g_1 - g_{1,0}). \tag{3.9}$$

The diffusion coefficient is no longer a constant, but a function of time

$$D(t, \tau) = \begin{cases} \left(\sqrt{D_{\mathrm{gr}}} \cdot \left(1 - \frac{t}{\tau}\right) + \sqrt{D_{\mathrm{nogr}}} \cdot \frac{t}{\tau}\right)^2 & t \leq \tau \\ D_{\mathrm{nogr}} & t > \tau \end{cases} \tag{3.10}$$

We chose this specific form for the diffusion coefficient because the interpolation between D_{gr} and D_{nogr} corresponds to a simple linear interpolation in the forcing strength[2].

In addition, we also now include the advection term in the Fokker–Planck equation. Specifically,

$$\mu(t, \tau) = \begin{cases} g_{1,\mathrm{gr}}/\tau & t \leq \tau \\ 0 & t > \tau \end{cases}. \tag{3.11}$$

If we ignore the diffusion, then this form of μ moves the precession frequency from the initial value of $g_{1,0}$ to $g_{1,0} - g_{1,gr}$ by time $t = \tau$, i.e. when $\alpha = 0$ and there is no more general relativistic precession.

Note that there are no free parameters in this extension of the model. All the parameters, most importantly D_{gr} and D_{nogr}, are already fixed by matching the simulations of Laskar & Gastineau (2009).

3.5 Results

The survival fraction for our entire ensemble compared to the model is presented in Fig. 3.3. It shows the results from our ensemble of 1280 N-body simulations compared against the advection–diffusion model with time-dependent coefficients. The mean and 2σ uncertainties expected for an ensemble size of 1280 are shown for the model.

For Fig. 3.4, we split our ensemble of simulations into four equally sized groups to show the dependence on τ. The colours match those used in Fig. 3.1. Each panel includes the observed numerical survival fraction in our N-body simulations along with the expected mean survival fraction given by our model and the corresponding 2σ confidence interval for an ensemble size of 320. The plots also include a dotted vertical line indicating when the last simulation in the bin has reached $\alpha(t, \tau) = 0$. A notable feature in some of the panels is that the model produces instabilities slightly

[2]Note that $D \sim t_c \cdot F^2$ where t_c is the characteristic forcing time-scale and F is the characteristic forcing strength in a random walk process (see e.g. Rein & Papaloizou, 2009).

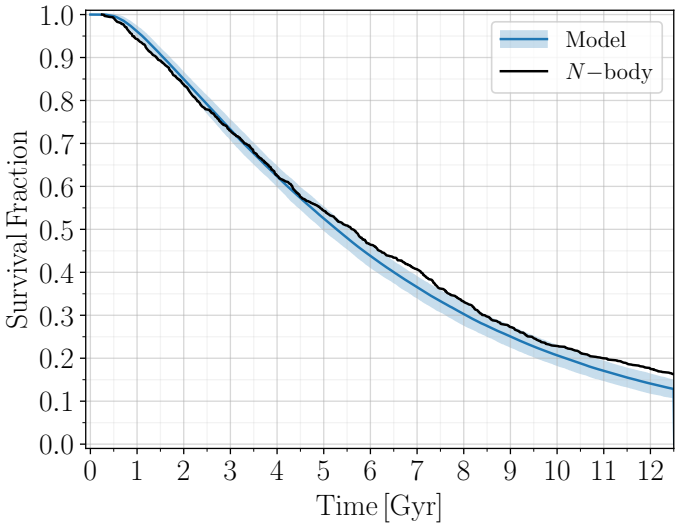

Figure 3.3: The survival fraction of the entire ensemble of simulations compared to the survival given by the model described in Section 3.4. The mean and 2σ uncertainties are shown for the model.

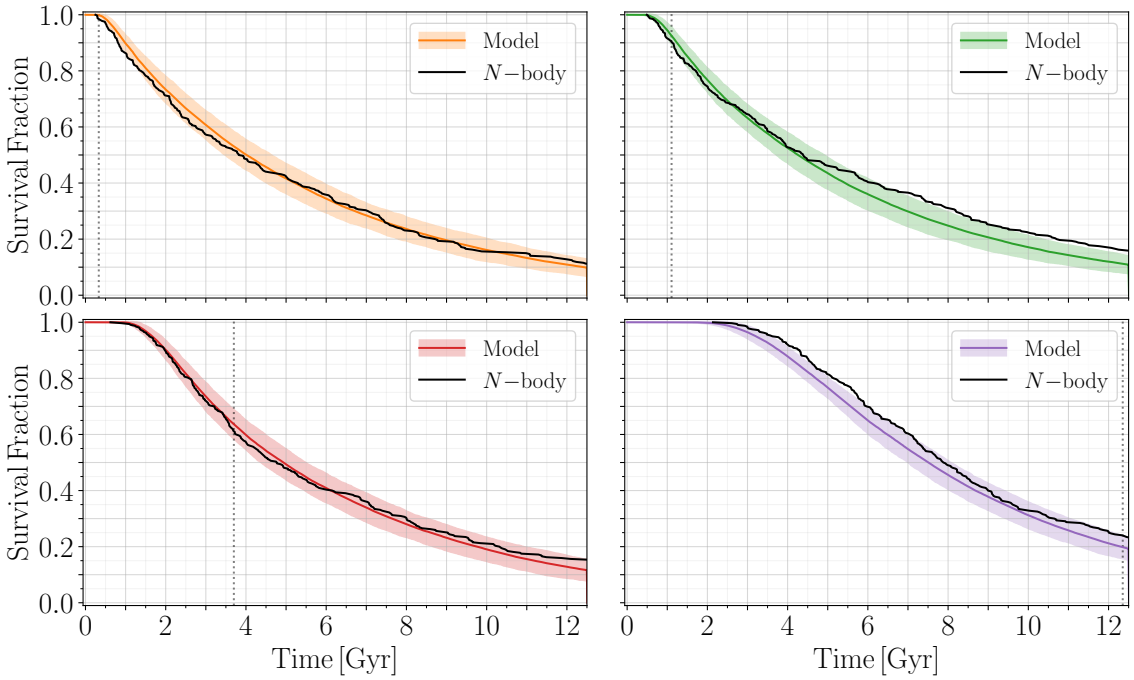

Figure 3.4: The survival fraction of the ensemble of N-body simulations separated into four bins of τ as shown in Fig. 3.1 is given in black. The mean survival of the model described in Section 3.4 is shown for each bin with 2σ uncertainties. The dotted vertical lines indicate when all of the N-body simulations in the bin have completely decoupled from general relativistic corrections. Thus, from $t = 0$ to the dotted line, GR corrections are gradually being turned off.

earlier than in the N-body experiments (starting around 4.5 Gyr). Even so, the model and the numerical simulations agree remarkably well. In particular, note that our model is not fitted to the data, but rather uses a physically motivated model and parameters that are solely determined by the limiting cases done in previous work by Laskar & Gastineau (2009) and Mogavero & Laskar (2021).

The top-left panel in Fig. 3.4 shows the survival fraction of simulations after removing the GR precession quickly[3]. The results match those by Laskar & Gastineau (2009): $\sim$ 60 per cent go unstable within 5 Gyr. Note that removing GR precession from these integrations (even in the far future) does not immediately cause instability. In fact, some simulations continue to remain stable (without GR) for more than 12 Gyr.

3.6 Conclusions

In this paper, we explored how sensitive the stability of the solar system is to changes in the perihelion precession caused by general relativistic corrections. Earlier work by Laskar & Gastineau (2009) has shown that turning off general relativistic corrections can increase the fraction of instability within 5 Gyr by a factor of 60. We develop a simple advection–diffusion model that can explain the results of previous N-body experiments that either include or exclude general relativistic precession; thus, extending the model of Mogavero & Laskar (2021). We then go beyond simply turning the GR precession on or off and instead vary the rate of GR precession smoothly over time. We do this not because we think this is something that will occur in the real solar system, but because it offers a way to experiment with this dynamical system in a controlled way.

We show that our advection–diffusion model can naturally explain the case of a time-varying general relativistic precession remarkably well without the introduction of any new free parameters. We are also confident that this model provides a sound extrapolation for the time to Mercury's dynamical instability beyond 5 Gyr (neglecting changes to the stellar life cycle of the Sun and other external factors). This confidence is based on the work of others mentioned throughout this paper as well as the addition of our N-body ensemble extending all the way to 12.5 Gyr (to date the largest set of solar system integrations extended to this time). The model shows strong agreement to N-body data for so many different regimes of general relativistic precession. Additionally, the model reproduces the statistical results across different analytical and numerical methods, again, without the introduction of any new free parameters.

Without general relativistic corrections, the precession frequency of Mercury, g_1, is closer to that of Jupiter, g_5, by about $0.4298''\mathrm{yr}^{-1}$. However, our results show that this alone does not explain the increased rate of instability observed in N-body experiments. We show that our advection–diffusion model can represent the instability rate only if we significantly decrease the diffusion time-scale (or increase the diffusion coefficient). In other words, although the g_1–g_5 resonance determines when Mercury's eccentricity reaches a critical value, the process to get to this resonance is much faster without GR corrections.

This result might not be surprising, given that the solar system is a complex chaotic system with way more degrees of freedom than our model (which just allows for a diffusion in g_1). Our

[3]Quickly here means that the simulations in this bin all have the general relativistic corrections removed on a time-scale shorter than the lower bound on the destabilization time of Mercury given by Mogavero & Laskar (2021) ($\sim$ 0.56 Gyr).

simulations with time-varying general relativistic precession allow us to gain some more insight into this process. As we have shown in Section 3.5, our model matches the N-body experiments very well given there are no free parameters aside from those used to match the limiting cases of GR being completely on or off. This leads to several conclusions. Firstly, there is no critical value of the general relativistic precession rate that needs to be crossed in order to significantly change the instability rate. Secondly, because this is such a smooth transition all the way from one limit to the other, we can rule out a process that involves a sweeping secular resonance. If this were not so smooth, we would see an increase in the instability rate at some critical GR precession frequency. This makes sense because the diffusion in g_1 is strong enough so that a small change due to the GR precession has a negligible effect. This provides additional evidence that the stability of the solar system is robust to moderate changes to the secular system (see also Laskar, 1990; Brown & Rein, 2022). The fact that we are able to model the evolution so well with a simple diffusion model also shows that current numerical results (Laskar & Gastineau, 2009; Zeebe, 2015; Abbot et al., 2021) are robust against small perturbations whether they are physical or numerical (Abbot et al., 2022). We expect that statistical results are in agreement as long as simulations resolve secular frequencies accurately enough so that physical diffusion (not numerical diffusion or advection) is the dominant driver of the instability.

In summary, we reconfirm that, even in the presence of other small perturbations, the solar system's evolution is well described by a simple (advection–)diffusion process. Here, we considered the perturbation to be the change in the general relativistic precession frequency, but any other physical effect that changes the planets' precession frequencies will lead to a similar result. The initial motivation of this project was to use the stability of the solar system as a test bed for additional physics that are typically not included in simulations of the solar system. For example, had our results shown that slowly changing the general relativistic precession frequency leads to significant increase in the instability rate, then we could have placed a limit on alternative theories of general relativity by noting that the solar system has not gone unstable yet. Clearly, this is not the case. For future work, we propose further investigation into the expected time to instability for other secularly evolving planetary systems and whether or not a one-dimensional advection–diffusion model is representative of more systems or only the solar system (see e.g. Hussain & Tamayo, 2020).

Acknowledgments

We would like to thank Scott Tremaine, Sam Hadden, Dang Pham, Mykhaylo Plotnykov, and David Veitch for useful discussions. This research has been supported by the Natural Sciences and Engineering Research Council (NSERC) Discovery Grants RGPIN-2014-04553 and RGPIN-2020-04513. This research was made possible by the open-source projects `Jupyter` (Kluyver et al., 2016), `iPython` (Pérez & Granger, 2007), `matplotlib` (Hunter, 2007; Droettboom et al., 2016), and `GNU Parallel` (Tange, 2022). This research was enabled in part by support provided by the Digital Research Alliance of Canada (formerly Compute Canada; alliancecan.ca). Computations were performed on the Niagara supercomputer (Loken et al., 2010; Ponce et al., 2019) at the SciNet HPC Consortium (scinethpc.ca). SciNet is funded by the following: the Canada Foundation for Innovation; the Government of Ontario; Ontario Research Fund – Research Excellence; and the University of Toronto.

Chapter 4

On flybys and long-term stability

A version of the following chapter was published as Brown & Rein (2022), overseen by Hanno Rein. In this chapter, this work explores the effects of weakly interacting stellar flybys on the long-term stability of the solar system. Before this work, much effort had been given to investigating the dynamical stability of planetary systems affected by stellar flybys. However, no work had yet undertaken to show the impact of stellar flybys on a system by simulating the dynamical lifetime of the system. Since Laskar & Gastineau (2009) had established a baseline level of expected instability over 5 Gyr, this work takes to understanding the effect of flybys on the long-term dynamical stability of the solar system.

Abstract

The architecture and evolution of planetary systems are shaped in part by stellar flybys. Within this context, we look at stellar encounters which are too weak to immediately destabilize a planetary system but are nevertheless strong enough to measurably perturb the system's dynamical state. We estimate the strength of such perturbations on secularly evolving systems using a simple analytic model and confirm those estimates with direct N-body simulations. We then run long-term integrations and show that even small perturbations from stellar flybys can influence the stability of planetary systems over their lifetime. We find that small perturbations to the outer planets' orbits are transferred between planets, increasing the likelihood that the inner planetary system will destabilize. Specifically, our results for the solar system show that relative perturbations to Neptune's semi-major axis of order 0.1 per cent are strong enough to increase the probability of destabilizing the solar system within 5 Gyr by one order of magnitude.

4.1 Introduction

Since Newton's formulation of his universal law of gravitation (Newton, 1687), the long-term stability of the solar system has been the subject of inquiry for centuries. While a closed-form, analytic solution to the two-body problem exists, systems with more particles are not integrable and have no closed form analytic solution (Poincaré, 1899). Through perturbative expansions Laplace and Lagrange came up with secular equations with regular solutions (for a comprehensive historical

review see Laskar, 2013). These early models were deterministic. However, using a computer assisted secular theory, Laskar (1989) showed that the solar system is chaotic. This implies that any single solution to the set of N-body equations describing the solar system only possesses specific predictive power for at most a few Lyapunov timescales ($\sim$ 100 Myrs). Finally, using a large ensemble of direct N-body integrations, Laskar & Gastineau (2009) showed that within a set of possible solutions to the solar system's future evolution, there is a 1 per cent chance that Mercury's orbit will destabilize (leading to a collision or escape) within the next 5 Gyr. Additional numerical and semi-analytic studies have mostly reconfirmed this result (Zeebe, 2015; Mogavero & Laskar, 2021; Abbot et al., 2021; Brown & Rein, 2020).

The simulations mentioned above typically consider the solar system in isolation, without any external perturbations. However, no system is completely isolated from the rest of the universe and in particular the effects of stellar flybys can be important depending on the stellar environment. Different authors have considered such flybys under various circumstances: outer solar system analogues (Malmberg et al., 2011; Li & Adams, 2015; Stock et al., 2020); planetary systems with one planet embedded in stellar clusters (Laughlin & Adams, 1998; Zheng et al., 2015), systems with five planets with equal masses and separations (Cai et al., 2017), the solar system excluding Mercury and Venus (Dotti et al., 2019); the late stages of the solar system (Zink et al., 2020); and planetary systems with Kuiper belt and Oort cloud type objects (Portegies Zwart & Jílková, 2015). The general conclusion of these studies is that in the case of the solar system in its current stellar neighbourhood, most flybys are weak and do not lead to an immediate dramatic destabilization of the system, and strong flybys are so rare that they are unlikely to occur within the solar system's lifetime.

What is new in this paper is that we do not only look for immediate destabilization, but consider flybys which lead to weak perturbations and their implications for the very long-term evolution of the planetary system. Specifically, we derive a relationship between a stellar flyby and the effect it has on the probability that the system goes unstable within the next 5 Gyr.

To do this, we begin with a discussion of various stellar environments in Section 4.2. We then review the effect of a single stellar flyby and multiple stellar flybys on a single planet system's binding energy. We discuss how perturbations to a system with two planets can be investigated through changes to the fundamental secular frequencies and how these frequencies are perturbed during flybys. In Section 4.3 we describe the numerical setup for our long-term ensemble of integrations of the solar system. We numerically verify the analytical estimate of the effects stellar flybys have on the secular frequencies of the solar system and numerically determine the smallest perturbation which can affect the stability of the solar system. We close in Section 4.4 with the conclusions.

4.2 Weak perturbations to planetary systems

4.2.1 Stellar environments

We want to draw statistical conclusions about the overall importance of stellar flybys for the solar system. For that, we need to know the number density of stars, as well as the stellar mass and velocity distributions of the stellar environment. In this paper, we consider the following stellar environments. The numerical parameters are also summarized in Table 4.1.

Table 4.1: A summary of the stellar densities n, typical velocities $\bar{v}$, and mass ranges $m_\star$ used to compute the data in Fig. 4.1 and Fig. 4.2. Additionally, a summary of the expected time to a numerically resolvable flyby τ, the expected time to a critical flyby $\tilde{\tau}_c$, and the expected lifetimes for the various stellar environments.

Environment	Density n [pc^{-3}]	Speed $\bar{v}$ [km s^{-1}]	Mass $m_\star$ [M$_\odot$]	Time to Flyby $\tau = \Gamma^{-1}$ [yrs]	Single Flyby $\tilde{\tau}_c$ [yrs]	Multiple Flybys $\tilde{\tau}_c$ [yrs]	Lifetime [yrs]
Local Region	0.14	26	0.01–10	$9.76 \cdot 10^7$	$1.70 \cdot 10^{11}$	$(1.28 \pm 0.88) \cdot 10^{11}$	-
Open Cluster	100	1	0.01–100	$1.44 \cdot 10^8$	$1.22 \cdot 10^9$	$(5.11 \pm 4.61) \cdot 10^8$	$\sim 10^8$
Globular Cluster	1,000	10	0.01–1	$1.72 \cdot 10^5$	$7.13 \cdot 10^7$	$(8.60 \pm 5.72) \cdot 10^7$	-
Milky Way Bulge	50	120	0.01–10	$5.49 \cdot 10^3$	$6.77 \cdot 10^8$	$(1.84 \pm 1.63) \cdot 10^8$	-
Milky Way Core	10,000	170	0.01–10	$1.17 \cdot 10^1$	$1.31 \cdot 10^6$	$(1.54 \pm 0.91) \cdot 10^6$	-

Local Stellar Neighbourhood. We take the mass density to be $\hat{n} = 0.04\,\mathrm{M}_\odot\,\mathrm{pc}^{-3}$ (Bovy, 2017) and combine it with the average mass from our initial mass function (IMF) for the neighbourhood, $\sim 0.3\,\mathrm{M}_\odot$. We note that the typical velocities of local stars are comparable to Earth's orbital speed (Bailer-Jones et al., 2018).

Open Clusters. We consider an open cluster environment as it might be similar to the solar system's stellar environment during its formation phase. Generally considered to remain gravitationally bound for about 100 Myrs (Adams, 2010), the variety, size, and density of open clusters can vary a lot, though Pfalzner & Vincke (2020) provide constraints on a possible cradle for the Sun. They find that solar system equivalents are more likely to be produced in areas where stellar densities range from $5 \cdot 10^4\,\mathrm{pc}^{-3} < n_{\mathrm{local}} < 2 \cdot 10^5\,\mathrm{pc}^{-3}$. Since these densities are not necessarily typical of where stars spend the majority of their time in open clusters, Laughlin & Adams (1998) suggest that for clusters that resemble isothermal spheres, the effective stellar density is a factor ~ 10 smaller than the maximum central density of the cluster. Here, we adopt a commonly used stellar density of $n = 100\,\mathrm{pc}^{-3}$. Relative velocities in typical open clusters are comparable to Neptune's orbital speed (Adams, 2010; Malmberg et al., 2011).

Globular Clusters. We consider the expected perturbation strengths that a solar system analogue would experience in a globular cluster, even though stars in such environments indicate they may be too metal poor to form such an analogue (Fischer & Valenti, 2005; Nascimbeni et al., 2012) and too dynamically hostile to maintain such an analogue (Cai et al., 2019). Globular clusters are generally old (Krauss & Chaboyer, 2003) with small stars $\lesssim 0.85\,\mathrm{M}_\odot$ (Mann et al., 2019), thus have the most restrictive mass range out of the environments we considered. The velocity dispersion of globular clusters are similar to Jupiter's orbital speed (Pryor & Meylan, 1993; Mann et al., 2019). Additionally, the stellar density of globular clusters can vary by many orders of magnitude depending on the distance from the centre. We adopt a conservative static estimate representing a general distance $\sim 15\,\mathrm{pc}$ from the centre (Jiménez-Torres et al., 2013).

Milky Way Centre. Due to the extreme nature of the centre of the Milky Way, we follow the work of Jiménez-Torres et al. (2013) and divide the galactic centre into two regimes, the core (the inner 1 pc) and the bulge (some 300 pc from the core). The velocity dispersion in the galactic centre is much greater than any orbital velocity in the solar system (Jiménez-Torres et al., 2013; Valenti et al., 2018). As was shown by McTier et al. (2020), with such high densities and velocities, as many as 4 in 5 stars in the galactic centre experience a flyby within 1000 AU within 1 Gyr. We also show that flybys within this distance are common for systems in the galactic centre and show that they

are also likely to disrupt planetary systems.

Incorporating the stellar density n, cross-section σ, and velocity dispersion $\bar{v}$, we can define the encounter rate Γ as the rate in which stars enter a sphere of influence around the Sun (Adams, 2010):

$$\Gamma = n\sigma\bar{v}\,. \tag{4.1}$$

We use this equation to calculate the average time it takes until a star comes within a certain distance from the Sun. In the reference frame of the central star with mass m_c, a passing star with mass $m_\star$ begins with a relative velocity at infinity denoted by v_∞. If we consider the effects of gravitational focusing, the cross-section is (Binney & Tremaine, 2008; Malmberg et al., 2011; Portegies Zwart & Jílková, 2015)

$$\sigma = \pi q_\star^2 \left(1 + \frac{2G(m_c + m_\star)}{q_\star v_\infty^2}\right)\,, \tag{4.2}$$

where $q_\star$ is the impact parameter of the incoming star and G is Newton's gravitational constant. Note that for the vast majority of encounters, the impact parameter $b_\star$ or the velocity are large and thus $\sigma \approx \pi b_\star^2$.

4.2.2 One planet

We review the effects that a stellar flyby has on a binary. In our case the binary consists of a central star (the Sun) with mass m_c and one planet with mass m, semi-major axis a, and eccentricity e. For a passing star on a hyperbolic trajectory, the star's mass $m_\star$, eccentricity $e_\star$, impact parameter $b_\star$, relative velocity at infinity v_∞, and perihelion $q_\star$ are related by (e.g. Spurzem et al., 2009)

$$e_\star = \sqrt{1 + \left(\frac{b_\star v_\infty^2}{G(m_c + m + m_\star)}\right)^2} \quad \text{and} \quad q_\star = b_\star\sqrt{\frac{e_\star - 1}{e_\star + 1}}\,.$$

Like other authors, we focus on adiabatic encounters where the velocity of the perturbing star at perihelion is less than that of the outermost planet. We return to whether this is a good assumption below. The binding energy of the central star and the planet is given by

$$\varepsilon = -\frac{Gm_c m}{2a}\,. \tag{4.3}$$

The change in binding energy of a binary system from an adiabatic encounter by a star on a hyperbolic trajectory is given by (Roy & Haddow, 2003; Heggie, 2006; Spurzem et al., 2009)

$$\begin{aligned}\Delta\varepsilon = &-\frac{\sqrt{\pi}}{8} G\mathcal{M} f_1(e_\star)\frac{a^2}{q_\star^3} K^{5/2} \exp\left[-\frac{2K}{3} f_2(e_\star)\right] \\ &\cdot F(e, i_\star, \omega_\star, \Omega_\star, nt_0)\,,\end{aligned} \tag{4.4}$$

where

$$K = \sqrt{\frac{2(m_c + m)q_\star^3}{(m_c + m_\star + m)a^3}} \qquad \text{and} \qquad \mathcal{M} = \frac{m_c\, m_\star\, m}{m_c + m}\,.$$

The precise form of F can be found in Appendix 4.A. F takes into account the orientation of the perturbing star's orbit relative to the elliptical orbit of the planet and is of order unity. The functions $f_1(e_\star)$ and $f_2(e_\star)$ which depend on the eccentricity of the flyby star are also given in Appendix 4.A.

In the parabolic case $f_1(1) = f_2(1) = 1$.

The relative change in binding energy due to a flyby can be used to calculate the relative change to the planet's semi-major axis, $\Delta a/a \approx -\Delta\varepsilon/\varepsilon$[1]. This change in semi-major axis is what we refer to as the *perturbation strength* of the stellar flyby. We investigate the use of the angular momentum deficit (AMD) as an alternative metric in Appendix 4.B.

Averaging over the incident angles, we obtain the average perturbation strength due to a flyby from equation (4.3) and equation (4.4) so that

$$\left|\frac{\Delta a}{a}\right| \simeq \left|\frac{\sqrt{\pi}}{2}\frac{m_\star}{m_c + m + m_\star} f_1(e_\star) K^{1/2} \exp\left[\frac{-2K}{3} f_2(e_\star)\right]\right|. \tag{4.5}$$

Note the exponential dependence on the perihelion of the flyby star (or more accurately the ratio of $q_\star/a$). This implies that flybys will only have a significant effect if they come close, i.e. a distance comparable to the semi-major axis a. From here we can probe the dependence of perturbation strength on the three main characteristics of perturbing stars: mass $m_\star$; distance $b_\star$; and speed v_∞. As an example, a flyby in the solar neighbourhood with $b_\star = 1000\,\mathrm{AU}$, $m_\star = 0.1\,\mathrm{M}_\odot$, and $v_\infty = 40\,\mathrm{km\ s^{-1}}$ (so $q_\star \approx 999\,\mathrm{AU}$) will result in a relative change in the semi-major axis of Neptune of $|\Delta a/a| \approx 8.4 \cdot 10^{-7}$

We can obtain a more intuitive understanding of the importance of stellar flybys by calculating the average time it takes for an encounter with a specific perturbation strength to occur. To do that, we sample the various stellar environments following the Monte Carlo approach of Zink et al. (2020) where for each flyby star we sample a mass, velocity, and impact parameter along with a random orientation centred on the Sun. The initial mass function (IMF) we use to generate the stellar masses smoothly combines the IMF for single stars in equation (17) by Chabrier (2003) for stars less than one solar mass and the standard power-law IMF from Salpeter (1955) for stars above one solar mass. We sample stellar velocities from a Maxwell–Boltzmann distribution with a standard deviation $\bar{v}$ specific to the stellar environment (see Table 4.1). We sample impact parameters uniformly over the cross-sectional area. With $m_\star$, v_∞, and $b_\star$, we compute the analytical estimate for the change in semi-major axis of Neptune orbiting the Sun using equation (4.5). We then take a subset of these samples and numerically measure the perturbation strength with 3-body simulations using `REBOUND` (Rein & Liu, 2012) to compare against the analytic estimate. We compute a weighted histogram of the collected samples for both estimates, scaled according to the number of events expected in a given time. We then cumulatively integrate the total number of flybys together such that a given flyby of perturbation strength $|\Delta a/a|$ or greater is expected after a given time (similarly for a flyby of certain perihelion or closer). The results are shown in Fig. 4.1.

The left panel of Fig. 4.1 shows a comparison between analytical estimates and numerically measured perturbation strengths from stellar flybys for different environments. Because we assume adiabatic encounters, we can see the greatest discrepancy between analytical and numerical results for impulsive flybys more often found in the environments with the largest velocity dispersion. Note that the comparison between the analytical and numerical methods shows that for the majority of stellar environments the most frequent type of stellar flybys are in the adiabatic regime and result in very weak perturbations. The flybys in open cluster environments in particular are almost always adiabatic. The right panel of Fig. 4.1 shows the perihelia from stellar flybys for different

[1] This holds so long as the relative changes are small.

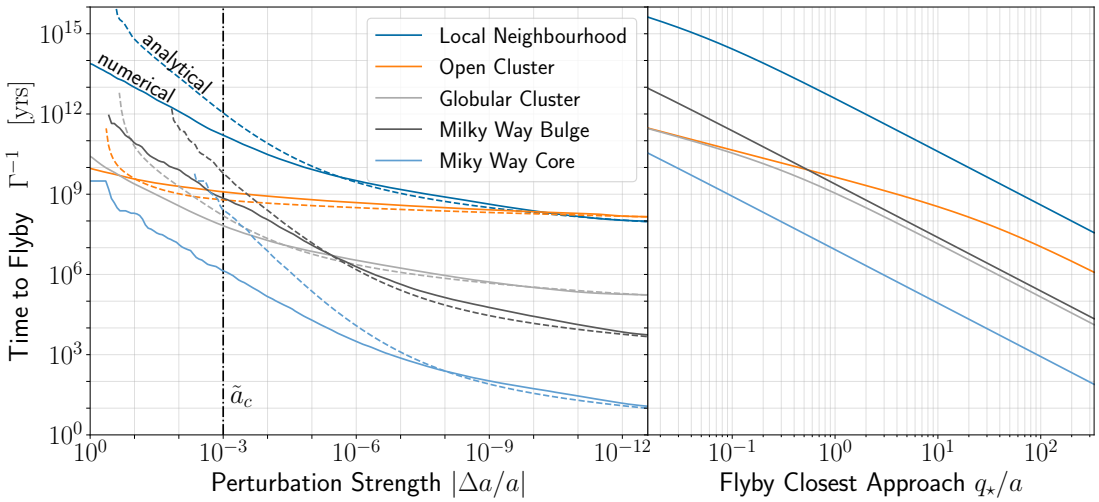

Figure 4.1: The average time until a stellar flyby occurs for various stellar environments. On the left panel, we plot the time as a function of perturbation strength. On the right panel, we use the more traditional perihelion distance of the perturbing star normalized to Neptune's semi-major axis. The solid lines on the left panel are numerically measured changes to Neptune's semi-major axis, whereas the dashed lines are analytical estimates. The vertical dashed line at $\tilde{a}_c = 10^{-3}$ indicates where the perturbations are strong enough to affect the solar system's long term stability (see Section 4.3.2).

environments, which is the inverse of equation (4.1).

Intuitively, the results in the left panel of Fig. 4.1 can be understood by considering the three main environment characteristics: n, $m_\star$, and $\bar{v}$. If we increase the density of the stellar region n (keeping everything else constant) then the likelihood of a flyby increases, thus translating the curve in the figure down. Similarly, if we increase the typical masses of the flyby stars $m_\star$, each individual perturbation would be more intense, translating the curve to the left. Finally, if we change the velocity dispersion of the stellar environment $\bar{v}$ this changes the shape of the curve, with a shallow curve indicative of a very low velocity dispersion and a steep curve representative of a very high velocity dispersion.

To summarise, Fig. 4.1 shows that the most common stellar flybys only cause weak perturbations to planetary systems. Furthermore, we can see that the adiabatic assumption is more accurate for weaker encounters. Finally, we can see that for secularly evolving systems, like the solar system, critical perturbations $|\Delta a/a| > 10^{-3}$ (see Section 4.3.2) are rare compared to the lifetime of the system. The numerical values for the rarity of these critical perturbations is also shown in the Single Flyby column of Table 4.1.

4.2.3 Successive flybys

We next consider the effects of stellar flybys on star-planet binary systems by simulating successive flybys to the same system. The importance of successive flybys on the resulting architecture of planetary systems has recently been shown in multiple studies (Cai et al., 2017; Stock et al., 2020). We begin with the same setup and Monte Carlo approach as Section 4.2.2 for a star-planet binary system where a Neptune-analogous planet orbits around a solar mass star. We simulate the evolution

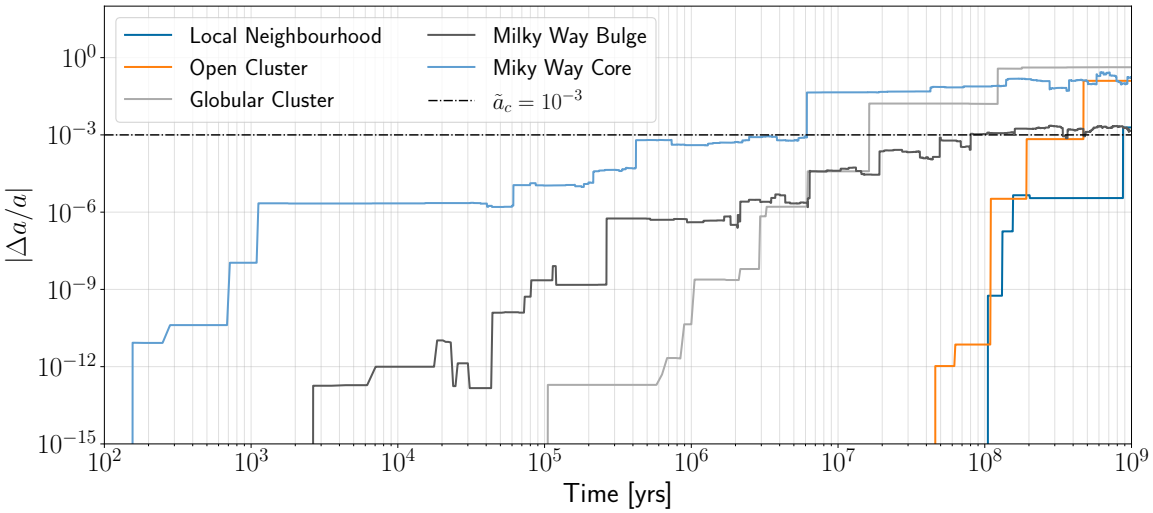

Figure 4.2: The impact of successive flybys on the binding energy (semi-major axis) of a Sun-Neptune system. The horizontal dashed line at $\tilde{a}_c = 10^{-3}$ indicates where the perturbations are strong enough to measurably affect the system's long-term stability (see Section 4.3.2). The most important feature is that the largest relative change is the most relevant. We also observe that the perturbation to the systems generally increase overtime and the effects are akin to Lévy flight.

of one planet orbiting a star for 1 Gyr. We divide the time into 1 Myr pieces and determine the number of flybys expected to occur for a given environment in each million years using equation (4.1). For each flyby that occurs, we randomly draw the three main characteristics of the perturbing stars (mass, velocity, and impact parameter) and simulate the flyby the same way we did in Section 4.2.2. We then assume that the resulting orbital parameters of the planet will remain constant until the next flyby and we repeat the processes of randomly drawing and simulating flybys for the duration of the 1 Gyr.

We simulate 1024 star-planet systems in each stellar environment and calculate the average time until $|\Delta a/a| > 10^{-3}$ has been reached. The results are in Table 4.1 under the Multiple Flybys column. When assuming that the star-planet system remains in an environment with a constant stellar density, the cumulative effects of successive flybys do not significantly change the expected time for a system to experience a critical level perturbation. A comparison between the columns in Table 4.1 for a single flyby and multiple flybys shows that on average, successive flybys increase the likelihood of a critical perturbation by at most about a factor of four (again, assuming a constant stellar density). This is because the effects of successive flybys are dominated by the most significant flybys. Note that this is consistent with the results shown in Fig. 4.1 which show that the kicks planetary systems experience are not all equal, but follow a distribution that includes rare but large kicks, reminiscent of a Lévy flight.

Fig. 4.2 shows one sample out of each set of 1024 simulations illustrating the typical evolution of the relative change in semi-major axis (compared to the original state) of a Neptune-like planet for each of the five stellar environments discussed above. The general trend for systems undergoing successive flybys is to deviate more and more from their initial state, but not in a purely random walk way where the effects grow as $\sqrt{t}$. The evolutionary paths for these systems are suggestive of a Lévy flight, with long periods of little change, interrupted by sudden jumps when a strong encounter

occurs (note the log-log scale). For dense environments, the systems are more quickly pushed from their initial states compared to less dense environments such as the Local Neighbourhood. Here we acknowledge some of the limitations of our approach for simulating successive flybys. Since we assume a constant stellar density throughout the entire 1 Gyr evolution, the particular path that a system might follow through a stellar environment will likely pass through more and less dense regions. This approach of adopting typical and conservative values for the parameters of each stellar environment does not take into account the continuity of stellar density. While this may change the overall likelihood by more than a factor of four, the qualitative features seen Fig. 4.2 remain the same. Mainly, the changes to the systems are dominated by the most significant flybys.

4.2.4 Two planets

Long-term variations of planetary orbits in the solar system are caused by the cumulative effects of planet-planet interactions, general relativity, tides, and other external perturbations. Because there are no significant mean motion resonances between the planets of the solar system, the dynamics (especially the inner planets) are dominated by secular dynamics, i.e. the shape of the orbits including semi-major axes, eccentricities, inclinations, perihelia, and ascending nodes, but not by the planets' phases. The frequencies of oscillations in perihelia (the rotation of the orbit in its orbital plane) and the ascending node (the rotation of the plane of the orbit in space) are referred to as secular frequencies. The dominant mechanism for instability in the solar system emerges from the overlap of secular resonances (see Section 4.3.3). For this reason, we will discuss how secular frequencies change if the solar system is perturbed by a flyby.

For a two planet system, with a semi-major axis ratio of the inner and outer planets $\alpha = a_1/a_2$, there are two secular modes associated with perihelion precession having eigenfrequencies (Murray & Dermott, 1999),

$$g_1 \simeq \frac{3}{4}\mu_2 n_1 \alpha^3 \quad \text{and} \quad g_2 \simeq \frac{3}{4}\mu_1 n_2 \alpha^2$$

assuming $\alpha \ll 1$, with reduced masses $\mu_1 = m_1/(m_c + m_2)$, $\mu_2 = m_2/(m_c + m_1)$, and mean motions $n_j^2 = G(m_c + m_j)/a_j^3$. With this dependence of the eigenfrequencies on the semi-major axes, we can determine the relative change in secular frequencies based on the change in semi-major axes of the planets. Namely,

$$\left|\frac{\Delta g_1}{g_1}\right| = \left|\frac{3}{2}\frac{\Delta a_1}{a_1} - 3\frac{\Delta a_2}{a_2}\right| \quad \text{and} \quad \left|\frac{\Delta g_2}{g_2}\right| = \left|2\frac{\Delta a_1}{a_1} - \frac{7}{2}\frac{\Delta a_2}{a_2}\right|.$$

Thus, we find that to first order $\Delta g/g \propto \Delta a/a$.

In the event of a flyby, the exponential dependence of a_j in equation (4.5) implies that $|\Delta a_j/a_j|$ will be smaller for the inner planet than for the outer planet. Therefore, the change in secular modes will be dominated by the changes to the semi-major axis of the outermost planet. Additionally, numerical studies involving stellar flybys have shown that changes to the architecture of a planetary system correlates with the number of planets and the initial semi-major axis of the outermost planet (Stock et al., 2022). Note that we now have a straightforward scaling relationship that goes from encounter parameters ($m_\star$, $b_\star$, v_∞) to $|\Delta g_j/g_j|$. As an example, consider a flyby in the solar neighbourhood with $b_\star = 1000\,\mathrm{AU}$, $m_\star = 0.1\,\mathrm{M}_\odot$, and $v_\infty = 40\,\mathrm{km\ s^{-1}}$. If we consider only Jupiter and Neptune, the relative change in secular frequencies is $|\Delta g/g| \approx 2.5 \cdot 10^{-6}$.

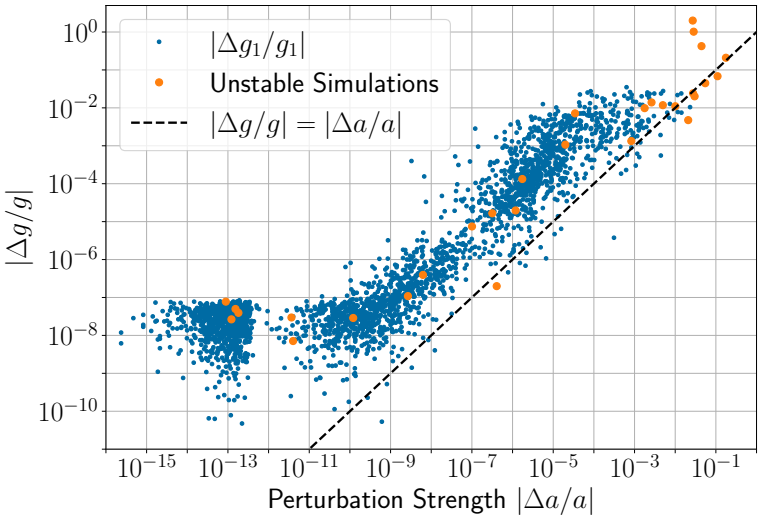

Figure 4.3: Changes to the secular mode g_1 as a function of the perturbation strength $\Delta a/a$, measured in Neptune's orbit. Perturbations with $\Delta a/a < 10^{-11}$ cannot be resolved due to finite floating point precision.

4.2.5 More than two planets

Above we have estimated the effects that a flyby has on the secular frequencies of a two planet system. We now consider the relative change in secular frequencies in the case of more than two planets. We will show with numerical simulations that stellar flybys cause relative changes to all secular modes on the same order of magnitude as the relative changes to Neptune's semi-major axis, i.e. $\Delta g_j/g_j \propto \Delta a_8/a_8$. Note that secular modes can never be exclusively associated with one single planet. So although one might refer to g_1 as Mercury's secular mode, it is really a mode of the entire solar system, and all modes are coupled to all planets.

To calculate the secular frequencies numerically, we follow the procedure developed by Laskar (1988, 1990, 1993, 2003) and known as modified frequency analysis. See also the work by Šidlichovský & Nesvorný (1996). We integrate an ensemble of 2880 stellar flybys to the solar system (for the precise numerical setup see Section 4.3). We measure the change in secular frequencies over 20 Myrs compared to an unperturbed case. The results are shown in Fig. 4.3.

One can see that the relationship between the relative change in g_1 and the numerically measured relative change in the semi-major axis of Neptune from stellar flybys (what we call the perturbation strength) is linear except where we reach the numerical floor at $\Delta a_8/a_8 < 10^{-11}$, and where the perturbations are of order unity. The other modes, $g_2, \ldots, g_8$ similarly show this linear behaviour. Thus, in spite of the rough estimates we made in Section 4.2, Fig. 4.3 shows that even though a stellar flyby is very unlikely to directly alter the orbit of Mercury in any significant way, secular interactions will eventually propagate perturbations of the outer planets' orbits to Mercury's orbit. The timescale for these changes to propagate from the outer planets to the inner planets is the secular timescale. The secular timescales for the solar system are in the hundreds of thousands to tens of millions of years (Lithwick & Wu, 2011). We note that changes in the secular frequencies can be calculated with high accuracy but this does not provide any immediate new insight into the physical state of the system for changes smaller than $\sim 10^{-4}$ (Rein et al., 2019a).

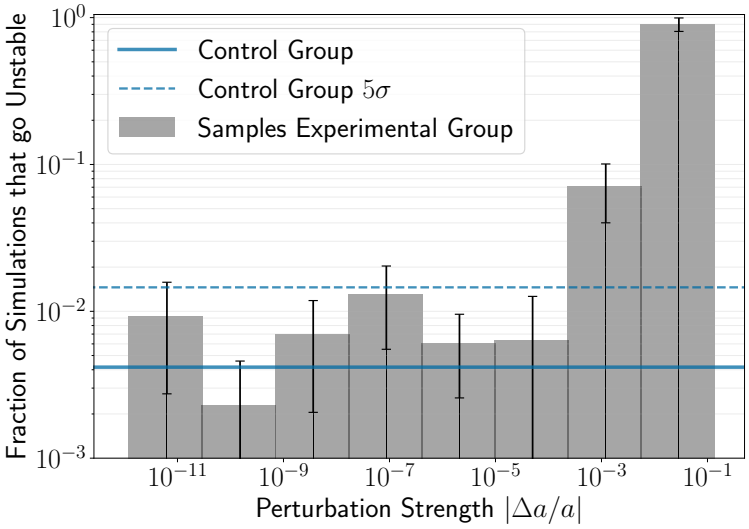

Figure 4.4: The fraction of simulations that lead to an instability before 5 Gyr grouped by perturbation strength $\Delta a/a$. For perturbation strengths larger than $\tilde{a}_c = 10^{-3}$ the fraction is significantly higher (more than 5σ) than in the control group.

4.3 Long-term stability

4.3.1 Numerical methods

For all our simulations, we use NASA JPL Horizons data at the J2000 epoch as initial conditions for the solar system (Sun and eight planets). We integrate simulations forward in time using `REBOUND` (Rein & Liu, 2012) and the Wisdom-Holman integrator Wisdom & Holman (1991) with symplectic correctors and the lazy implementation of the kernel method, `WHCKL` (Wisdom et al., 1996). This integrator is well suited to provide highly accurate results for secularly evolving systems (Rein et al., 2019b). We include general relativistic corrections with `REBOUNDx` (Tamayo et al., 2020a) using the `gr_potential` module. We used a fixed timestep of $dt = \sqrt{65} \approx 8.062$ days.

4.3.2 Solar system stability

In this section we present the stability results of an ensemble of 2880 long-term integrations of the solar system. Each simulation begins with a flyby star passing along on a random hyperbolic trajectory. The flybys are sampled from an open cluster environment and we record the perturbation strength for each of them. We then integrate the simulations for 4.8 Gyr, or until a collision or escape event occurs.

We divide the simulations into a control group, where the perturbations are too small to be resolved from numerical noise, and an experimental group, where relative perturbations range from numerical noise to near unity. From the control group, we find that 4 of the 960 simulations (0.42 per cent) ended with a Mercury–Venus collision because of a dramatic increase in the eccentricity of Mercury. Within the experimental group, we find that 26 of the 1920 simulations (1.35 per cent) ended in instability—20 were collisions between Mercury and Venus, one was a collision between Earth and Mars, two resulted in the escape of Uranus, two ended in the escape of Neptune, and one finished with the escape of Mercury. A more detailed breakdown of the results can be found in Appendix 4.C.

Let us consider more closely the effect of the different strengths of stellar flybys on the solar system. Fig. 4.4 shows the fraction of systems that go unstable as a function of the numerically measured perturbation strength, $\Delta a/a$. There is a clear qualitative change in the fraction of unstable simulations starting at around $|\Delta a/a| \simeq 10^{-3}$ when the fraction of unstable simulations is more than five standard deviations beyond the mean of the control group. We thus define the critical perturbation strength to be $\tilde{a}_c = 10^{-3}$. Perturbations stronger than $\tilde{a}_c$ can significantly alter the dynamical state of the solar system in a way that affects its long-term stability. On the other hand, the solar system appears to be robust to perturbations of less than $\tilde{a}_c$ as they do not significantly alter the probability of an instability occurring.

Note that nearly 100 per cent of the simulations go unstable around $|\Delta a/a| \simeq 10^{-1}$, corresponding to Neptune's semi-major axis changing by about 3 AU. Our analytic approximations break down in that regime as the perturbations are no longer weak. An example of a flyby in the solar neighbourhood that results in this strong of a perturbation would be $m_\star = 1\,\mathrm{M}_\odot$, $b_\star = 250\,\mathrm{AU}$, and $v_\star = 20\,\mathrm{km\ s}^{-1}$ (so $q_\star \approx 245\,\mathrm{AU}$).

As we did not carry out any simulations beyond a collision or escape, the remaining systems could be stable for many billions of years, or could entirely destabilize (Laskar & Gastineau, 2009).

4.3.3 Secular resonances

As we've argued in Section 4.2.5, perturbations to the orbit of the outermost planet have effects on all secular frequencies. This is important because it can push planets in to or out of secular resonances with each other (Laskar, 2000; Zakamska & Tremaine, 2004). For example, a resonance involving the longitude of perihelion and the longitude of the ascending node of Earth and Mars has been identified as a possibly important secular resonance in the inner solar system (Laskar et al., 1992; Sussman & Wisdom, 1992; Lithwick & Wu, 2011). This resonance is related to the secular frequencies g_3 and g_4. These frequencies are already close to a commensurability in the present-day unperturbed solar system with a relative difference of only $\sim 3.1 \cdot 10^{-2}$ (Laskar et al., 2011; Rein et al., 2019a). In our long-term N-body simulations, we see correlations of secular resonances with eccentricity pumping and, eventually, planetary collisions. Another resonance, and in fact the one most correlated with instability in our simulations, is the g_1–g_5 secular resonance between Mercury and Jupiter (Mogavero & Laskar, 2021). When the solar system falls into this resonance, the eccentricity of Mercury increases on short timescales (Batygin et al., 2015).

To investigate this effect further we ran an additional 240 N-body simulations. We initialize these simulations by first integrating the present day solar system a random time (between 0 and 10,000 years) forward in time to randomize the orbital phases. Rather than perturbing the system with a flyby we artificially perturb the orbital elements of Neptune by a small amount. Each simulation is then integrated for 20 Myrs, or until a collision or escape event occurs.

In Fig. 4.5, we plot the resonant angle $[1, -1]$ which is related to the g_3 and g_4 secular frequencies (see Lithwick & Wu, 2011, for details) as a function of time and perturbation strength. We only show one angle for this illustration, but we note that other angles show very similar behaviour. In the unperturbed state (far left of the plot), the system is not in resonance in the first 20 Myrs as the angle is circulating. However, for larger perturbation strengths, the resonant angle can be pushed into a librating state, at least temporarily. This can be seen in the figure as the colour remains the same for an extended period of time compared to some of the neighbouring simulations which

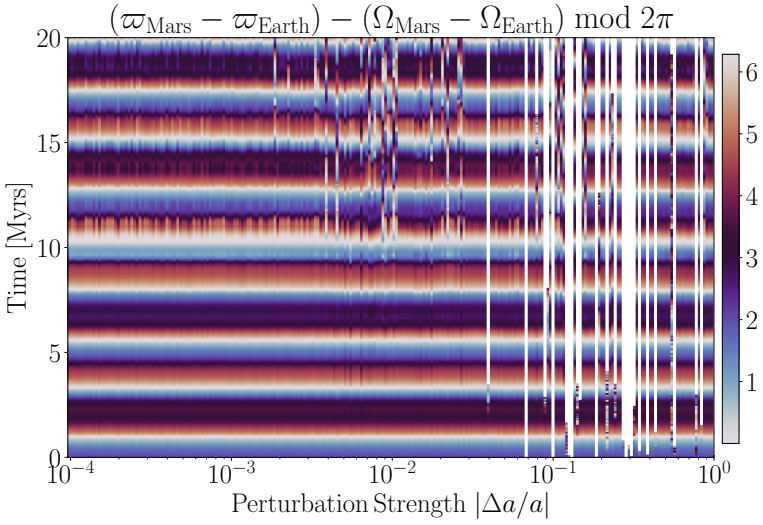

Figure 4.5: Secular resonant angle $[1, -1]$ between Earth and Mars (Lithwick & Wu, 2011) as a function of perturbation strength and time for 240 different simulations. Even on this timescale, small perturbation to Neptune's orbit of $\Delta a/a \gtrsim 10^{-3}$ can alter the resonant structure of the inner solar system. Almost instantaneous instability events (vertical white lines) can occur at $\Delta a/a \gtrsim 10$ per cent.

carry on normally. Fig. 4.5 shows that clear deviations from the normal secular structure of the solar system begin with relative changes around $\tilde{a}_c$ and become catastrophic around $|\Delta a/a| \simeq 10^{-1}$, consistent with the results from our long-term simulations. Furthermore, one can see that about half of the simulations in the range $10^{-1} \leq |\Delta a/a| \leq 10^{0}$ remain stable for the first 20 Myrs following the perturbation. Note that we are now in a highly non-linear regime. The perturbations change the secular dynamics of the solar system significantly and we expect many of the simulations which are stable on short timescales will destabilize after a few secular timescales as energy and angular momentum are exchanged through planet-planet interactions.

4.4 Discussion and Conclusions

In this paper, we explored the sensitivity of solar system stability due to weak perturbations such as those resulting from distant stellar flybys. Our numerical, long-term integrations show that the solar system's stability is not affected by perturbations as long as they change the planets' orbital parameters by less than 0.1 per cent ($\tilde{a}_c = 10^{-3}$). We showed that for stellar environments similar to our local neighbourhood, flybys with such perturbation strengths only occur once every 100 Gyr. However, for stars which are part of more dense environments, strong encounters are much more likely. We estimate that encounters with $\tilde{a}_c > 10^{-3}$ will occur during a system's lifetime and likely play an important role in shaping such planetary systems.

We also explored the evolution of star-planet systems within various stellar contexts as they undergo multiple successive flybys. The effects of successive flybys behave like a Lévy flight where the outcome is mostly set by the largest perturbation, rather than the cumulative effect of equal perturbations in a random walk. Thus, in most cases it is sufficient to consider only the strongest perturbation to see whether the stability of a system is affected.

We derived a set of equations which allow us to estimate the effects from a stellar flyby on the semi-major axes of planets and the secular frequencies of planetary systems. These estimates are working well for weak (or adiabatic) encounters, but break down for strong encounters. We've shown that all secular modes are affected during flybys, i.e. not only those typically associated with the

outer planets.

The solar system appears to be in a somewhat stable region of parameter space. The path to instability is ultimately determined by stochastic processes and chaos (Mogavero & Laskar, 2022). We argue that the critical perturbation strength to affect the long-term stability of the solar system is $\tilde{a}_c = 10^{-3}$. Perturbations stronger than $\tilde{a}_c$ lead to changes in the secular frequencies of the order of $\Delta g/g \approx 10^{-3}$. Such perturbations are strong enough to affect the secular dynamics and push planets in and out of resonances which ultimately changes the probability of the system going unstable. We note there is of course no one-to-one correspondence between changes to the secular frequencies and dynamical instability because of the chaotic nature of the system.

We also note that our study did not include stellar binaries, even though as many as half of stars are part of a binary system (Chabrier, 2003) and more work needs to be done to better estimate the occurrence rate of such encounters along with their impact on perturbation strength. We anticipate it would increase the strength of the perturbations by about 2 to 3.6 times (Li & Adams, 2015) and thus decrease the occurrence of a critical flyby in the Local Neighbourhood to about once every 64 to 75 Gyr. We also did not investigate the effects that Planet 9 (Batygin et al., 2019) would have on the solar system's stability in the context of a stellar flyby. Given its proposed distance from the Sun, we expect it to experience the largest relative change from a stellar flyby. However, we also expect the secular coupling between Planet 9 and the rest of the solar system to be weak.

Whereas our analytical estimates are general and apply to any planetary system, our numerical simulations focused on the solar system, the system for which we have the most accurate ephemeris. A natural direction for future work would be to look more closely at the effects of weak stellar flybys on exoplanet systems.

4.A Adiabatic change in energy from a stellar flyby

Here we present the conclusions of Roy & Haddow (2003) and Heggie (2006) for the change in energy of a binary star system due to the flyby of a third star. The authors assume a hard binary, or that the binding energy of the binary far exceeds the kinetic energy of the passing star. Although this traditional interpretation of a hard binary assumption is not consistent with planetary systems, the following analytical description for the change in energy of a star-planet system from a stellar flyby still holds for flybys in the adiabatic regime (see the discussion in Section 2.1 by Spurzem et al., 2009). The change in energy for a star-planet system due to an adiabatic flyby is given by equation (4.4). The functions $f_1(e_\star)$ and $f_2(e_\star)$ in that equation are

$$f_1(e_\star) = \frac{(e_\star + 1)^{3/4}}{2^{3/4}\, e_\star^2} \text{ and} \tag{4.6}$$

$$f_2(e_\star) = \frac{3}{2\sqrt{2}} \frac{\sqrt{e_\star^2 - 1} - \arccos(1/e_\star)}{(e_\star - 1)^{3/2}}\,. \tag{4.7}$$

For convenience, let us define the following functions of the planet's eccentricity e,

$$e_1 = J_{-1}(e) - 2eJ_0(e) + 2eJ_2(e) - J_3(e) \tag{4.8}$$

$$e_2 = J_{-1}(e) - J_3(e) \tag{4.9}$$

$$e_4 = J_{-1}(e) - eJ_0(e) - eJ_2(e) + J_3(e) \tag{4.10}$$

where J_n is the Bessel function of the first kind of order n. With that notation,

$$\begin{aligned}
F(e,&i_\star,\omega_\star,\Omega_\star,nt_0) = \\
&= e_1\{\sin(2\omega_\star + nt_0)\,[\cos(2i_\star) - 1] - \sin(2\omega_\star + nt_0)\cos(2i_\star)\cos(2\Omega_\star) - \\
&\quad - 3\sin(2\omega_\star + nt_0)\cos(2\Omega_\star) - 4\sin(2\Omega_\star)\cos(2\omega_\star + nt_0)\cos(i_\star)\} + \\
&+ e_2(1-e^2)\{\sin(2\omega_\star + nt_0)\,[1 - \cos(2i_\star)] - \sin(2\omega_\star + nt_0)\cos(2i_\star)\cos(2\Omega_\star) - \\
&\quad - 3\sin(2\omega_\star + nt_0)\cos(2\Omega_\star) - 4\cos(2\omega_\star + nt_0)\sin(2\Omega_\star)\cos(i_\star)\} + \\
&+ e_4\sqrt{1-e^2}\{-2\cos(2i_\star)\cos(2\omega_\star + nt_0)\sin(2\Omega_\star) - \\
&\quad - 6\cos(2\omega_\star + nt_0)\sin(2\Omega_\star) - 8\cos(2\Omega_\star)\sin(2\omega_\star + nt_0)\cos(i_\star)\}\,,
\end{aligned} \tag{4.11}$$

where $n = \sqrt{G(m_c + m)/a^3}$ is the mean motion of the planet and t_0 is the time of pericentric passage of the planet where $t = 0$ is when the flyby star passes perihelion. The angles $\omega_\star, \Omega_\star$, and $i_\star$ are defined for the flyby star with respect to the orientation of the star-planet system and are laid out in detail in equation (18) by Roy & Haddow (2003). Using the fact that the planet's semi-minor axis b is related to its semi-major axis a by $b = a\sqrt{1-e^2}$, we recover equation (11) from Heggie (2006).

4.B Angular momentum deficit

The angular momentum deficit (AMD) of a multi-planet system is a measure of how eccentric and inclined the orbits of the planets are compared to a hypothetical system with the same mass and semi-major axis arrangement, but with circular, co-planar orbits. For an N-planet system in heliocentric coordinates, the AMD is defined as (Laskar, 2000)

$$C = \sum_{j=1}^{N} m_j\sqrt{Gm_c a_j}\left(1 - \cos i_j\sqrt{1-e_j^2}\right) \tag{4.12}$$

where the planetary inclinations i_j are defined with respect to the plane of the total angular momentum. The measure of AMD can be used to determine stability, where a system is termed AMD-stable if the amount of AMD is insufficient to permit planet-planet collisions (Laskar & Petit, 2017).

In Fig. 4.6 we plot the relative difference to the AMD $\Delta C/C$ versus the relative difference to Neptune's semi-major axis $\Delta a/a$, similar to Fig. 4.3. Although the AMD is slightly more sensitive at very small perturbation strengths ($\Delta a/a \lesssim 10^{-11}$), we find no difference in using the AMD to predict the long-term stability of the solar system compared to using the changes in the semi-major axis of Neptune. This might not be surprising, given the solar system in its current state is already AMD-unstable (Tamayo et al., 2020b). The criterion for AMD-stability only indicates a worst-case scenario, whereas the probability of the solar system being long-term stable is ultimately determined

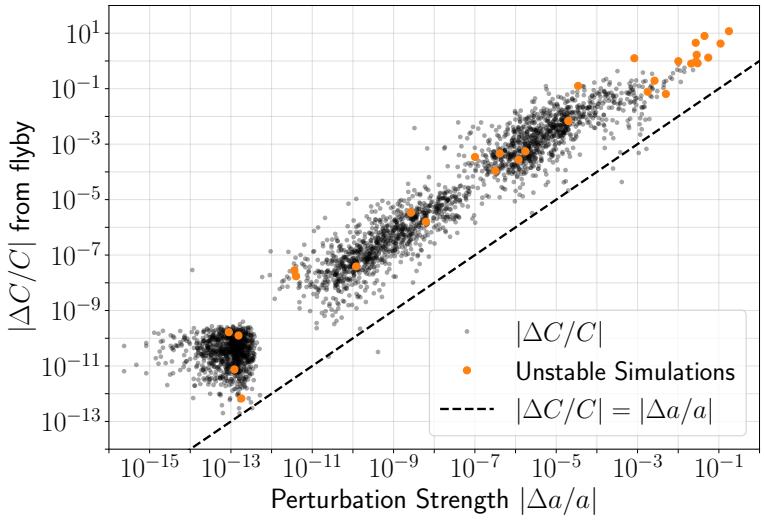

Figure 4.6: Relative changes to the angular momentum deficit (AMD) of the entire solar system (Sun and eight planets) $\Delta C/C$ as a function of the perturbation strength $\Delta a/a$, measured in Neptune's orbit all due to stellar flybys.

by secular dynamics. This is why in the main paper, we decided to measure changes to semi-major axes and then relate them to changes in secular frequencies.

4.C Details of numerical results

Fig. 4.7 shows the cumulative number of simulations that go unstable with respect to the time that the instability event occurs. There were 2880 simulations in total and 30 instability events. For all of the 24 events that were collisions between Mercury and Venus, there is a consistent correlation between a g_1–g_5 Mercury-Jupiter resonance and an increase in the eccentricity of Mercury preceding its collision with Venus. All 4 of the 960 simulations in the control group and 20 of the 1920 simulations in the experimental group ended with a Mercury–Venus collision. The timing of these Mercury–Venus collisions are spread throughout the remaining lifetime of the solar system, but there is a concentration of them around 3.5–4.5 Gyr.

There was one simulation that ended with a collision between Earth and Mars and there is correlational evidence suggesting that the collision was preceded by an Earth–Mars secular resonance that pumped the eccentricities of both planets leading to a collision. The remaining five events were escapes—Uranus twice, Neptune twice, and Mercury once. These early escapes of Uranus and Neptune are consistent with previous studies involving strong perturbations from stellar flybys (Malmberg et al., 2011; Stock et al., 2020). The Uranus escapes were the result of extremely large perturbations from the flyby star which dramatically increased the eccentricity of Uranus and led to a close encounter with Saturn. The Neptune escapes followed from a close encounter with Uranus and correlation evidence suggests that the close encounter was enabled by a series of eccentricity pumping from secular resonances with Uranus. The path to Mercury's escape was complicated and is very difficult to disentangle. We find correlations between various resonances on and off in different ways with many of the other planets coinciding with increases in Mercury's eccentricity and inclination. All of this precedes Mercury experiencing a close encounter with the Sun and subsequent ejection from the system. Further investigation should be done into the correlations between secular

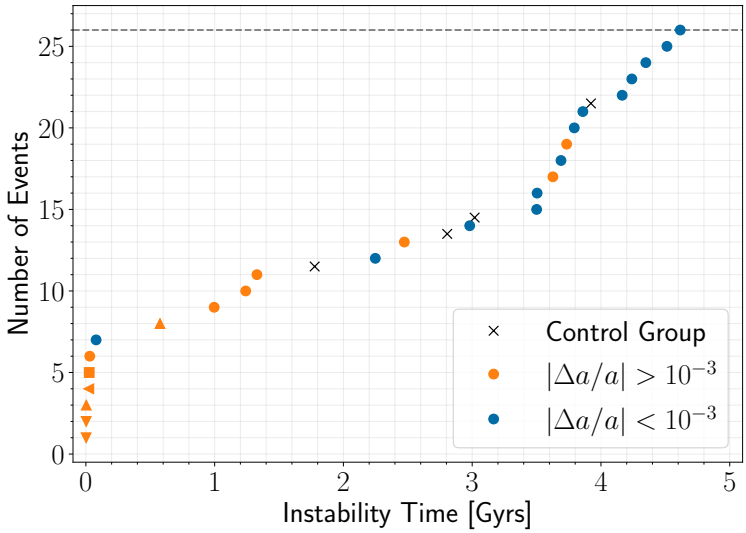

Figure 4.7: All events that triggered the simulations from Section 4.3.2 to end before 5 Gyr. The color indicates if the initial perturbation is smaller or larger than $\tilde{a}_c = 10^{-3}$. The 24 events that were collisions between Mercury and Venus are indicated by circles (◯) for the experimental group and crosses for the control group (×). The square (□) indicates a collision between Earth and Mars. The triangles indicate when the instability event was due to an escape rather than a collision. The triangle orientations indicate which planet escaped: Neptune (△), Uranus (▽), and Mercury (◁).

resonances and eccentricity pumping within these simulations as the causal link to instability.

Acknowledgments

We are very grateful to Maxwell Xu Cai for a helpful review which significantly improved the substance and quality of this paper. We would like to thank Scott Tremaine, Sam Hadden, Dan Tamayo, and Nathan Sandholtz for useful discussions. This research has been supported by the NSERC Discovery Grants RGPIN-2014-04553 and RGPIN-2020-04513. This research was made possible by the open-source projects `Jupyter` (Kluyver et al., 2016), `iPython` (Pérez & Granger, 2007), `matplotlib` (Hunter, 2007; Droettboom et al., 2016), and `GNU Parallel` (Tange, 2022). This research was enabled in part by support provided by the Digital Research Alliance of Canada (formerly Compute Canada; alliancecan.ca). Computations were performed on the Niagara supercomputer (Loken et al., 2010; Ponce et al., 2019) at the SciNet HPC Consortium (scinethpc.ca). SciNet is funded by: the Canada Foundation for Innovation; the Government of Ontario; Ontario Research Fund - Research Excellence; and the University of Toronto.

Chapter 5

Conclusions

Advancements in understanding the motion of the planets have been driven by improvements to both mathematical models and physical insight (Kepler, 1609; Newton, 1687; Laplace, 1775; Lagrange, 1776; Einstein, 1915, to highlight a few). Additionally, the availability of fast and programmable computers have enabled an exploration of the intractable N-body problem, assisted by algorithmic and implementation enhancements (Poincaré, 1899; Wisdom & Holman, 1991; Rein & Tamayo, 2015). Together, the advancements in mathematical models and availability in computing power have enabled this work on the long-term stability of the solar system.

The general focus of this work has been on the impact of flyby encounters on the solar system, offering a substellar-mass flyby encounter as a possible explanation for the origins of the secular modes (Chapter 2) and providing estimates on how likely it will be for a flyby to impact the future long-term stability of the solar system (Brown & Rein, 2022, Chapter 4). Futhermore, this work employed the long-term stability of the solar system as a mechanism for understanding possible changes to the general theory of relativity over billions of years (Brown & Rein, 2023, Chapter 3). The common thread throughout this work is the interplay between the secular modes of the solar system, particularly the dominant path to instability resulting from a linear secular resonance between Mercury and Jupiter (Laskar et al., 1992; Sussman & Wisdom, 1992). This interplay is explored in the context of the origins of the secular modes, the role of general relativity in influencing the Mercury–Jupiter resonance, and the potential impact of stellar flybys on both the secular modes and the long-term stability of the solar system. Additional contributions to numerical methods have also resulted from this work (Rein et al., 2019; Rein et al., 2019a,b; Brown & Rein, 2020).

In Chapter 2, this work showed that the likelihood that a substellar flyby could produce the secular architecture of the solar system is at best 1 in 1000. We determined this likelihood by simulating flyby encounters of the gas giants, drawing flyby parameters from an open star cluster environment, but most importantly, by investigating the overlooked regions of parameter space that include substellar-mass objects and encounters with extremely close perihelia. This 1-in-1000 likelihood changes based on how long the solar system remains in the open star cluster, how dense the cluster is, and the formation rate of substellar-mass objects, but we emphasize that this explanation for the secular modes is surprisingly efficient. We also introduced a novel application of the log-spectral distance to construct a metric that ranks how close the secular architecture of a flyby system is to the solar system.

In Chapter 3, this work reconfirmed, in a novel way, that including general relativistic corrections to Newtonian models of the solar system are necessary for achieving accurate, long-term solar system integrations (Laskar & Gastineau, 2009). In particular, we showed that the expected instability rate of the solar system (defined as a Mercury–Venus collision) can be modelled with a Fokker–Plank, advection–diffusion model. To show this, we used an ensemble of solar system simulations, each with a unique changing rate of general relativistic corrections to the perihelion precession of the planets. We did this not because we think this is something that will occur in the real solar system, but because it offers a way to experiment with this dynamical system in a controlled way. Thus, we showed that our advection–diffusion model can naturally explain the case of a time-varying general relativistic precession remarkably well without the introduction of any new free parameters.

In Chapter 4, this work showed that weak perturbations to the solar system from stellar flybys can lead to an increased chance of instability over the lifetime of the solar system. We showed this by running thousands of long-term solar system integrations for 5 Gyr beyond a stellar flyby event. It was also shown that successive flybys are less important than a single, larger perturbation. Indeed, the perturbations from stellar flybys are akin to a Lèvy flight, that is most alterations are small with the occasional large change. This work also was able to show that changes to secular modes from perturbations to Neptune can be detected and can impact the stability of the terrestrial planets. Additionally, as the time to an instability in the solar system is on the order of the expected lifetime of the system, this places the solar system on the edge of instability (Mogavero et al., 2023; Tamayo, 2023). Whether the result of a previous instability (Tremaine, 2023), or something else, we showed that in spite of this closeness to instability, the solar system is generally in a stable region of parameter space that is robust to perturbations from stellar flybys.

Future Work

The possibility of a substellar flyby encounter as the origin of the secular modes of the solar system provides an exceptional jumping-off point for future work. A more comprehensive investigation into the effects of substellar flybys on the entire solar system may reveal flyby parameters that provide even clearer matches with the solar system's architecture. Considering the effectiveness of substellar-mass flybys over stellar-mass flybys on producing the secular modes of the solar system, a focused study including all eight planets may provide tighter constraints on possible flyby candidates.

Additionally, this work submits that a substellar encounter deep within the solar system is not unlikely. Since many of the flyby candidates that pass between 1–10 AU successfully produce solar system–like architectures, an exploration into the impact of a substellar-mass object passing through a cold asteroid belt would reveal whether any lasting signatures of the flyby would remain after millions of years. An over-excited or depleted asteroid belt would provide additional constraints on the possibility of a substellar flyby as the origin of the secular modes. In a similar way, an investigation into the impact of a substellar flyby on the trans-Neptunian objects (TNOs) would provide additional constraints. The distribution of TNOs provides strong evidence of a stellar flyby encounter with the young solar system (Pfalzner et al., 2024). The preliminary work shown in Section 2.4.3 indicates that even a substellar flyby may be able to produce some of the features of the TNOs. However, a more thorough investigation is needed. Also, the likelihood of both a stellar flyby and a substellar flyby would certainly be less than only one flyby, but the uniqueness of the

solar system does not preclude any number of rare events occurring throughout its history.

This work also provides data and methodology that may be used to explore the relationships between flyby encounters and the secular modes in general. A perturbative understanding regarding changes to the secular modes may be gleaned from a deeper analysis of the data. Specific questions concerning the relative phases of the planets when the flyby is at perihelion and the amplitudes of the secular modes, or relationships between the incident angles and the phases of the secular modes, may expose means for inferring a flyby candidate that more closely matches the architecture of the solar system without expensive N-body integrations.

This work proposes a novel use of the log-spectral distance (Gray & Markel, 1976; Rabiner & Juang, 1993, see also equation (2.1)) to build a metric $\mathcal{M}$, defined in equation (2.4), that determines the similarity between two planetary systems. While the metric proved very useful in the case of the giant planets, there were clear shortcomings when the metric was applied to the entire solar system. Additional research into an improved implementation of the metric, or an alternative metric that ranks similarity between two planetary systems, would be beneficial to the community. Since the dominant frequencies associated with the dynamics of the solar system are within $\pm 30''$/yr, a suggested starting point is to add a low-pass filter. This is because the metric $\mathcal{M}$ equally considers all frequency values. Reducing the importance of the highest frequency values may provide a better comparison. However, this may not be broadly applicable and may not transfer if $\mathcal{M}$ is used for planetary systems other than the solar system. Additionally, a study on the effect of sample spacing, windowing functions, and window lengths to understand the impact that aliased frequencies and numerical artifacts may have on the ranking would be reassuring.

Following Brown & Rein (2023) where we modelled the instability of the solar system with a Fokker–Planck, advection–diffusion model, Abbot et al. (2024) reported on the use of a subdiffusion model that more accurately reproduces the instability statistics seen in N-body results (Abbot et al., 2022), especially for earlier instability times. While these improvements provide better results over the expected remaining life of Mercury ($\sim$5 Gyr), the remarkable results of Brown & Rein (2023) are that the Fokker–Planck, advection–diffusion model works surprisingly well without introducing any additional parameters. However, the questions brought up by Abbot et al. (2024) remain unanswered. Therefore, we also suggest further research into whether or not the instability times of planetary systems, in general, are better modelled by a subdiffusive process compared to a diffusive process. This exploration would aid in determining why the g_1 secular mode seems to subdiffuse rather than diffuse (Abbot et al., 2024). Additional work into a physical cause for the restoring upper boundary of the g_1 mode may partially be answered by the work of Mogavero et al. (2023); however, a more thorough and specific investigation is needed (Abbot et al., 2024).

In pursuit of a different question, Raymond et al. (2024) reconfirmed the general results of Brown & Rein (2022). Namely, stellar flybys that lead to larger changes in Neptune's semi-major axis correlate with systems that are more likely to go unstable. However, there are two shortcomings in this comparison. First, Raymond et al. (2024) did not integrate the remaining main sequence–time of the Sun following the flyby, meaning that extending the integrations to 5 Gyr might reveal additional instabilities. Second, the number of systems in Brown & Rein (2022) where $|\Delta a/a| > 10^{-3}$ for Neptune is much lower compared to the rest of their dataset. Furthermore, when Brown & Rein (2022) selected flybys to use in their study, they did not know a priori whether or not there was a critical threshold that would impact stability. Therefore, we suggest that a reproduction of the work

focused more on the parameters around the threshold region would clarify some of the uncertainties in the results. Additionally, a study of this kind may also explore how the amplitudes of the secular modes change following weak flybys (see Chapter 2). Changes to the amplitudes of the secular modes may be more directly related to the increase in instability than changes to the frequency values (see Chapter 3). Finally, an exploration emphasizing binary flybys may also reveal whether or not the increase in instability is different by the anticipated factor of $\sim$3.

Additional questions arose throughout the work of Chapter 2. The suggestion to consider the giant planets at semi-major axes different from what is observed today relates to the expectation that planetary systems form in more compact configurations due to migration within a protoplanetary disk (Armitage, 2020). With this in mind, an investigation into the effect of flybys on systems in mean motion resonance (MMR) could lead to a flyby as a triggering event to the planet-planet scattering proposed by solar system formation hypotheses (Tsiganis et al., 2005; Morbidelli et al., 2007; Nesvorný & Morbidelli, 2012; Raymond et al., 2020; Nesvorný, 2018; Clement et al., 2021; Griveaud et al., 2024). Moreover, analytical understandings of the impact of stellar flybys on stellar-binary systems is much more extensive (Heggie, 1975; Heggie & Rasio, 1996; Roy & Haddow, 2003; Heggie, 2006) than the analytical derivations for the impact of flybys on star-planet systems (Spurzem et al., 2009; Malmberg et al., 2011), with only semi-analytical explorations of the impact of flybys on multi-planet systems (Rodet & Lai, 2022). Our expectations from this work suggest that flyby-planet interactions can be modelled for each planet independently when the perturbations with the flyby object are greater than the planet-planet perturbations. However, planets in MMRs interact more quickly than secularly interacting planets, possibly reducing the ability for a flyby object to alter the eccentricities, inclinations, or semi-major axes of the planets. Furthermore, there is also a need for the extension to hyperbolic flybys for the results in the appendix of Malmberg et al. (2011) on the effect of stellar flybys on the inclinations of planets.

Closing Remarks

The contributions of this work to the long-term stability of the solar system are a modest addition to the ongoing exploration of planetary dynamics within our own system and beyond. The intricacies of secular dynamics, while often baffling, have proven to be both rewarding and intellectually stimulating. Moreover, the opportunity to delve into innovative numerical methods has been a source of great pleasure and professional satisfaction.

I acknowledge the privilege of dedicating years of my life to the pursuit of fundamental knowledge, even if its immediate applications to humanity's pressing concerns may be limited. It is my hope that this work serves as a solid foundation for future research and, at the very least, a tangible testament to humanity's natural and enduring curiosity about the cosmos.

Appendix A

AIRBALL

`AIRBALL` (Brown et al., 2024) is a package for running and managing flybys using `REBOUND` (Rein & Liu, 2012). It is an extension to `REBOUND`, the popular, open-source, N-body integrator. `AIRBALL` provides logic for handling the geometry of adding, running, and removing a flyby object in a `REBOUND` simulation, stellar environments for generating and managing randomly generated stars from different stellar environments throughout the galaxy, initial mass functions for quickly generating samples from probability distributions, `Astropy.units` integration to help manage the mess of units and scales, and interactive examples for teaching and exploring `AIRBALL`'s functionality. For the latest details regarding the source code, API, and interactive examples, please visit `https://airball.readthedocs.io/`.

`AIRBALL` has been written to provide a reproducible framework for flyby simulations. Many papers simulating flyby encounters describe how the flybys are simulated, but do not provide reference code. The combination of unintuitive geometries and coordinate systems can make reproducing a flyby scenario practically impossible. Additionally, `AIRBALL` enables inexperienced individuals to avoid unknown pitfalls that range from choosing an appropriate starting (and ending) distance for the flyby object, to knowing when to call `sim.ri_whfast.recalculate_coordinates_this_timestep = 1`, to correctly sampling flyby parameters isotropically. The development of `AIRBALL` is ongoing. One major extension could be to include a framework for managing and handling binary flyby encounters. Another improvement would be to add time-evolving stellar densities to the `StellarEnvironment` class.

Bibliography

Abbot, D. S., Hernandez, D. M., Hadden, S., et al. 2022, arXiv e-prints, arXiv:2212.14844. https://arxiv.org/abs/2212.14844 28, 30, 38, 57

—. 2023, ApJ, 944, 190, doi: 10.3847/1538-4357/acb6ff 6

Abbot, D. S., Webber, R. J., Hadden, S., Seligman, D., & Weare, J. 2021, ApJ, 923, 236, doi: 10.3847/1538-4357/ac2fa8 28, 30, 38, 40

Abbot, D. S., Webber, R. J., Hernandez, D. M., Hadden, S., & Weare, J. 2024, ApJ, 967, 121, doi: 10.3847/1538-4357/ad3e5f 57

Adams, F. C. 2010, ARA&A, 48, 47, doi: 10.1146/annurev-astro-081309-130830 10, 12, 20, 22, 41, 42

Adams, F. C., & Myers, P. C. 2001, ApJ, 553, 744, doi: 10.1086/320941 20

Applegate, J. H., Douglas, M. R., Gursel, Y., Sussman, G. J., & Wisdom, J. 1986, AJ, 92, 176, doi: 10.1086/114149 5, 6

Armitage, P. J. 2020, Astrophysics of planet formation, 2nd edn. (Cambridge, UK: Cambridge University Press) 10, 11, 58

Arnol'd, V. I. 1963, Russian Mathematical Surveys, 18, 9, doi: 10.1070/RM1963v018n05ABEH004130 4, 29

Artymowicz, P. 1992, PASP, 104, 769, doi: 10.1086/133051 10, 11

Babb, S. E. 1977, Isis, 68, 426. http://www.jstor.org/stable/231318 1

Bailer-Jones, C. A. L., Rybizki, J., Andrae, R., & Fouesneau, M. 2018, Astronomy & Astrophysics, 616, A37, doi: 10.1051/0004-6361/201833456 41

Battinelli, P., & Capuzzo-Dolcetta, R. 1991, MNRAS, 249, 76, doi: 10.1093/mnras/249.1.76 20

Batygin, K., Adams, F. C., Batygin, Y. K., & Petigura, E. A. 2020, AJ, 159, 101, doi: 10.3847/1538-3881/ab665d 20

Batygin, K., Adams, F. C., Brown, M. E., & Becker, J. C. 2019, Physics Reports, 805, 1, doi: 10.1016/j.physrep.2019.01.009 51

Batygin, K., & Laughlin, G. 2008, The Astrophysical Journal, 683, 1207 6, 28

Batygin, K., Morbidelli, A., & Holman, M. J. 2015, ApJ, 799, 120, doi: 10.1088/0004-637X/799/2/120 30, 49

Baum, R., & Sheehan, W. 1997, In search of planet Vulcan : the ghost in Newton's clockwork universe (New York: Plenum Press) 4

Binney, J., & Tremaine, S. 2008, "Galactic Dynamics: Second Edition" (Princeton, NJ: Princeton University Press) 12, 42

Blanes, S., Casas, F., Farrés, A., et al. 2013, Applied Numerical Mathematics, 68, 58, doi: https://doi.org/10.1016/j.apnum.2013.01.003 7

Bovy, J. 2017, Monthly Notices of the Royal Astronomical Society, 470, 1360, doi: 10.1093/mnras/stx1277 41

Brasser, R., Duncan, M. J., & Levison, H. F. 2006, Icarus, 184, 59, doi: 10.1016/j.icarus.2006.04.010 10, 12, 22

Brouwer, D., & Clemence, G. M. 1961, Methods of celestial mechanics (New York: Academic Press) 10, 11, 17

Brown, G., & Rein, H. 2020, Research Notes of the American Astronomical Society, 4, 221, doi: 10.3847/2515-5172/abd103 6, 14, 15, 40, 55

—. 2022, Monthly Notices of the Royal Astronomical Society, 515, 5942, doi: 10.1093/mnras/stac1763 10, 12, 20, 21, 22, 30, 38, 39, 55, 57

—. 2023, MNRAS, 521, 4349, doi: 10.1093/mnras/stad719 19, 27, 55, 57

Brown, G., Rein, H., Mohsin, H., et al. 2024, AIRBALL: a package for running and managing flybys using REBOUND, https://airball.readthedocs.io/ 8, 13, 26, 59

Butcher, J. 1996, Applied Numerical Mathematics, 20, 247, doi: https://doi.org/10.1016/0168-9274(95)00108-5 4

Cai, M. X., Kouwenhoven, M. B. N., Zwart, S. F. P., & Spurzem, R. 2017, Monthly Notices of the Royal Astronomical Society, 4353, 4337, doi: 10.1093/mnras/stx1464 10, 12, 40, 44

Cai, M. X., Portegies Zwart, S., Kouwenhoven, M. B. N., & Spurzem, R. 2019, Monthly Notices of the Royal Astronomical Society, 489, 4311, doi: 10.1093/mnras/stz2467 41

Chabrier, G. 2003, Publications of the Astronomical Society of the Pacific, 115, 763, doi: 10.1086/376392 12, 43, 51

Chabrier, G., & Lenoble, R. 2023, ApJ, 944, L33, doi: 10.3847/2041-8213/acadd3 12, 20

Chan, M. H., & Lee, C. M. 2023, MNRAS, 518, 6238, doi: 10.1093/mnras/stac3509 28

Chirikov, B. V. 1979, Phys. Rep., 52, 263, doi: 10.1016/0370-1573(79)90023-1 7

Clement, M. S., Raymond, S. N., Kaib, N. A., et al. 2021, Icarus, 355, 114122, doi: 10.1016/j.icarus.2020.114122 10, 11, 22, 58

Clerke, A. M. 1902, A popular history of astronomy during the nineteenth century, 4th edn. (London: A. and C. Black) 4

Cohen, C. J., & Hubbard, E. C. 1965, AJ, 70, 10, doi: 10.1086/109674 5, 6

Cohen, C. J., Hubbard, E. C., & Oesterwinter, C. 1973, Celestial Mechanics, 7, 438, doi: 10.1007/BF01227509 5

Cromer, A. 1981, American Journal of Physics, 49, 455, doi: 10.1119/1.12478 4

De Vogelaere, R. 1956, Methods of Integration which Preserve the Contact Transformation Property of the Hamilton Equations, Tech. rep., University of Notre Dame, doi: 10.7274/24733422.v1 5

Donnelly, D., & Rogers, E. 2005, American Journal of Physics, 73, 938, doi: 10.1119/1.2034523 5

Dotti, F. F., Kouwenhoven, M. B., Cai, M. X., & Spurzem, R. 2019, Monthly Notices of the Royal Astronomical Society, 489, 2280, doi: 10.1093/mnras/stz2346 40

Droettboom, M., Hunter, J., Caswell, T. A., et al. 2016, matplotlib: matplotlib v1.5.1, doi: 10.5281/zenodo.44579 26, 38, 54

Eckert, W. J., Brouwer, D., & Clemence, G. M. 1951, Astronomical papers prepared for the use of the American ephemeris and nautical almanac ; v. 12, 12, 1 5, 6

Eddington, A. S. 1923, The mathematical theory of relativity (The University Press) 4, 28

Einstein, A. 1915, Sitzungsberichte der Königlich Preußischen Akademie der Wissenschaften, 844 4, 28, 55

Elmegreen, B. G., & Clemens, C. 1985, ApJ, 294, 523, doi: 10.1086/163320 20

English, N. 2011, The Refracting Telescope: A Brief History (New York, NY: Springer New York), 3–20, doi: 10.1007/978-1-4419-6403-8_1 4

Euler, L. 1768, Institutionum calculi integralis, volumen primum (St. Petersburg: Imperial Academy of Sciences) 4

Feuchter, C. A. 1984, Sky & Telescope, 67, 358 5, 6

Fischer, D. A., & Valenti, J. 2005, The Astrophysical Journal, 622, 1102, doi: 10.1086/428383 41

Gingerich, O. 1985, Vistas in Astronomy, 28, 339, doi: https://doi.org/10.1016/0083-6656(85)90044-3 2, 3

Girard, T. M., Grundy, W. M., Lopez, C. E., & van Altena, W. F. 1989, AJ, 98, 227, doi: 10.1086/115139 12

Goldreich, P., & Tremaine, S. 1980, ApJ, 241, 425, doi: 10.1086/158356 10, 11

Gray, A., & Markel, J. 1976, IEEE Transactions on Acoustics, Speech, and Signal Processing, 24, 380, doi: 10.1109/TASSP.1976.1162849 13, 57

Griveaud, P., Crida, A., Petit, A. C., Lega, E., & Morbidelli, A. 2024, A&A, 688, A202, doi: 10.1051/0004-6361/202450340 10, 11, 18, 21, 22, 58

Hadden, S. 2023, History of Planetary N-body Simulations. https://shadden.github.io/nbody_history/ 6

Hairer, E., Lubich, C., & Wanner, G. 2006, Geometric numerical integration: structure-preserving algorithms for ordinary differential equations, Vol. 31 (Springer Science & Business Media) 5

Hairer, E., Wanner, G., & Lubich, C. 2009, Geometric Numerical Integration, Springer Series in Computational Mathematics (Berlin, Heidelberg: Springer Berlin Heidelberg), doi: 10.1007/3-540-30666-8 5

Hamilton, W. R. 1833, On a general method of expressing the paths of light, & of the planets, by the coefficients of a characteristic function (Dublin: Printed by P.D. Hardy). http://books.google.com/books?id=--44AAAAMAAJ 5

Hao, W., Kouwenhoven, M. B. N., & Spurzem, R. 2013, MNRAS, 433, 867, doi: 10.1093/mnras/stt771 10, 12

Heggie, D. C. 1975, MNRAS, 173, 729, doi: 10.1093/mnras/173.3.729 58

Heggie, D. C. 2006, in Few-Body Problem: Theory and Computer Simulations, Vol. 358 (University of Turku), 20–28. https://arxiv.org/abs/0512504 42, 51, 52, 58

Heggie, D. C., & Rasio, F. A. 1996, MNRAS, 282, 1064, doi: 10.1093/mnras/282.3.1064 23, 58

Hoang, N. H., Mogavero, F., & Laskar, J. 2022, MNRAS, 514, 1342, doi: 10.1093/mnras/stac1299 4, 10, 11, 29

Huang, Y., & Gladman, B. 2024, ApJ, 962, L33, doi: 10.3847/2041-8213/ad2686 10, 12, 22

Hunter, J. D. 2007, Computing In Science & Engineering, 9, 90 26, 38, 54

Hussain, N., & Tamayo, D. 2020, MNRAS, 491, 5258, doi: 10.1093/mnras/stz3402 38

Ida, S., & Lin, D. N. C. 2004, ApJ, 604, 388, doi: 10.1086/381724 10, 11

Ito, T., & Tanikawa, K. 2002, MNRAS, 336, 483, doi: 10.1046/j.1365-8711.2002.05765.x 10, 11

Jacobsen, T. S. 1999, "Planetary systems from the ancient Greeks to Kepler" (University of Washington Press) 1, 2

Javaheri, P., Rein, H., & Tamayo, D. 2023, The Open Journal of Astrophysics, 6, 29, doi: 10.21105/astro.2307.05683 6, 7, 13, 19

Jiménez-Torres, J. J., Pichardo, B., Lake, G., & Segura, A. 2013, Astrobiology, 13, 491, doi: 10.1089/ast.2012.0842 20, 41

Joblib Development Team. 2024, Joblib: running Python functions as pipeline jobs, https://joblib.readthedocs.io/ 26

Kane, S. R., & Wittenmyer, R. A. 2024, ApJ, 962, L21, doi: 10.3847/2041-8213/ad2463 22

Kenyon, S. J., & Bromley, B. C. 2004, Nature, 432, 598, doi: 10.1038/nature03136 10, 12, 22

Kepler, J. 1609, Astronomia Nova (Heidelberg: E. Vögelin). https://archive.org/details/Astronomianovaa00Kepl/page/n7/mode/2up 2, 55

—. 1619, Harmonices Mundi (Johannes Plancus, Linz, Austria). https://archive.org/details/ioanniskepplerih00kepl/page/n9/mode/2up 2

Kepler, J., Aiton, E., Duncan, A., & Field, J. 1997, The Harmony of the World, American Philosophical Society: Memoirs of the American Philosophical Society (Philadelphia, Pennsylvania: American Philosophical Society). https://books.google.ca/books?id=rEkLAAAAIAAJ 2

Kepler, J., & Donahue, W. H. 1992, New astronomy (Cambridge, England: Cambridge University Press) 2

Kinoshita, H., & Nakai, H. 1984, Celestial Mechanics, 34, 203, doi: 10.1007/BF01235802 5, 6

Kley, W., & Nelson, R. P. 2012, ARA&A, 50, 211, doi: 10.1146/annurev-astro-081811-125523 10, 11

Kluyver, T., Ragan-Kelley, B., Pérez, F., et al. 2016, Positioning and Power in Academic Publishing: Players, Agents and Agendas, 87 26, 38, 54

Kolmogorov, A. N. 1954, in Dokl. Akad. Nauk SSSR, Vol. 98, 527–530 4, 29

Krauss, L. M., & Chaboyer, B. 2003, Science, 299, 65, doi: 10.1126/science.1075631 41

Kutta, W. 1901, Zeitschrift fur Angewandte Mathematik und Physik, 46, 435 4

Lada, C. J., & Lada, E. A. 2003, ARA&A, 41, 57, doi: 10.1146/annurev.astro.41.011802.094844 20

Lagrange, J. 1776, in Œuvres de Lagrange, ed. J. A. Serret & G. Darboux (Gauthier-Villars), 255–271 3, 29, 55

Lagrange, J. L. 1778, Recherches sur les équations séculaires des mouvemens des noeuds, et des inclinaisons des orbites des planètes (de l'Imprimerie Royale) 3, 29

—. 1781, Théorie des variations séculaires des éléments des planètes, Première partie (Nouveaux Mémoires de l'Académie des Sciences et Belles-Lettres de Berlin) 3, 29

—. 1782, Théorie des variations séculaires des éléments des planètes, Seconde partie contenant la détermination de ces variations pour chacune des plaètes principales (Nouveaux Mémoires de l'Académie des Sciences et Belles-Lettres de Berlin) 3, 29

—. 1783a, Théorie des variations périodiques des mouvements des planètes, Première partie (Nouveaux Mémoires de l'Académie des Sciences et Belles-Lettres de Berlin) 3, 29

—. 1783b, Sur les variations séculaires des mouvements moyens des planètes (Nouveaux Mémoires de l'Académie des Sciences et Belles-Lettres de Berlin) 3, 29

—. 1784, Théorie des variations périodiques des mouvements des planètes, Seconde partie (Nouveaux Mémoires de l'Académie des Sciences et Belles-Lettres de Berlin) 3, 29

Laplace, P. S. 1775, Mémoire de l'Académie royale des sciences de Paris 3, 29, 55

—. 1776, Mémoire de l'Académie royale des sciences de Paris, 8, 199 3, 29

Laskar, J. 1985, A&A, 144, 133 4, 6, 29

—. 1986, A&A, 157, 59 4, 6, 29

Laskar, J. 1988, Astronomy and Astrophysics, 198, 341 4, 6, 10, 11, 17, 47

Laskar, J. 1989, Nature, 338, 237, doi: 10.1038/338237a0 4, 6, 29, 40

Laskar, J. 1990, Icarus, 88, 266 4, 6, 10, 11, 12, 14, 17, 29, 30, 38, 47

—. 1993, Physica D: Nonlinear Phenomena, 67, 257, doi: 10.1016/0167-2789(93)90210-R 6, 17, 47

Laskar, J. 1996, Celestial Mechanics and Dynamical Astronomy, 64, 115, doi: 10.1007/BF00051610 10, 11

Laskar, J. 1997, Astronomy and Astrophysics, 317, 75 13

—. 2000, Physical Review Letters, 84, 3240, doi: 10.1103/PhysRevLett.84.3240 13, 30, 49, 52

—. 2003, arXiv:math/0305364. https://arxiv.org/abs/0305364 6, 17, 47

—. 2013, in Chaos (Springer), 239–270. https://arxiv.org/abs/1209.5996 3, 4, 29, 40

Laskar, J., Fienga, A., Gastineau, M., & Manche, H. 2011, Astronomy & Astrophysics, 532, A89, doi: 10.1051/0004-6361/201116836 10, 11, 49

Laskar, J., & Gastineau, M. 2009, Nature, 459, 817, doi: 10.1038/nature08096 6, 10, 11, 27, 28, 30, 31, 33, 34, 35, 37, 38, 39, 40, 49, 56

Laskar, J., & Petit, A. C. 2017, Astronomy & Astrophysics, 605, A72, doi: 10.1051/0004-6361/201630022 52

Laskar, J., Quinn, T., & Tremaine, S. 1992, Icarus, 95, 148, doi: 10.1016/0019-1035(92)90196-E 6, 29, 49, 55

Laskar, J., & Robutel, P. 2001, Celestial Mechanics and Dynamical Astronomy, 80, 39, doi: 10.1023/A:1012098603882 7

Laskar, J., Robutel, P., Joutel, F., et al. 2004, A&A, 428, 261, doi: 10.1051/0004-6361:20041335 10, 11, 15

Laughlin, G., & Adams, F. C. 1998, The Astrophysical Journal, 508, L171, doi: 10.1086/311736 10, 12, 40, 41

—. 2000, Icarus, 145, 614, doi: 10.1006/icar.2000.6355 10, 12

Le Verrier, U. 1840, J. Math. Pures Appli, 4, 220 3, 29

—. 1841, J. Math. Pures Appli, 28 3, 29

Le Verrier, U.-J. 1845, Théorie du mouvement de Mercure (Paris: Bachelier Imprimeur-Libraire) 4

Levison, H. F., Morbidelli, A., & Dones, L. 2004, AJ, 128, 2553, doi: 10.1086/424616 10, 12, 22

Li, D., Mustill, A. J., & Davies, M. B. 2019, MNRAS, 488, 1366, doi: 10.1093/mnras/stz1794 10, 12, 22

—. 2020, MNRAS, 496, 1149, doi: 10.1093/mnras/staa1622 10, 12

Li, G., & Adams, F. C. 2015, Monthly Notices of the Royal Astronomical Society, 448, 344, doi: 10.1093/mnras/stv012 10, 12, 22, 40, 51

Lithwick, Y., & Wu, Y. 2011, ApJ, 739, 31, doi: 10.1088/0004-637X/739/1/31 6, 29, 30, 47, 49, 50

Loken, C., Gruner, D., Groer, L., et al. 2010, Journal of Physics: Conference Series, 256, 012026, doi: 10.1088/1742-6596/256/1/012026 26, 38, 54

Lubow, S. H., Seibert, M., & Artymowicz, P. 1999, ApJ, 526, 1001, doi: 10.1086/308045 10, 11

Malmberg, D., Davies, M. B., & Heggie, D. C. 2011, Monthly Notices of the Royal Astronomical Society, 411, 859, doi: 10.1111/j.1365-2966.2010.17730.x 10, 12, 40, 41, 42, 53, 58

Malmberg, D., de Angeli, F., Davies, M. B., et al. 2007, MNRAS, 378, 1207, doi: 10.1111/j.1365-2966.2007.11885.x 10, 12

Mann, C. R., Richer, H., Heyl, J., et al. 2019, The Astrophysical Journal, 875, 1, doi: 10.3847/1538-4357/ab0e6d 41

Maschberger, T. 2013, MNRAS, 429, 1725, doi: 10.1093/mnras/sts479 12, 20

McTier, M. A. S., Kipping, D. M., & Johnston, K. 2020, Monthly Notices of the Royal Astronomical Society, 495, 2105, doi: 10.1093/mnras/staa1232 41

Milgrom, M. 1983, ApJ, 270, 365, doi: 10.1086/161130 28

Mills, A. A., Turvey, P. J., Jones, R. V., & Paton, W. D. M. 1979, Notes and Records of the Royal Society of London, 33, 133, doi: 10.1098/rsnr.1979.0009 4

Moffat, J. W., & Toth, V. T. 2008, ApJ, 680, 1158, doi: 10.1086/587926 28

Mogavero, F., Hoang, N. H., & Laskar, J. 2023, Physical Review X, 13, 021018, doi: 10.1103/PhysRevX.13.021018 4, 56, 57

Mogavero, F., & Laskar, J. 2021, A&A, 655, A1, doi: 10.1051/0004-6361/202141007 4, 10, 11, 28, 29, 30, 33, 34, 37, 40, 49

—. 2022, arXiv e-prints, arXiv:2205.03298. https://arxiv.org/abs/2205.03298 4, 10, 11, 29, 51

Morbidelli, A., Brasser, R., Tsiganis, K., Gomes, R., & Levison, H. F. 2009, A&A, 507, 1041, doi: 10.1051/0004-6361/200912876 22

Morbidelli, A., & Levison, H. F. 2004, AJ, 128, 2564, doi: 10.1086/424617 10, 12, 22

Morbidelli, A., Tsiganis, K., Crida, A., Levison, H. F., & Gomes, R. 2007, AJ, 134, 1790, doi: 10.1086/521705 10, 11, 22, 58

Möser, J. 1962, Nachr. Akad. Wiss. Göttingen, II, 1 4, 29

Murray, C. D., & Dermott, S. F. 1999, Solar system dynamics (Cambridge, UK: Cambridge university press) 10, 11, 29, 46

Nascimbeni, V., Bedin, L. R., Piotto, G., De Marchi, F., & Rich, R. M. 2012, Astronomy and Astrophysics, 541, 1, doi: 10.1051/0004-6361/201118655 41

Nesvorný, D. 2018, ARA&A, 56, 137, doi: 10.1146/annurev-astro-081817-052028 10, 11, 22, 58

Nesvornỳ, D., & Morbidelli, A. 2012, The Astronomical Journal, 144, 117 10, 11, 18, 21, 22, 23, 58

Newcomb, S. 1874, On the general integrals of planetary motion (Philadelphia, Pennsylvania: Smithsonian Contributions to Knowledge) 3

Newhall, X. X., Standish, E. M., & Williams, J. G. 1983, A&A, 125, 150 5, 6

Newton, I. 1687, Philosophiae Naturalis Principia Mathematica (London, England: Societatis Regiae) 2, 5, 28, 39, 55

Newton, I., Cohen, I. B., & Whitman, A. 1999, The Principia: Mathematical Principles of Natural Philosophy (Berkeley, California: University of California Press) 2

Nobili, A., & Roxburgh, I. W. 1986, in IAU Symposium, Vol. 114, Relativity in Celestial Mechanics and Astrometry. High Precision Dynamical Theories and Observational Verifications, ed. J. Kovalevsky & V. A. Brumberg, 105–110 31

Ossendrijver, M. 2016, Science, 351, 482, doi: 10.1126/science.aad8085 4

Papaloizou, J. C. B., Nelson, R. P., & Masset, F. 2001, A&A, 366, 263, doi: 10.1051/0004-6361:20000011 10, 11

Park, R. S., Folkner, W. M., Konopliv, A. S., et al. 2017, The Astronomical Journal, 153, 121, doi: 10.3847/1538-3881/aa5be2 4, 30

Pérez, F., & Granger, B. E. 2007, Computing in Science and Engineering, 9, 21, doi: 10.1109/MCSE.2007.53 26, 38, 54

Pfalzner, S. 2013, A&A, 549, A82, doi: 10.1051/0004-6361/201218792 20

Pfalzner, S., Bhandare, A., Vincke, K., & Lacerda, P. 2018, ApJ, 863, 45, doi: 10.3847/1538-4357/aad23c 20

Pfalzner, S., Govind, A., & Portegies Zwart, S. 2024, Nature Astronomy, doi: 10.1038/s41550-024-02349-x 10, 12, 22, 56

Pfalzner, S., & Vincke, K. 2020, ApJ, 897, 60, doi: 10.3847/1538-4357/ab9533 20, 41

Pham, D., & Rein, H. 2024, MNRAS, 530, 2526, doi: 10.1093/mnras/stae986 13

Pham, D., Rein, H., & Spiegel, D. S. 2024, The Open Journal of Astrophysics, 7, 1, doi: 10.21105/astro.2401.02849 13

Poincaré, H. 1898, Annuaire du Bureau des Longitudes pour l'an 1898 3, 29

—. 1899, Les méthodes nouvelles de la mécanique céleste (Gauthier-Villars et fils, imprimeurs-libraires) 4, 29, 39, 55

Pollack, J. B., Hubickyj, O., Bodenheimer, P., et al. 1996, Icarus, 124, 62, doi: 10.1006/icar.1996.0190 10, 11

Ponce, M., van Zon, R., Northrup, S., et al. 2019, in Proceedings of the Practice and Experience in Advanced Research Computing on Rise of the Machines (Learning), PEARC '19 (New York, NY, USA: Association for Computing Machinery), doi: 10.1145/3332186.3332195 26, 38, 54

Portegies Zwart, S. F., & Jílková, L. 2015, Monthly Notices of the Royal Astronomical Society, 451, 144, doi: 10.1093/mnras/stv877 40, 42

Pryor, C., & Meylan, G. 1993, in Astronomical Society of the Pacific Conference Series, Vol. 50, Structure and Dynamics of Globular Clusters, ed. S. G. Djorgovski & G. Meylan, 357 41

Quinn, T. R., Tremaine, S., & Duncan, M. 1991, AJ, 101, 2287, doi: 10.1086/115850 5, 6

Rabiner, L., & Juang, B. 1993, Fundamentals of Speech Recognition, Prentice-Hall Signal Processing Series: Advanced monographs (Hoboken, NJ: PTR Prentice Hall) 13, 57

Ranocha, H., & Ketcheson, D. I. 2020, Journal of Scientific Computing, 84, 17, doi: 10.1007/s10915-020-01277-y 5

Raymond, S. N., Izidoro, A., & Morbidelli, A. 2020, in Planetary Astrobiology, ed. V. S. Meadows, G. N. Arney, B. E. Schmidt, & D. J. Des Marais (Tucson, AZ: The University of Arizona Press), 287, doi: 10.2458/azu_uapress_9780816540068 10, 11, 22, 58

Raymond, S. N., Kaib, N. A., Selsis, F., & Bouy, H. 2024, MNRAS, 527, 6126, doi: 10.1093/mnras/stad3604 10, 12, 22, 57

Rein, H., Brown, G., & Tamayo, D. 2019a, Monthly Notices of the Royal Astronomical Society, doi: 10.1093/mnras/stz2942 8, 30, 47, 49, 55

Rein, H., & Liu, S. F. 2012, A&A, 537, A128, doi: 10.1051/0004-6361/201118085 8, 13, 26, 30, 43, 48, 59

Rein, H., & Papaloizou, J. C. B. 2009, A&A, 497, 595, doi: 10.1051/0004-6361/200811330 35

Rein, H., & Spiegel, D. S. 2015, Monthly Notices of the Royal Astronomical Society, 446, 1424, doi: 10.1093/mnras/stu2164 13

Rein, H., & Tamayo, D. 2015, MNRAS, 452, 376 7, 30, 55

Rein, H., & Tamayo, D. 2019, Research Notes of the AAS, 3, 16, doi: 10.3847/2515-5172/aaff63 3

Rein, H., Tamayo, D., & Brown, G. 2019b, Monthly Notices of the Royal Astronomical Society, 489, 4632, doi: 10.1093/mnras/stz2503 8, 13, 30, 48, 55

Rein, H., Hernandez, D. M., Tamayo, D., et al. 2019, Monthly Notices of the Royal Astronomical Society, 485, 5490, doi: 10.1093/mnras/stz769 8, 55

Rodet, L., & Lai, D. 2022, MNRAS, 509, 1010, doi: 10.1093/mnras/stab3046 58

Roy, A., & Haddow, M. 2003, Celestial Mechanics and Dynamical Astronomy, 87, 411, doi: 10.1023/B:CELE.0000006767.34371.2f 42, 51, 52, 58

Roy, A. E. 2004, Orbital motion, 4th edn. (Boca Raton: CRC Press) 5

Roy, A. E., Walker, I. W., Macdonald, A. J., et al. 1988, Vistas in Astronomy, 32, 95, doi: 10.1016/0083-6656(88)90399-6 5

Runge, C. 1895, Mathematische Annalen, 46, 167. http://eudml.org/doc/157756 4

Rupp, K. 2020, 42 Years of Microprocessor Trend Data. https://www.karlrupp.net/2018/02/42-years-of-microprocessor-trend-data/ 6

Saha, P., & Tremaine, S. 1994, AJ, 108, 1962, doi: 10.1086/117210 31

Salpeter, E. E. 1955, ApJ, 121, 161, doi: 10.1086/145971 12, 43

Schoettler, C., & Owen, J. E. 2024, MNRAS, doi: 10.1093/mnras/stae1900 10, 12

Šidlichovský, M., & Nesvorný, D. 1996, Celestial Mechanics and Dynamical Astronomy, 65, 137, doi: 10.1007/BF00048443 6, 17, 47

Skeel, R. D. 1993, BIT Numerical Mathematics, 33, 172, doi: 10.1007/BF01990352 5

Skeel, R. D., & Cieśliński, J. L. 2020, arXiv e-prints, arXiv:2003.12268, doi: 10.48550/arXiv.2003.12268 5

Spurzem, R., Giersz, M., Heggie, D. C., & Lin, D. N. 2009, Astrophysical Journal, 697, 458, doi: 10.1088/0004-637X/697/1/458 10, 12, 42, 51, 58

Stock, K., Cai, M. X., Spurzem, R., Kouwenhoven, M. B. N., & Portegies Zwart, S. 2020, Monthly Notices of the Royal Astronomical Society, 497, 1807, doi: 10.1093/mnras/staa2047 40, 44, 53

Stock, K., Veras, D., Cai, M. X., Spurzem, R., & Portegies Zwart, S. 2022, Monthly Notices of the Royal Astronomical Society, 512, 2460, doi: 10.1093/mnras/stac602 46

Sussman, G. J., & Wisdom, J. 1992, Science, 257, 56 6, 29, 49, 55

Tamayo, D. 2023, Physics Online Journal, 16, 57, doi: 10.1103/Physics.16.57 56

Tamayo, D., Rein, H., Shi, P., & Hernandez, D. M. 2020a, Monthly Notices of the Royal Astronomical Society, 491, 2885, doi: 10.1093/mnras/stz2870 31, 48

Tamayo, D., Cranmer, M., Hadden, S., et al. 2020b, Proceedings of the National Academy of Sciences, 117, 18194, doi: 10.1073/pnas.2001258117 52

Tange, O. 2022, GNU Parallel 20221022 ('Nord Stream'), Zenodo, doi: 10.5281/zenodo.7239559 38, 54

—. 2023, GNU Parallel 20240522 ('Tbilisi'), https://doi.org/10.5281/zenodo.11247979, Zenodo, doi: 10.5281/zenodo.11247979 26

Tremaine, S. 2023, Dynamics of Planetary Systems (Princeton, NJ: Princeton University Press) 5, 10, 11, 56

Tsiganis, K., Gomes, R., Morbidelli, A., & Levison, H. F. 2005, Nature, 435, 459, doi: 10.1038/nature03539 10, 11, 22, 58

Turrini, D., Zinzi, A., & Belinchon, J. A. 2020, A&A, 636, A53, doi: 10.1051/0004-6361/201936301 13

Valenti, E., Zoccali, M., Mucciarelli, A., et al. 2018, Astronomy & Astrophysics, 616, 8, doi: 10.1051/0004-6361/201832905 41

van den Bergh, S. 1981, PASP, 93, 712, doi: 10.1086/130912 20

Verlinde, E. 2017, SciPost Physics, 2, 016, doi: 10.21468/SciPostPhys.2.3.016 28

Winn, J. N., & Fabrycky, D. C. 2015, ARA&A, 53, 409, doi: 10.1146/annurev-astro-082214-122246 22

Wisdom, J. 2018, Monthly Notices of the Royal Astronomical Society, 474, 3273, doi: 10.1093/mnras/stx2906 6

Wisdom, J., & Holman, M. 1991, AJ, 102, 1528, doi: 10.1086/115978 6, 7, 30, 48, 55

Wisdom, J., Holman, M., & Touma, J. 1996, Fields Institute Communications, 10, 217 7, 30, 48

Yoshida, H. 1993, Celestial Mechanics and Dynamical Astronomy, 56, 27, doi: 10.1007/BF00699717 5

Zakamska, N. L., & Tremaine, S. 2004, The Astronomical Journal, 128, 869, doi: 10.1086/422023 30, 49

Zeebe, R. E. 2015, ApJ, 798, 8, doi: 10.1088/0004-637X/798/1/8 10, 11, 28, 30, 38, 40

Zheng, X., Kouwenhoven, M. B., & Wang, L. 2015, Monthly Notices of the Royal Astronomical Society, 453, 2759, doi: 10.1093/mnras/stv1832 40

Zink, J. K., Batygin, K., & Adams, F. C. 2020, AJ, 160, 232, doi: 10.3847/1538-3881/abb8de 12, 40, 43